Cell

An antibiotic from an uncultured bacterium binds to an immutable target

Graphical abstract

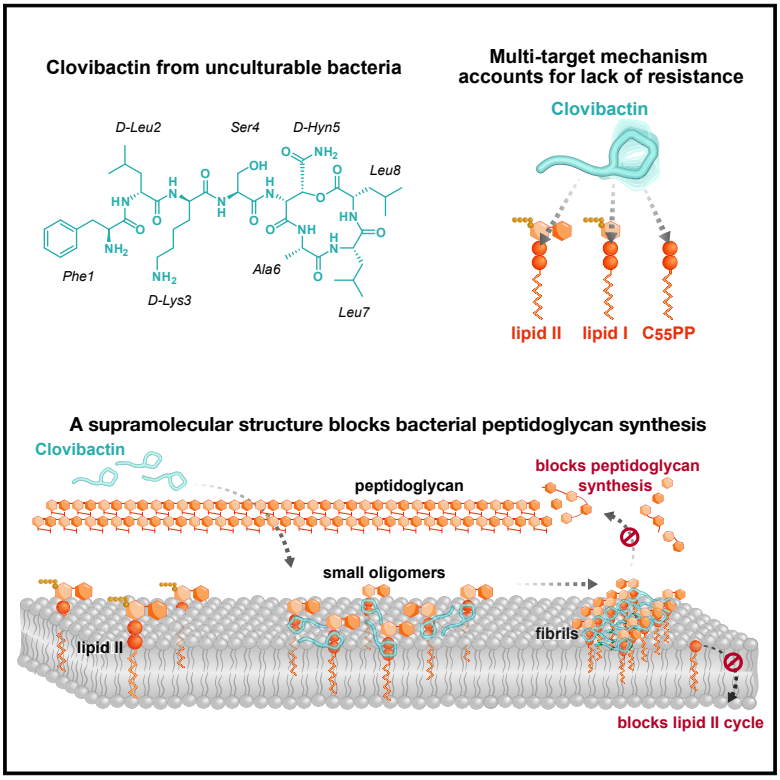

Highlights

- Clovibactin was discovered in a previously uncultivated bacterium
- Kills without resistance and is efficacious in a mouse model of *S. aureus* infection
- It blocks the cell wall biosynthesis by targeting distinct, essential precursors
- Clovibactin uses an unusual hydrophobic interface to target immutable pyrophosphate

Authors

Rhythm Shukla, Aaron J. Peoples, Kevin C. Ludwig, ..., Kim Lewis, Tanja Schneider, Markus Weingarth

Correspondence

tschneider@uni-bonn.de (T.S.), m.h.weingarth@uu.nl (M.W.)

In brief

Clovibactin, a new antibiotic isolated from soil bacteria, blocks bacterial cell wall synthesis by targeting essential peptidoglycan precursors, allowing it to kill drug-resistant bacterial pathogens without detectable resistance.

Shukla et al., 2023, Cell *186*, 4059–4073
September 14, 2023 © 2023 The Authors. Published by Elsevier Inc.
https://doi.org/10.1016/j.cell.2023.07.038

CellPress

Cell

CellPress
OPEN ACCESS

Article

An antibiotic from an uncultured bacterium binds to an immutable target

Rhythm Shukla,[1,2,14] Aaron J. Peoples,[3,14] Kevin C. Ludwig,[4] Sourav Maity,[5] Maik G.N. Derks,[1,2] Stefania De Benedetti,[4] Annika M. Krueger,[5] Bram J.A. Vermeulen,[1] Theresa Harbig,[7] Francesca Lavore,[1] Raj Kumar,[1] Rodrigo V. Honorato,[1] Fabian Grein,[4,8] Kay Nieselt,[7] Yangping Liu,[9] Alexandre M.J.J. Bonvin,[1] Marc Baldus,[1] Ulrich Kubitscheck,[6] Eefjan Breukink,[2] Catherine Achorn,[3] Anthony Nitti,[3] Christopher J. Schwalen,[10] Amy L. Spoering,[3] Losee Lucy Ling,[3] Dallas Hughes,[3] Moreno Lelli,[11,12] Wouter H. Roos,[5] Kim Lewis,[13] Tanja Schneider,[4,8,*] and Markus Weingarth[1,15,*]

[1]NMR Spectroscopy, Department of Chemistry, Utrecht University, Padualaan 8, 3584 CH Utrecht, the Netherlands
[2]Membrane Biochemistry and Biophysics, Department of Chemistry, Utrecht University, Padualaan 8, 3584 CH Utrecht, the Netherlands
[3]NovoBiotic Pharmaceuticals, Cambridge, MA 02138, USA
[4]Institute for Pharmaceutical Microbiology, University Hospital Bonn, University of Bonn, Bonn, Germany
[5]Moleculaire Biofysica, Zernike Instituut, Rijksuniversiteit Groningen, Nijenborgh 4, 9747 AG Groningen, the Netherlands
[6]Clausius-Institute for Physical and Theoretical Chemistry, University of Bonn, Bonn, Germany
[7]Integrative Transcriptomics, Center for Bioinformatics, University of Tübingen, 72070 Tübingen, Germany
[8]German Center for Infection Research (DZIF), partner site Bonn-Cologne, Bonn, Germany
[9]The Province and Ministry Co-sponsored Collaborative Innovation Center for Medical Epigenetics, Tianjin Key Laboratory on Technologies Enabling Development of Clinical Therapeutics and Diagnostics, School of Pharmacy, Tianjin Medical University, Tianjin 300070, China
[10]Novartis Institutes for Biomedical Research, Cambridge, MA 02139, USA
[11]Magnetic Resonance Center (CERM) and Department of Chemistry "Ugo Schiff", University of Florence, via della Lastruccia 3, Sesto Fiorentino 50019, Italy
[12]Consorzio Interuniversitario Risonanze Magnetiche MetalloProteine (CIRMMP), via Sacconi 6, Sesto Fiorentino 50019, Italy
[13]Antimicrobial Discovery Center, Northeastern University, Department of Biology, Boston, MA 02115, USA
[14]These authors contributed equally
[15]Lead contact
*Correspondence: tschneider@uni-bonn.de (T.S.), m.h.weingarth@uu.nl (M.W.)
https://doi.org/10.1016/j.cell.2023.07.038

SUMMARY

Antimicrobial resistance is a leading mortality factor worldwide. Here, we report the discovery of clovibactin, an antibiotic isolated from uncultured soil bacteria. Clovibactin efficiently kills drug-resistant Gram-positive bacterial pathogens without detectable resistance. Using biochemical assays, solid-state nuclear magnetic resonance, and atomic force microscopy, we dissect its mode of action. Clovibactin blocks cell wall synthesis by targeting pyrophosphate of multiple essential peptidoglycan precursors ($C_{55}PP$, lipid II, and lipid III_{WTA}). Clovibactin uses an unusual hydrophobic interface to tightly wrap around pyrophosphate but bypasses the variable structural elements of precursors, accounting for the lack of resistance. Selective and efficient target binding is achieved by the sequestration of precursors into supramolecular fibrils that only form on bacterial membranes that contain lipid-anchored pyrophosphate groups. This potent antibiotic holds the promise of enabling the design of improved therapeutics that kill bacterial pathogens without resistance development.

INTRODUCTION

The introduction of antibiotics has revolutionized medicine, providing effective treatment for infectious diseases that were once fatal and enabling modern medicine, such as surgery and organ transplantation. Widespread resistance development thwarts the effectiveness and lifespan of antibiotics, calling for the discovery of new drugs in the perpetual standoff against human pathogens.[1–4]

Most antibiotics used in the clinic originate from natural product scaffolds that were discovered by screening soil dwelling bacteria.[5] This approach, ushered in by the "Waksman platform," was vastly successful in the 1940s to 1960s, considered the golden age of antibiotics discovery, and it eventually led to the introduction of compounds such as streptomycin, vancomycin, or tetracycline. However, to date, traditional screening sources seem overmined because they tend to yield previously known compounds. Because the drug discovery pipeline has considerably thinned, it is prudent to search for new antibiotics with unprecedented mechanism of action among untapped groups of bacterial producers.

Uncultured bacteria represent a vast (~99% of all species), unexploited source of new natural product scaffolds.[6,7] Recently, the development of the iChip technique[8] provided

This is an open access article under the CC BY license (http://creativecommons.org/licenses/by/4.0/).

access to a broad diversity of uncultured bacterial species, leading to the discovery of teixobactin,[9] isolated from the soil bacterium *Eleftheria terrae*. Teixobactin shows excellent antibacterial activity and has a unique chemical structure. Teixobactin blocks cell wall biosynthesis by specific binding to highly conserved lipid precursors,[9] leading to the formation of supramolecular structures that perturb membrane stability.[10] Additional antibiotics with novel modes of action that came out of screening uncultured bacteria are lassomycin, an inhibitor of the ClpP1P2C1 protease, and amycobactin, an inhibitor of the SecY protein exporter, both acting selectively against mycobacteria.[11,12] Uncultured bacteria hence appear to offer a rich source of compounds with new chemical and mechanistic characteristics, which bodes well for the sustained discovery of effective leads to develop next-generation antibiotics.

Here, we report the discovery and mode of action of clovibactin, an antibiotic without detectable resistance, identified from a screen of uncultured bacteria.

RESULTS

Discovery of clovibactin

Some environmental bacteria, as well as spores, may require a prolonged incubation to initiate growth *in vitro*.[13,14] This allows access to microorganisms that would be missed by standard cultivation techniques. Colonies that were detected after 12 weeks of incubation were sub-cultured and screened for antimicrobial activity on nutrient agar plates overlaid with *Staphylococcus aureus*. One of the producers showed a prominent zone of inhibition, and based on 16S rDNA sequence, it is 99% identical to *E. terrae*. We refer to this isolate as *E. terrae ssp. carolina*; the sandy soil it was isolated from comes from North Carolina. The genus *Eleftheria* that belongs to β-proteobacteria is very rare, and the original *E. terrae* we isolated several years ago by growth *in situ* is the producer of teixobactin.[9] *E. terrae* belong to "uncultured" bacteria that are not recovered by conventional methods. We therefore decided to identify the antimicrobial compound produced by *E. terrae ssp. carolina*.

Bioassay-guided fractionation of an extract resulted in the isolation of kalimantacin, a known antibiotic. However, extracts of the fermented broth showed activity against *Bacillus subtilis*, whereas kalimantacin is not active against this species.[15] Upon an initial separation of the crude extract by high-pressure liquid chromatography (HPLC), we identified another fraction of the extract that showed activity against both *B. subtilis* and *S. aureus*. In an attempt to increase metabolic flux to novel compound production and simplify isolation, we set out to disrupt genes responsible for kalimantacin production. Whole-genome sequencing led to the identification of a biosynthetic gene cluster (BGC) with 55% identity to the kalimantacin/batumin operon.[16] Production of kalimantacin was reduced below detectable levels by interrupting the first gene in the operon, *bat1*, using homologous recombination of a suicide vector.[17]

Fermentation broth of *E. terrae ssp. carolina Δbat1* was separated by HPLC, and bioassay-guided isolation produced a fraction with a compound having a mass of 903.5291 $[M+H]^+$. According to Antibase, this mass is unique. A combination of mass spectrometry and solution nuclear magnetic resonance (NMR) resolved the structure of this compound, which is a novel depsipeptide that we named clovibactin (Figure 1). Stereochemistry was confirmed by Marfey's analysis. Clovibactin features two D-amino acids in its linear N terminus and an uncommon residue D-3-hydroxyasparagine in the depsi-cycle. The compound's molecular scaffold bears some resemblance to the depsi-peptide teixobactin, as reflected by a Tanimoto coefficient of 0.8761. However, clovibactin has a considerably shorter linear N terminus (four residues in clovibactin, seven residues in teixobactin) that harbors the two positive charges present in the compound. Additionally, teixobactin contains one of its two positively charged amino acids in the macrolactone that also contains an unusual enduracididine residue, missing in clovibactin.

The genome of *E. terrae ssp. carolina* was sequenced using PacBio. *E. terrae ssp. carolina* contains 19 predicted BGCs overall, of which 14 have non-ribosomal peptide synthase (NRPS)-like elements (either pure NRPS or NRPS/PKS hybrid). The gene cluster associated with the biosynthesis of clovibactin was identified by antiSMASH[18] version 5.1.1.[19] It contains two NRPS genes (*cloA* and *cloB*), a transporter gene (*cloC*) and a tailoring enzyme (*cloD*). The proposed biosynthetic pathway of clovibactin (Figure 1) proceeds through assembly line condensation of 8 amino acids with 3 epimerizations carried out by dual-function condensation domains and a β-hydroxylation on Asn5 by the CloD, a TauD/TfdA dioxygenase. This hydroxylation provides the cyclization point for release from the NRPS and formation of the macrocyclic lactone. When comparing the clovibactin and teixobactin BGCs, the identity is 72% by BLASTN alignment (Figure 1).

Clovibactin exhibited antibacterial activity against a broad range of Gram-positive pathogens, including methicillin-resistant *S. aureus* (MRSA), daptomycin-resistant and vancomycin-intermediate-resistant *S. aureus* (VISA) strains, and difficult to treat vancomycin-resistant *Enterococcus faecalis*[20] and *E. faecium* (vancomycin-resistant enterococci [VRE]) (Tables 1 and S1). *Escherichia coli* was only marginally affected compared with an outer membrane deficient *E. coli* WO153 strain, probably reflecting insufficient penetration of the compound.

Clovibactin is bactericidal, with *S. aureus* minimal bactericidal concentration (MBC) of 2 × MIC (minimal inhibitory concentration). We then examined the time-dependent killing in more detail (Figure 2A). Clovibactin was more effective in killing *S. aureus* compared with vancomycin, the first line of defense antibiotic. We noticed that clovibactin produced unusually strong lysis of the cell culture and quantified this effect (Figures 2B, 2C, and S1A). Teixobactin was previously demonstrated to be rapidly bactericidal and to induce lysis[9] mediated by AtlA,[1] the major cell wall autolysin of *S. aureus*. To investigate the contribution of AtlA to the activity of clovibactin, the antibacterial activity against an Δ*atlA* deletion mutant was examined and compared with wild-type *S. aureus*. Clovibactin (2 × MIC) induced strong lysis, more pronounced than teixobactin (Figures 2B and 2C). Strikingly, lytic events were only slightly affected in the Δ*atlA* mutant, suggesting that clovibactin-induced lysis does not primarily rely on AtlA activity. Moreover, killing of *S. aureus* by clovibactin was almost unaffected in both wild type and in the Δ*atlA* mutant, in contrast to teixobactin (Figure 2D). In agreement, clovibactin-treated *S. aureus* cells did not release AtlA into

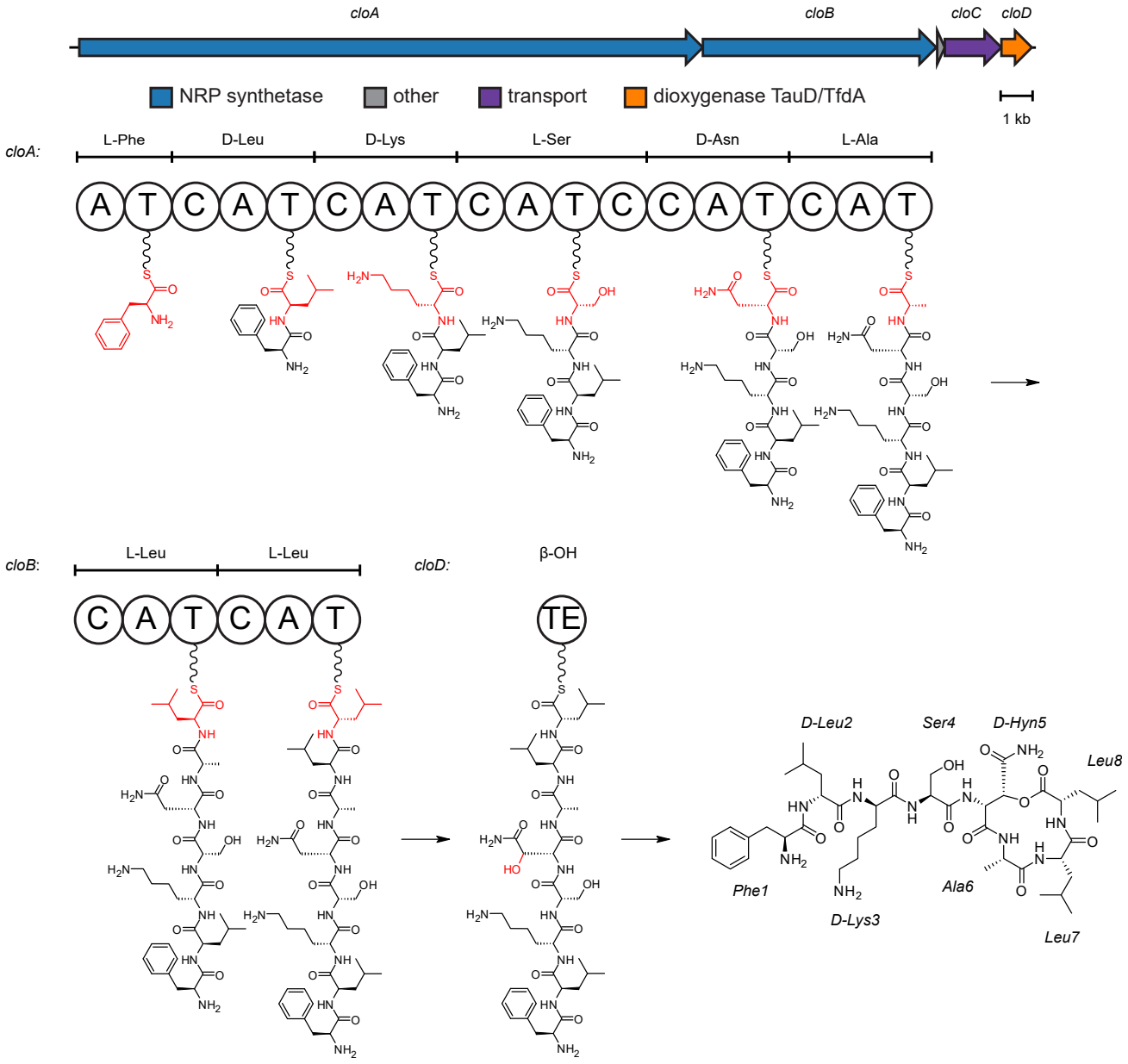

Figure 1. Biosynthetic gene cluster and proposed biosynthesis of clovibactin

The gene cluster associated with the biosynthesis of clovibactin (*cloABCD*) was identified via whole-genome sequencing. NRPS modules are labeled as follows: A, adenylation; T, thiolation/peptidyl carrier protein; C, condensation; TE, thioesterase.

See also Tables 1 and S1.

supernatant as observed for teixobactin as revealed by zymographic analysis[1] (Figure S1B) and comparative transcriptomic sequencing (RNA-seq) of clovibactin- and teixobactin-treated *S. aureus* showed differential regulation of autolysins and hydrolases controlled by the essential WalRK two-component system (TCS) (Figure S1C), pointing to distinct cellular mechanisms of action of the two compounds. Such pronounced lysis is typically observed with detergent-like compounds that rapidly destroy the cell membrane. However, lysis induced by clovibactin is not the result of rapid pore formation or membrane disruption, as evidenced by the absence of membrane effects in permeabilization assays in contrast to the pore-forming lantibiotic nisin (Figure S1E). Similarly, clovibactin treatment did not lead to rapid membrane depolarization as determined using the membrane potential sensitive dye DiSC2(5) or enable penetration of SYTOX. This contrasts with the action of teixobactin that thins and depolarizes bacterial membranes.[10] In agreement with this, clovibactin did not affect the cellular localization of the

Table 1. Antimicrobial activity of clovibactin

Strain	MIC (μg/mL)
Staphylococcus aureus	
NCTC 8325–4 (MSSA)	0.5–1
ATCC 29213 (MSSA)	0.5–1
ATCC 700699 (GISA)	1–2
NRS71 (epidemic MRSA)	1
NRS108 (MRSA, also synercid^{R})	1
ATCC 33591 (MRSA)	1–2
Mu50 (VISA)	2
SG511	0.125
HG001	2
Staphylococcus epidermidis	
ATCC 35982 (*mecA* positive)	0.5
NRS8 (*mecA* positive)	0.5
Staphylococcus haemolyticus	
NRS9 (*mecA* positive)	1
NRS69 (*mecA* positive)	0.5
Other Gram-positive	
Enterococcus faecium BM4147 (VRE) (*aac(6′)-Ie-aph-(2′)*)	0.5–1
E. faecalis ATCC 51299 (VRE)	0.5–2
Bacillus subtilis trpC2 1A1	1–2
B. subtilis 168 DSM 23778	2
Bacillus anthracis Sterne	0.25
Streptococcus pneumoniae ATCC 10813	0.25–0.5
Streptococcus pyogenes ATCC 19615	0.25–0.5
Staphylococcus warneri NRS138	1
Mycobacterium smegmatis MC^2 155	2
Mycobacterium *tuberculosis* MC^2 6020	0.5–1
Gram-negative	
Haemophilus influenzae SJ7	2
Escherichia coli K12	64
E. coli WO153 (AB1157:*asmB1 ΔtolC:kan*)	1–2
Pseudomonas aeruginosa PA-01	>128

Related to Figure 1. Minimal inhibitory concentrations (MICs) of clovibactin were determined by broth microdilution against selected strains and pathogenic bacteria. GISA, glycopeptide intermediate resistant *S. aureus*; MSSA, methicillin-sensitive *S. aureus*; MRSA, methicillin-resistant *S. aureus*; VISA, vancomycin-intermediate-resistant *S. aureus*; VRE, vancomycin-resistant enterococci. See also Table S1.

cell-division protein MinD in *B. subtilis* (Figure S1F). MinD is normally localized to cell poles and division sites and becomes delocalized upon dissipation of the membrane potential.[21]

Clovibactin did not show any cytotoxicity against mammalian NIH/3T3 and HepG2 cells at 100 μg/mL (highest concentration tested). Given the strong antimicrobial activity of clovibactin and low cytotoxicity, we next examined the action of this antibiotic *in vivo*. We first performed a pharmacokinetic (PK) study to evaluate the systemic exposure and blood residence time of the compound. A single dose of clovibactin was administered to mice at up to 40 mg/kg intravenously and was tolerated. Blood was drawn at different times, and clovibactin plasma levels were determined by LC-MSMS, and PK parameters were determined using the software package Watson LIMS (Figure 2E).

Next, clovibactin was evaluated in a neutropenic mouse thigh infection model with *S. aureus*. In this model, mice are treated with cyclophosphamide to disable the immune response. Antibiotics are then evaluated for their ability to control infection without the assistance of the immune system. Clovibactin was comparable to vancomycin in diminishing the bacterial burden (Figure 2F).

Target identification

Given the novelty of the structure and the promising properties of this compound as a developmental lead, we sought to identify the molecular target of clovibactin. First, we determined the frequency of resistance, which is essential to know for advancing a compound. From a drug development standpoint, a desirable frequency of resistance is $<10^{-8}$[22]—low enough to provide extended lifetime in the clinic. The added benefit of this determination is target identification by whole-genome sequencing of resistant mutants. However, plating *S. aureus* on media containing clovibactin even at a low concentration (4 × MIC) produced no resistant mutants. We therefore estimate the frequency of resistance to be $<10^{-10}$. We then sought to determine a possible biosynthetic pathway that clovibactin might inhibit. For this, we followed the incorporation of labeled precursors into the major biosynthetic pathways of *S. aureus*—DNA, RNA, protein, and peptidoglycan. Clovibactin specifically interfered with the incorporation of radiolabeled N-acetylglucosamine (GlcNAc) into the cell wall, whereas DNA, RNA, and protein biosynthesis remained unaffected (Figure 3A). In a parallel approach, we used pathway-selective bioreporter strains of *B. subtilis* treated with clovibactin.[23] Expression of LacZ was specifically induced by clovibactin in *B. subtilis* P_{ypuA}-*lacZ*, indicative of interference with cell wall biosynthesis (Figure 3B). Treatment of *B. subtilis* with clovibactin induced cell-shape deformations as visualized by phase-contrast microscopy. This blebbing phenotype is characteristically induced by many cell-wall-acting antibiotics and was similarly observed with teixobactin,[9] hypeptin,[24] or vancomycin but not the protein synthesis inhibitor clindamycin used as a control (Figures 3C and S1D), further supporting direct interference with cell wall biosynthesis. To narrow down the molecular target within the cell wall biosynthesis pathway, *lial-lux* induction was monitored over time. LiaRS is a TCS, known to respond to antibiotics that interfere with lipid II biosynthesis. Clovibactin strongly induced P_{lial}-*lux*, suggesting that it may directly interact with the lipid II biosynthesis pathway (Figure 3D).

Synthesis of the peptidoglycan precursor lipid II occurs in two different compartments of the bacterial cell. In the cytoplasm, the soluble sugar building blocks UDP-N-acetylmuramic acid pentapeptide (UDP-MurNAc-pp) and UDP-GlcNAc are synthesized and transferred to the lipid carrier undecaprenyl phosphate ($C_{55}P$) to build lipid II that is flipped across the membrane to the exterior of the cell and incorporated into the growing peptidoglycan network (Figure S2). Antibiotics that block late stages of peptidoglycan biosynthesis, such as vancomycin, are known to trigger the intracellular accumulation of the last soluble peptidoglycan precursor UDP-MurNAc-pp. As observed for

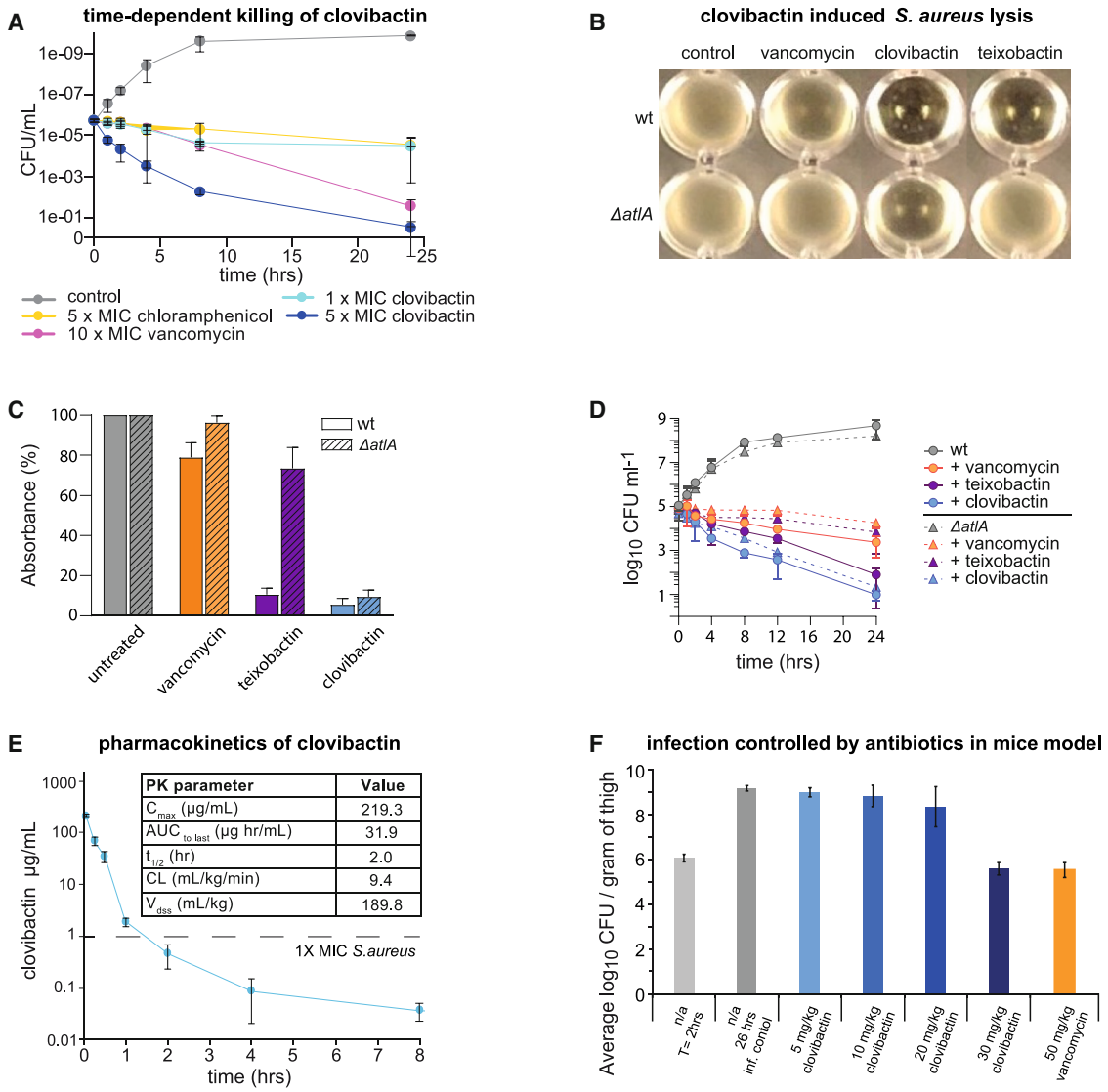

Figure 2. Clovibactin kills *S. aureus in vitro* and *in vivo*

(A) Time-dependent killing of *S. aureus* (clovibactin [1 × MIC], clovibactin [5 × MIC], vancomycin [10 × MIC], and chloramphenicol [5 × MIC]). Data are means of three independent experiments ± standard deviation.

(B and C) Clovibactin-induced lysis in *S. aureus*. Cells of *S. aureus* SA113 and a *ΔaltA* mutant were incubated with each compound at 2 × MIC (B) and 5 × MIC (C) for 24 h, as indicated. Representative of four independent experiments (B) and mean values from three independent experiments (C) are shown. In (C), error bars represent standard deviation.

(D) Time-dependent killing of *S. aureus* and *S. aureus ΔatlA* (clovibactin, teixobactin, and vancomycin [2 × MIC each]). Error bars represent standard deviation.

(E) Pharmacokinetic parameters of clovibactin in mice model determined using Watson LIMS software. The analysis was performed using three animals per time point. The data points are the mean plasma concentration and the standard deviation from all three animals within each time point.

(F) The bacterial load from the thigh infection model prior to dosing and 24 h after treatment. The infection controls demonstrated a bioload of 6.07 $\log_{10}$ colony-forming units (CFUs)/gram of thigh at the time of treatment (2 h). Clovibactin was delivered as two IV doses (2 and 4 h post infection) of 5, 10, 20, and 30 mg/kg. Vancomycin was delivered as a single IV dose at 50 mg/kg. There were four animals per group. The data points are the average CFU/gram of thigh and the standard deviation from all four animals within each group.

See also Figure S1 and Tables 1 and S1.

vancomycin, treatment of *S. aureus* with clovibactin at increasing concentrations led to an accumulation of UDP-MurNAc-pp in the cytoplasm (Figure 3E). A fluorescent clovibactin-Bodipy-FL derivative bound preferentially to the septum of dividing staphylococcal cells, a site enriched in lipid II (Figure S3A). Preincubation of cells with teixobactin strongly diminished clovibactin-FL binding to the septum, suggesting that both compounds interact with the same targets (Figure S3A).

Based on the results obtained with whole cells, the impact of clovibactin on the late steps of cell wall biosynthesis was analyzed

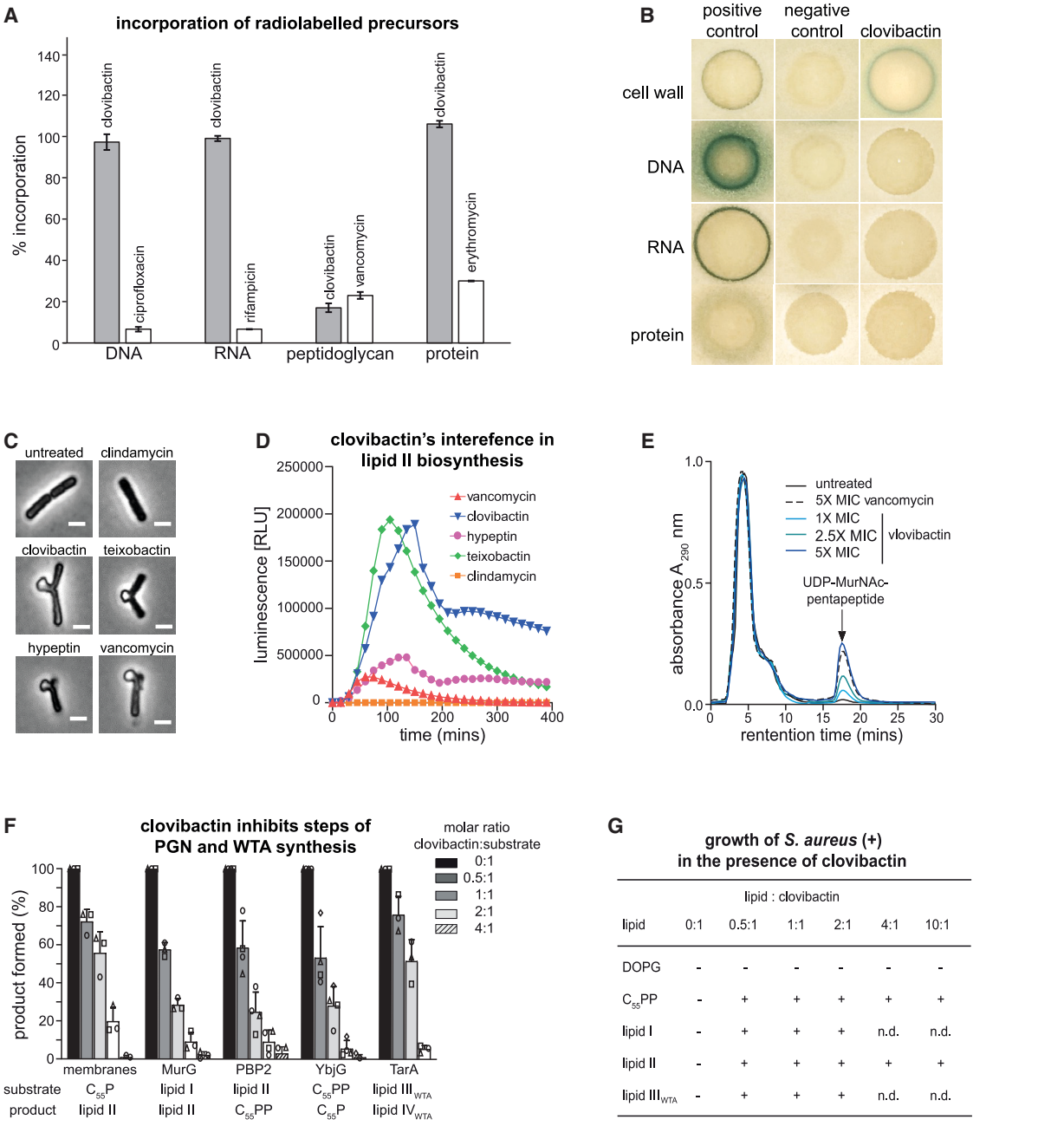

G

growth of *S. aureus* (+) in the presence of clovibactin

	lipid : clovibactin					
lipid	0:1	0.5:1	1:1	2:1	4:1	10:1
DOPG	-	-	-	-	-	-
$C_{55}PP$	-	+	+	+	+	+
lipid I	-	+	+	+	n.d.	n.d.
lipid II	-	+	+	+	+	+
lipid III_{WTA}	-	+	+	+	n.d.	n.d.

Figure 3. Clovibactin targets cell wall biosynthesis

(A) Effect of clovibactin on macromolecular biosyntheses in *S. aureus*. Incorporation of ^{3}H-thymidine (DNA), ^{3}H-uridine (RNA), ^{3}H-leucine (protein), and ^{3}H-glucosamine (peptidoglycan) was determined in cells treated with clovibactin at 2 × MIC (gray bars). Ciprofloxacin (8 × MIC), rifampicin (4 × MIC), vancomycin (2 × MIC), and erythromycin (2 × MIC) were used as positive controls (white bars). Data are averages of two independent experiments. Error bars are standard deviation.

(B) *B. subtilis* bioreporter strains with selected promotor-*lacZ* fusions were used to identify interference with major biosynthesis pathways. β-galactosidase (*lacZ*) is fused to promotors P_{ypuA} (cell wall), P_{yorB} (DNA), P_{yvgS} (RNA), and P_{yheI} (protein) and induction of a specific stress response is visualized by a blue halo at the edge of the inhibition zone. Antibiotics vancomycin, ciprofloxacin, rifampicin, and clindamycin were used as positive controls.

(C) Clovibactin treatment results in cell-shape deformations and characteristic blebbing as observed by phase-contrast microscopy of *B. subtilis*. Cell wall active antibiotics teixobactin, hypeptin, vancomycin, and protein synthesis inhibitor clindamycin were used as controls. Scale bars, 2 μm.

(D) Clovibactin (1 × MIC, blue) strongly induced P_{lial} as observed by expression of the *lux* operon in *B. subtilis* P_{lial}-*lux*. Teixobactin, hypeptin, vancomycin, and clindamycin were used as control antibiotics.

(E) Intracellular accumulation of the soluble cell wall precursor UDP-MurNAc-pp after treatment of *S. aureus* with different concentrations of clovibactin. Untreated and VAN-treated (5 × MIC) cells were used as controls. Experiments are representatives of three independent experiments.

(legend continued on next page)

in vitro to identify the molecular target—clovibactin was thus tested in individual biosynthesis assays using purified enzymes and substrates (Figure 3F). Clovibactin inhibited all cell wall biosynthesis reactions that consume lipid I, lipid II, lipid III_{WTA}, or undecaprenyl-pyrophosphate ($C_{55}PP$) as a substrate in a dose-dependent fashion, suggesting binding to these lipid intermediates, rather than inhibiting enzyme function. Of note, clovibactin equally inhibited reactions consuming $C_{55}PP$ and lipid II as a substrate. Corroborating this result, the addition of purified cell wall lipid intermediates antagonized the antimicrobial activity of clovibactin and restored growth of *S. aureus* (Figures 3G and S3D). Interestingly, similar molar concentrations of $C_{55}PP$ and lipid II were required to fully antagonize clovibactin activity, whereas antagonization of teixobactin activity required a 10-fold higher concentration of $C_{55}PP$ compared with lipid II (Figure S3D), suggesting differences in the binding mode. In agreement with this, higher concentrations of teixobactin[9] were needed to completely block the YbjG-catalyzed dephosphorylation compared with clovibactin (Figures 3F and S3E), suggesting that $C_{55}PP$ is a primary target for clovibactin. This is further substantiated by the antagonization of the clovibactin-induced liaI-lux stress response, which was equally antagonized by $C_{55}PP$ and lipid II (Figure S3F). In contrast, although teixobactin-induced liaI-lux stress response was efficiently antagonized by lipid II, significantly higher concentrations of $C_{55}PP$ were required (Figure S3F).

Oligomerization upon target binding

Next, we studied the interaction between clovibactin and lipid II in lipid bilayers using solid-state NMR (ssNMR), which allows the investigation of molecular mechanism of antibiotics binding to membrane targets under near-native conditions.[10,25,26] To make the drug amenable to a comprehensive ssNMR characterization, we produced uniformly ^{13}C,^{15}N-labeled clovibactin by fermentation of *E. terrrae spp. carolina Δbat* in ^{13}C,^{15}N-enriched media (see STAR Methods section). Co-assembly of clovibactin and lipid II in membranes resulted in high-quality 2D ssNMR correlation spectra that demonstrate the formation of a well-defined complex. We fully assigned the chemical shifts of clovibactin in the complex using 2D CC, CN, and NH spectra (Figure S4). Large signal shifts of the backbone amide protons show that clovibactin undergoes a major conformational change upon lipid II binding (Figure 4A). An analysis of the ^{13}C chemical shifts[27] suggests that the short linear N terminus of clovibactin does not adopt a classical secondary structure but seems to contain elements of β-structuring (Figure S4). Subsequently, we investigated the site-resolved dynamics of clovibactin in the lipid II-bound state using ssNMR relaxation measurements[28,29] (Figures 4B and 4C). Globally, clovibactin is immobilized in the complex, indicative of the formation of a larger supramolecular structure. Strikingly, the N terminus (Leu2 and Lys3) strongly rigidifies upon complex formation, which is reminiscent of the antimicrobial action of teixobactin, whose N terminus drives the self-assembly into large clusters upon target binding.[10,30]

We used confocal microscopy to probe the assembly of the complex on the surface of giant unilamellar vesicles (GUVs) doped with a low (0.1 mol %) concentration of Atto-tagged lipid II. Microscopy images clearly show the formation of large clovibactin-lipid II patches, whereas such accumulation was not observed without clovibactin (Figure 4G). These data confirm the formation of large supramolecular clovibactin-lipid II domains.

Next, we investigated at high resolution how clovibactin molecules arrange in the supramolecular assemblies. We acquired 2D ssNMR PARISxy[32] CC spectra of the complex, in which we observed numerous clear head-to-tail contacts between N-terminal (Phe1) and C-terminal (Hyn5 and Leu8) clovibactin residues. In agreement with the formation of a supramolecular structure, these are likely intermolecular contacts between clovibactin molecules because the intramolecular distances between N-terminal and C-terminal residues appear too far for CC magnetization transfer with a distance threshold of approximately 8 Å (Figures 4D, 4E, and S5A). The contacts that we observe are consistent with an antiparallel dimeric organization of clovibactin molecules (Figures 4F and S5B). The formation of supra-structures is also demonstrated by dynamic nuclear polarization (DNP) ssNMR studies using an equimolar mixture of ^{13}C-labeled and ^{15}N-labeled clovibactin samples (Figures S5C–S5F). In line with our structural model of the complex, these fluorescence resonance energy transfer (FRET)-like DNP-ssNMR experiments show that intermolecular clovibactin-clovibactin contacts in the suprastructure are predominantly backbone-backbone mediated and mainly involve N-terminal residues.

Flexible fibrils

To examine the supramolecular nature and the membrane interactions of clovibactin-lipid II complex in more detail, we first used high-speed atomic force microscopy (HS-AFM), a dynamic technique that provides biomolecular-scale structural resolution in real time.[33,34] Within minutes after the addition of 5 μM of clovibactin to membranes doped with lipid II, HS-AFM data show the formation of fibrils on the membrane surface (Figures 4H, 4J, and S5G). These fibrils only formed in the presence of both clovibactin and lipid II (Figure S5H). The observed fibrils showed a limited extend of lateral nucleation, forming thin, flat strings of associated fibrils.

The clovibactin concentrations required to observe supramolecular structures by HS-AFM are comparable to the MIC,

(F) Clovibactin inhibits membrane-associated steps of peptidoglycan (PGN) and wall teichoic acid (WTA) synthesis *in vitro*. The antibiotic was added in molar ratios from 0.5 to 4 with respect to the amount of the lipid substrate $C_{55}P$, $C_{55}PP$, lipid II, or lipid III_{WTA} used in the individual test systems. Reaction product synthesized in the absence of antibiotic was taken as 100%. Mean values from three independent experiments are shown. Error bars represent standard deviation.

(G) Antagonization of the antimicrobial activity of clovibactin by cell wall precursors. *S. aureus* was incubated with clovibactin (8 × MIC) in nutrient broth in microtiter plates, and growth was measured after a 24 h incubation at 37°C. Putative HPLC-purified antagonists (undecaprenyl-pyrophosphate [$C_{55}PP$], lipid I, lipid II, and lipid III_{WTA}) and 1,2-dioleoyl-*sn*-glycero-3-phospho-glycerol (DOPG) were added at molar ratios with respect to the antibiotic. Experiments were performed with biological replicates. + antagonization/growth; − no antagonization/no growth; n.d. not determined.

See also Figures S2 and S3.

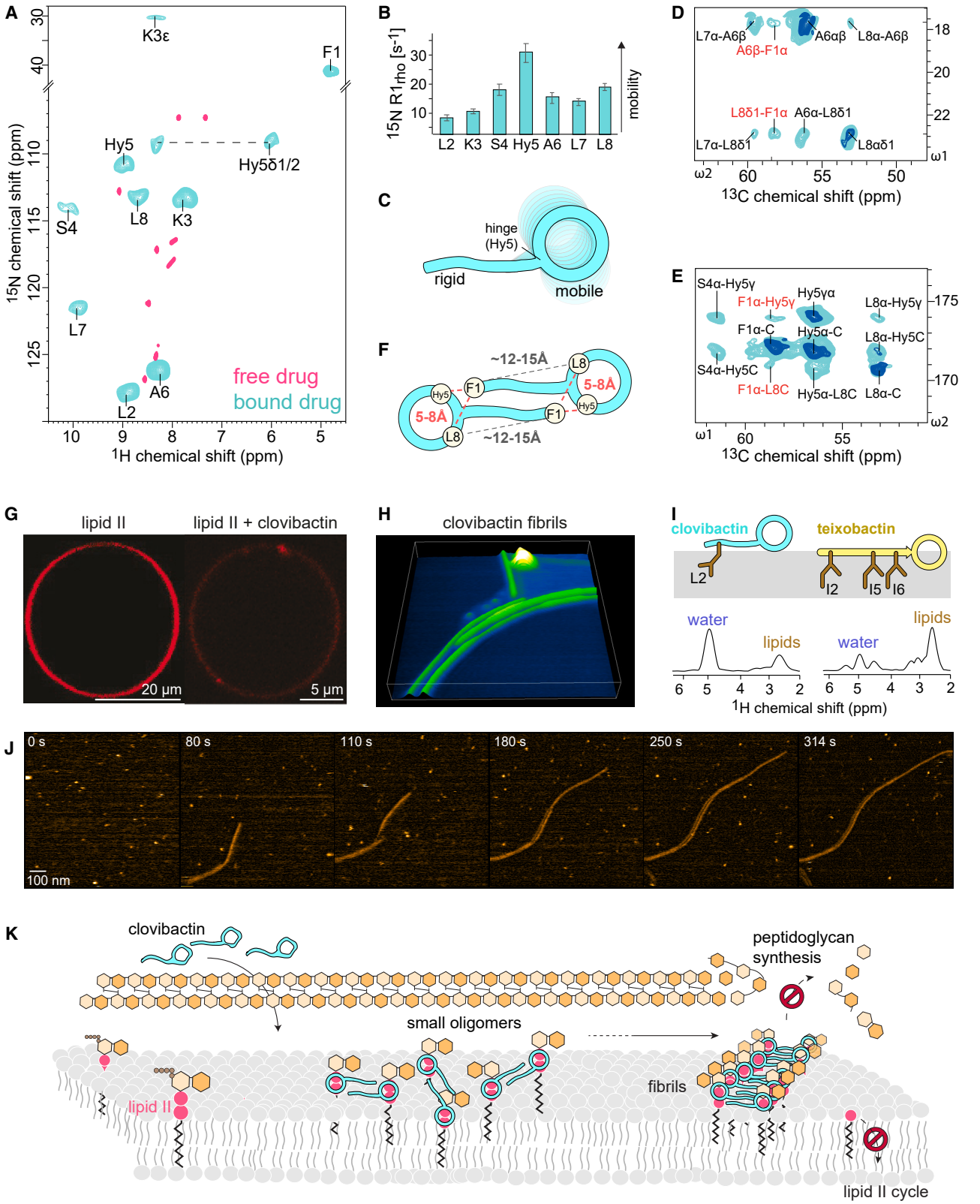

(legend on next page)

suggesting that the oligomerization upon target binding is important or even critical for the mode of action of clovibactin (Tables 1 and S1). The differential nature of the supramolecular structures of clovibactin and teixobactin[10] is also in line with mobility measurements in supported bilayers using single-molecule tracking. These measurements agree with higher concentration requirements for the formation of clovibactin fibrils and show that lipid II remains more mobile in assemblies formed by clovibactin (Figure S5I).

To better understand the nature of clovibactin-lipid II assemblies, we next looked at its membrane topology at high resolution using ssNMR experiments that qualitatively monitor the exposure of the antibiotic to water and phospholipid phases[31] (Figures 4I, S6A–S6C, and S6I). Previous ssNMR studies with teixobactin-lipid II fibrils showed a pronounced interaction with phospholipid tails, which agreed well with the deep insertion of teixobactin fibrils into the membrane observed by AFM and computational studies.[10] On the other hand, clovibactin-lipid II supra-structures interact only weakly with lipid tails, implying that supra-structures formed by clovibactin are much less deeply inserted and presumably lie on top of the membrane surface (Figure 4K). The differential membrane insertion can be rationalized by the presence of three long hydrophobic anchors (Ile2, Ile5, and Ile6) in the N terminus of teixobactin, whereas the much shorter N terminus of clovibactin features only a single hydrophobic anchor (Leu2). The shallow membrane insertion of the clovibactin supramolecular structure is in agreement with the high localization of the fibrils above the membrane surface observed by HS-AFM (1.2 ± 0.2 nm above the membrane surface for clovibactin fibrils, 0.8 ± 0.1 nm above the membrane surface for teixobactin fibrils) (Figure S5G) and also appears in line with the increased mobility of lipid II in clovibactin assemblies (Figure S5I). Given that samples of the clovibactin complex yielded similar ssNMR spectra after weeks of storage at 5°C, the supra-structures are apparently very stable on biological timescales.

The complex interface

Next, we sought to determine precisely how clovibactin targets lipid II, a complex lipid with a conserved pyrophosphate (PPi) group, a headgroup composed of the sugars MurNAc and GlcNAc and a pentapeptide whose variation confers resistance to antibiotics such as vancomycin[35] (Figure 5A).

First, we investigated how clovibactin targets the PPi group. Upon addition of clovibactin, 1D ^{31}P ssNMR data showed marked changes in the pyrophosphate signals of lipid II, suggesting a direct coordination (Figures 5B, S7A, and S7B). A similar signal shift was observed for lipid I (which lacks the GlcNAc sugar). Furthermore, the emergence of intense sidebands in 1D ^{31}P ssNMR data demonstrate that clovibactin also binds and immobilizes C_{55}PP (which lacks the sugars and the pentapeptide), in line with our biochemical binding analysis. Together, these data confirm that clovibactin is a multi-targeting antibiotic that blocks cell wall biosynthesis at several distinct, indispensable stages. To pinpoint the role of the lipid II PPi group in complex formation, we acquired a 2D ^{31}P^{1}H ssNMR spectrum, which monitors magnetization transfer from amino protons of clovibactin to PPi (Figure 5B). These data demonstrate that the backbone amino protons of clovibactin directly coordinate the PPi group with the amino protons of the depsi-cycle (Hyn5, Ala6, and Leu8). Furthermore, a weaker, but clearly discernible, signal shows that Ser4 of the N terminus-depsi-cycle junction is in proximity close to the PPi group. These direct contacts with the PPi group agree with the stark signal changes observed upon addition of the drug.

Subsequently, to resolve the role of the lipid II sugars and the pentapeptide for target binding, we prepared a complex of ^{13}C,^{15}N-clovibactin and ^{13}C,^{15}N-lipid II to measure a series of 2D PARISxy[32] ^{13}C^{13}C spectra at ultra-high magnetic fields of 950 and 1,200 MHz (Figures 5C and S7C). We observed a total of 12 unambiguous interfacial contacts between clovibactin and the lipid II sugars, 10 of which relate to Ala6 and Leu8 (Figure 5D), confirming that the depsi-cycle directly interacts with the lipid II headgroup. This is also in line with additional ambiguous interfacial contacts that we observed between Leu7 and the sugars. Together, our data show that all hydrophobic residues of the depsi-cycle are in direct proximity to the lipid II sugars. Almost all interfacial clovibactin-lipid II contacts are with MurNAc, the sugar that is covalently attached to the pyrophosphate, whereas we observed only three weak contacts

Figure 4. ssNMR structural model and oligomerization of the clovibactin/lipid II complex in membranes

(A) 2D NH ssNMR spectrum of lipid-II-bound clovibactin in membranes (cyan), superimposed on free clovibactin in aqueous solution (rose).

(B) Site-resolved ^{15}N R_{1rho} dynamics of lipid-II-bound teixobactin and clovibactin in 1,2-dioleoyl-*sn*-glycero-3-phosphocholine (DOPC) membranes. The error bars show the standard error of the fit.

(C) Illustration of the NMR-derived dynamics. Although clovibactin's N terminus is rigid, the depsi-cycle shows elevated dynamics.

(D and E) Zooms into a 2D CC spectrum of the complex show head-to-tail contacts in clovibactin, suggesting a dimeric (supramolecular) arrangement of clovibactin in the complex. Data acquired at 1,200 MHz magnetic field using 50 (cyan) and 250 ms (dark blue) CC mixing time.

(F) Schematic illustration of the head-to-tail contacts between Phe1-Hyn5 and Phe1-Leu8 seen in (D) and (E).

(G) Confocal microscopy of DOPC GUVs doped with Atto-labeled lipid II and treated with clovibactin show domain/cluster formation.

(H) 3D rendered HS-AFM image show the formation of clovibactin-lipid II supramolecular fibrils after 10 min of interactions.

(I) Lower panel: mobility-edited[31] ssNMR experiments show that clovibactin is much more water-accessible than teixobactin in the lipid II-bound state. Upper panel: ssNMR-derived topology and membrane insertion of clovibactin and teixobactin.

(J) Snapshots of a time-lapse HS-AFM video (Video S1) following the assembly of clovibactin-lipid II fibrils. Images were obtained on a supported lipid bilayer containing 4% (mol) lipid II in the presence of 5 μM clovibactin, added at 0 s. Image acquisition rate of 0.5 frames per second.

(K) Model of the mode of action of clovibactin. At the membrane surface, clovibactin binds lipid II and forms small oligomers that serve as nuclei for the formation of fibrils. Fibril formation enables a stable binding of lipid II and other cell wall precursors, blocking cell wall biosynthesis.

See also Figures S4, S5, and S6.

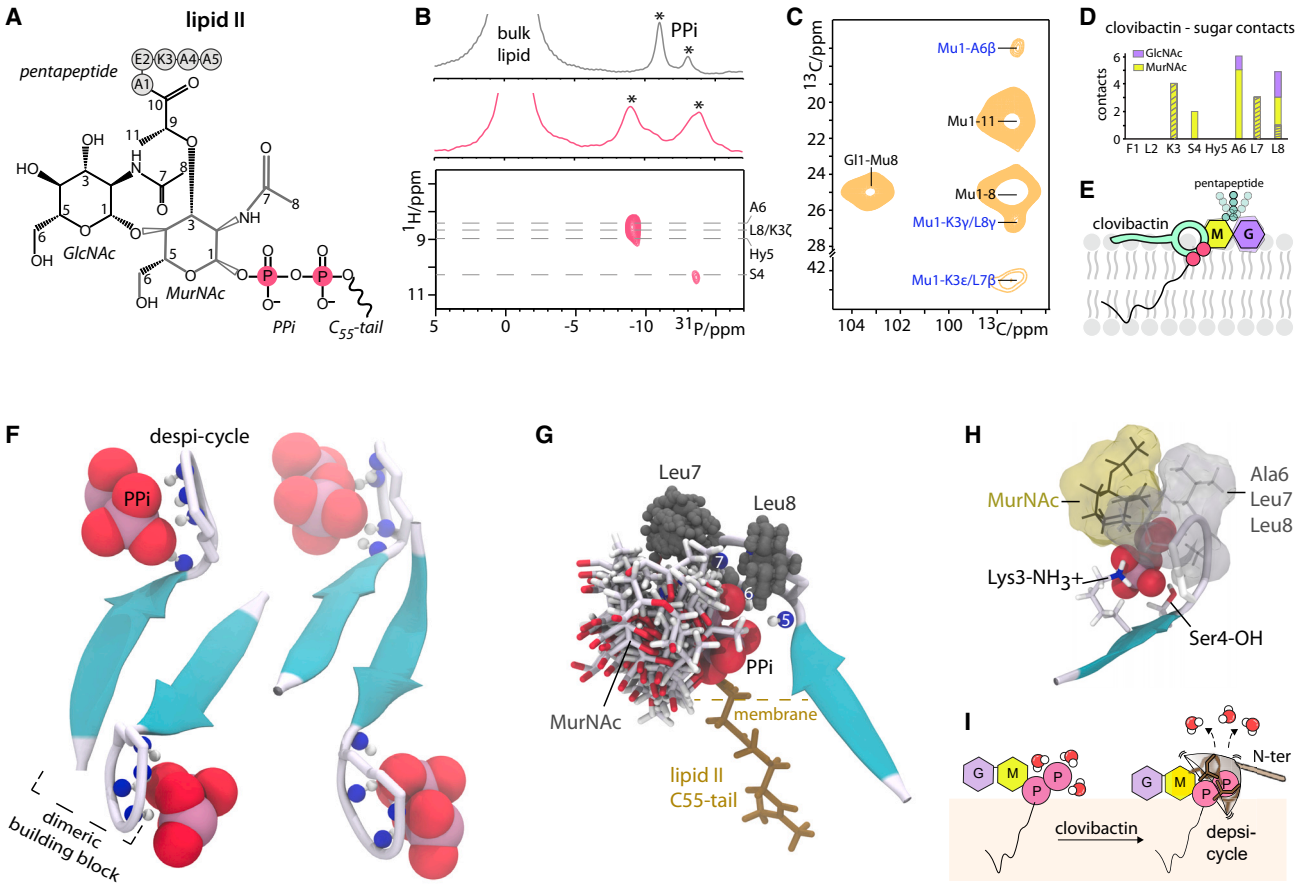

Figure 5. The interface and supramolecular structure

(A) Chemical structure of lipid II.

(B) 1D ^{31}P ssNMR data in liposomes show marked changes of the lipid II PPi signals upon addition of clovibactin. 2D ^{1}H^{31}P ssNMR spectrum establishes direct interactions between the backbone of the depsi-cycle and PPi.

(C) 2D CC ssNMR data of the ^{13}C,^{15}N-clovibactin-^{13}C,^{15}N-lipid II complex in liposomes show interfacial contacts with the MurNAc sugar and the hydrophobic side chains of the depsi-cycle. Interfacial clovibactin-lipid II contacts in blue. Data acquired at 950 MHz using 300 ms CC mixing time.

(D) Sum of interfacial contacts of clovibactin with the sugars of lipid II. Shaded bars show ambiguous contacts of MurNAc with either K3 or L7.

(E) Illustration of the interface: PPi and MurNAc are in direct proximity, GlcNAc is distal, the pentapeptide is flexible and not involved in the interface.

(F) ssNMR-derived structural model of the clovibactin-lipid II complex.

(G) Calculated interfaces of ssNMR structural models superimpose well and show that the hydrophobic depsi-cycle side chains (Ala6, Leu7, and Leu8) wrap like a glove around lipid II PPi group, interacting with the hydrophobic side of MurNAc.

(H) The cationic K3 and the polar S4 side chains favorably interact with the lipid II PPi group.

(I) Hydrophobic residues of clovibactin embrace the PPi group like a glove, which appears entropically favorable by the release of boundary water.

See also Figures S7 and S8.

with the GlcNAc sugar. This means that MurNAc is directly present at the interface with clovibactin, whereas the GlcNAc sugar is distal to this interface.

Strikingly, most residues of the lipid II pentapeptide were not observable in dipolar-based 2D CC spectra, in which we could only detect the first two residues (Ala*1 and γGlu*2). Because only rigid residues are observable in dipolar ssNMR spectra, our data strongly suggest that the pentapeptide is mobile and not part of the complex interface. This was confirmed with a complimentary scalar spectrum,[36] which gives a read-out on the mobile residues, in which we exclusively detected the last four residues (γGlu*2, Lys*3, Ala*4, and Ala*5) of the pentapeptide (Figures 5E and S7D).

Structural model of the complex

We next calculated a structural model of the complex using HADDOCK.[37] Although the dimeric (2 × 2) clovibactin is likely the minimal binding arrangement to stably bind lipid II, we calculated a (4 × 4) arrangement to get a better idea about the supramolecular structure. The structure calculations were based on intermolecular clovibactin-clovibactin distance restraints and interfacial clovibactin-lipid II distance restraints. Hydrogen bonding restraints were applied among and between the dimeric units (Figure S7J).

The obtained structures superimposed well (2.50 ± 0.85 Å average backbone root-mean-square deviation [RMSD] for clovibactin in the complex) (Figures 5F and S7E–S7G) and show

antiparallel dimeric units of clovibactin that could elongate to fiber-like supramolecular structures, in agreement with supramolecular structures observed by HS-AFM. A secondary structure analysis[38] shows about 60%–70% β strand propensity for clovibactin's short N terminus, an unusual molecular conformation that could foster oligomerization and fibril formation (Figure S6H). Enabled by the sequence of alternating D- and L-amino acids, hydrophobic (Leu2), and hydrophilic (Lys3 and Ser4) side chains are divided below and above the sheet-like arrangement, positioned to face lipid and water phases, respectively (Figure S6I).

The clovibactin-lipid II interface is well defined by several unambiguous distance restraints (1.47 ± 0.40 Å interfacial RMSD defined by residues Ala6, Leu7, and Leu8 of clovibactin, PPi, and MurNAc of lipid II) and shows that the backbone amino protons of the depsi-cycle directly coordinate the PPi group of lipid II. Strikingly, the hydrophobic residues of the despi-cycle (Ala6, Leu7, and Leu8) neatly wrap around the PPi moiety, reminiscent of a hydrophobic glove structure, in agreement with ssNMR distance measurements (Figure 5G). In this configuration, the hydrophobic depsi-cycle side chains of clovibactin do not form specific interactions with the sugars. Instead, they form a plastic, adjustable interface with the hydrophobic side of the MurNAc sugar, in agreement with unambiguous contacts between Leu8δ1-MurNAcC3, Ala6Cβ-MurNAcC11, or ambiguous contacts between Leu7Cβ-MurNAcC3 that are all within the hydrophobic patch of MurNAc. The lack of specific interactions with the MurNAc sugar also matches well with the increased dynamics of clovibactin's depsi-cycle in the complex observed by ssNMR relaxation data, and the relatively weak interfacial clovibactin-sugar contacts observed in 2D CC ssNMR spectra. Residue 5 (3-hydroxyasparagine) that attaches the depsi-cycle to the linear N terminus shows by far the strongest dynamics and hence acts as a sort of hinge that uncouples the dynamics of the PPi-binding depsi-cycle from the N-terminal oligomerization domain (Figures 4B and 4C). The lack of specific interactions between clovibactin and the sugars is also buttressed by phosphorous ssNMR dynamics studies (Figures S8A and S8B) that show that the lipid II PPi group is markedly more mobile in the clovibactin complex than in the teixobactin complex, in the latter of which the unusual enduracididine residue specifically interacts with the sugars.[10] Together, these data clearly agree with differential lipid II binding modes for clovibactin and teixobactin (Figure S8C).

The structures consistently show favorable closer-distance interactions between the anionic lipid II PPi group and the cationic (Lys3) and the polar (Ser4) side chains of the N terminus (Figure 5H). This agrees with clear interfacial clovibactin-lipid II ssNMR distance restraints Ser4Cβ-MurNAcC1 and Ser4Cβ-MurNAcC3 that show that Ser4-hydroxyl group is in proximity of the lipid II headgroup, and it matches well with the high rigidity of the Lys3 side chain that is observable in dipolar 2D NH spectra (Figures 4A and S4). 2D NH spectra also show that the protons of the cationic N-terminal amino-group of Phe1 are in fast exchange with water, which implies that they are not bound in a tight interaction.

The absence of specific interactions with the hydrophobic depsi-cycle side chains (Ala6, Leu7, and Leu8) is one of the reasons why clovibactin is able to efficiently (K_d for lipid II = 0.086 ± 0.007 μM) bind a broad spectrum of cell wall precursors with a PPi group (C_{55}PP, lipid I, and lipid II) (Figures 3E, 3F, and S9). This conclusion is supported by isothermal titration calorimetry (ITC) measurements that compare the affinity of clovibactin and teixobactin to different precursors showing that clovibactin's affinity is less affected by the presence of the sugars, explaining why clovibactin binds C_{55}PP with significantly higher affinity than teixobactin. The lack of specific interactions between clovibactin and the sugars is likely compensated by favorable entropic contributions of the hydrophobic cage, which remains flexible but strips off boundary water molecules that coordinate the PPi group (Figure 5I). Critically, we did not observe binding of clovibactin to soluble PPi (Na-pyrophosphate) in ITC experiments (Figure S9), demonstrating that clovibactin selectively binds lipid-anchored pyrophosphate groups. This suggests that settling on the membrane surface and the formation of stable supramolecular structures contribute to the effective binding of precursors.

DISCUSSION

Traditional screening platforms have failed to introduce new antibiotics in the last decades, in part due to overmining of *Actinomycetes*, the traditional source of antibiotics. Novel antibiotics are likely to be discovered by accessing silent operons, uncovering compounds masked by abundantly produced antimicrobials, and by growing previously uncultured bacteria.[4,5]

Clovibactin was isolated from an uncultured soil Gram-negative β-proteobacterium *E. terrae ssp. carolina*. It is a cell-wall-acting antibiotic with an unusual structure and mode of action. The extract from the producing organism was active against *S. aureus* but isolating the major compound responsible for this activity led to kalimantacin, a known antibiotic.[15] Kalimantacin is produced by *Pseudomonas* and *Alcaligenes* and inhibits the FabI enoyl-acyl carrier protein reductase of the fatty acid biosynthesis. Kalimantacin is inactive against *B. subtilis* carrying a different biosynthetic enzyme, but the extract was active against *B. subtilis* as well. Upon further examination of the extract, we isolated clovibactin, which was a relatively low abundant compound relative to kalimantacin. In order to simplify the isolation of clovibactin, we inactivated the kalimantacin operon. Inactivating the biosynthesis of abundant compounds to help detect and isolate minor compounds from extracts of interesting producers should be generally applicable to antibiotic discovery. In a similar approach, we recently reported isolation of a novel prodrug antibiotic aminodeoxyguanosine from a silent operon of *Photorhabdus luminescens* by first fractionating and concentrating an extract and then screening.[39]

Clovibactin binds to the pyrophosphate moiety of multiple essential cell wall precursors C_{55}PP, lipid II, and lipid III_{WTA} from different cell wall biosynthetic pathways. Clovibactin binds to the PPi moiety of these precursors. In general, PPi seems as an unsuitable target for an antibiotic because it will be released from dead cells together with PPi-containing nucleoside phosphates, and it is commonly present in the environment. At the same time, pyrophosphate is both an essential and immutable moiety of cell wall lipid intermediates, unlike other portions of the molecules, such as the pentapeptide of lipid II or sugars

that can be modified in, e.g., mycobacteria[40] or mutated. Moreover, a D-Ala-D-Lac substitution in the lipid II pentapeptide is a common mechanism of resistance to vancomycin that binds to the terminal D-Ala-D-Ala motif. Binding to immutable PPi would explain the lack of detectable resistance to this compound. How clovibactin manages to bind PPi of the central peptidoglycan precursor lipid II tightly and selectively is a fascinating question that we address in this study by performing a detailed structural analysis.

From the external medium, clovibactin settles at the membrane surface where it binds cell wall precursors. The leucine side chain on the N terminus helps partition clovibactin into the membrane at the site of its targets. Backbone amino protons of clovibactin's depsi-cycle directly coordinate the PPi, whereas the hydrophobic depsi-cycle side chains (Ala6, Leu7, and Leu8) surround the PPi group similar to an adjustable glove, an unusual interaction that is presumably entropically favorable by replacing boundary water and which enables efficient binding to distinct, indispensable cell wall precursors. Attacking a highly polar target (PPi) with a hydrophobic warhead is a striking, counter-intuitive mode of action. Clovibactin does not noticeably bind to PPi in solution, whereas ssNMR data acquired in membranes show that this is the principle moiety that clovibactin engages in the lipid II target. Apparently, selective binding to the PPi moiety of lipid precursors is achieved by the formation of a supramolecular complex and subsequent oligomerization into a stable higher-order fibrillar assembly of interacting clovibactin molecules bound to the target. This is presumably enabled by an antiparallel arrangement of clovibactin molecules, in which the short N terminus acts as oligomerization domain. The comparable concentrations for antibacterial action and for the formation of clovibactin fibrils suggests that supra-structures are an important or even essential part of the killing mechanism. The unique presence of readily accessible PPi-carrying molecules on the outside of bacterial membranes enables the formation of this structure and accounts for the lack of clovibactin toxicity against mammalian cells. A surprising feature of clovibactin is its superior ability to cause cell lysis, which is mechanistically distinct from teixobactin and independent of the major autolysin AtlA of *S. aureus*. This agrees well with the differential cellular response and expression pattern of genes controlled by the WalRK TCS. WalRK is the only essential TCS in *S. aureus* and plays a major role in controlling cell wall metabolism, mainly by controlling the transcription of cell wall lytic enzymes. The formation of a stable supramolecular structure will have favorable consequences for the *in vivo* activity of this compound, concentrating it onto bacterial surfaces where it belongs and continuing to act long after the soluble compound has been cleared from the body. Clovibactin's action against the PPi of cell wall precursors, a simple immutable target, expands our understanding of antibiotics evolved to avoid resistance, and points the way to rationally designing compounds with a long clinically useful life.

Limitations of the study

Further studies will be needed to conclusively establish the arrangement of the clovibactin-lipid II suprastructure. Although the clovibactin-lipid II interface is well described by unambiguous ssNMR distance restraints, we cannot conclusively rule out alternative clovibactin-clovibactin arrangements in the suprastructure. Establishing the precise supramolecular arrangement will likely require novel ssNMR methods, including synthetic routes to selectively isotope-label clovibactin. Another limitation of the study is that, at this point, we did not identify a specific hydrolase or glucosaminidase responsible for the strong lytic effect induced by clovibactin.

STAR★METHODS

Detailed methods are provided in the online version of this paper and include the following:

- KEY RESOURCES TABLE
- RESOURCE AVAILABILITY
  - Lead contact
  - Materials availability
  - Data and code availability
- EXPERIMENTAL MODEL AND SUBJECT DETAILS
  - Bacterial strains
  - Cell Lines
  - Mice
- METHOD DETAILS
  - Isolation of strain producing clovibactin
  - Clovibactin Isolation Procedure
  - Clovibactin Mass Spectrometry
  - Clovibactin 1D and 2D solution NMR Experiments
  - Whole genome sequencing of P9846
  - Biosynthetic analysis of P9846 genome
  - Annotation of clovibactin biosynthetic gene cluster
  - Determination of MICs
  - Mammalian cytotoxicity
  - Minimum bactericidal concentration (MBC)
  - Time-kill curves
  - Macromolecular synthesis assay
  - Resistance studies
  - Single dose PK in mice
  - Neutropenic mouse thigh infection study
  - Producing ^{13}C -^{15}N labeled clovibactin
  - β-galactosidase reporter assays
  - Quantification of intracellular UDP-N-acetylmuramic acid-pentapeptide
  - Luciferase reporter antagonization assays
  - Bacterial cell wall integrity assay
  - MIC-type antagonization assays
  - Synthesis and purification of lipid intermediates
  - *In vitro* lipid II synthesis with isolated membranes
  - *In vitro* PGN synthesis reactions using purified proteins and substrates
  - Complex formation clovibactin
  - Lysis assay
  - Zymographic analysis
  - MinD delocalization studies
  - Fluorescence labeling and fluorescence microscopy
  - Transcriptomics
  - RNA-Seq data assessment and analysis
  - Normalization and differential gene expression

- Analysis of single molecule mobility in supported lipid bilayers
- Synthesis and purification of isotopically labelled Lipid II
- Solid-state NMR sample preparation
- Solid-state NMR spectroscopy
- Fluorescence Microscopy
- Isothermal Titration Calorimetry
- High Speed-Atomic Force Microscopy (HS-AFM) Imaging
- Permeabilization assay
- Structure Calculations
- Structure calculation protocol

● QUANTIFICATION AND STATISTICAL ANALYSIS

SUPPLEMENTAL INFORMATION

Supplemental information can be found online at https://doi.org/10.1016/j.cell.2023.07.038.

ACKNOWLEDGMENTS

This work was funded by the Netherlands Organisation for Scientific Research (NWO, grant numbers 723.014.003 and 711.018.001 to M.W. and 718.015.001 to A.M.J.J.B.). This project has received funding from the European Union's Horizon Europe grant and innovation programme under grant agreement no. 101045485 (to M.W.). Funding for T.S., K.C.L., F.G., S.D.B., T.H., K.N., U.K., and A.M.K. was provided by the Deutsche Forschungsgemeinschaft (DFG, German Research Foundation), project ID 398967434—TRR 261, and funding to T.S. and F.G. was provided by the German Center for Infection Research (DZIF). Funding was also provided by NIH grant AI136137 to L.L.L., NIH grant AI091224 to A.L.S., NIH grant P01AI118687 to A.L.S. and K.L., and NIH grant RO1AI170962 to K.L. NMR experiments at the 950 and 1,200 MHz instruments were supported by uNMR-NL, an NWO-Funded Roadmap NMR Facility (no. 184.032.207). Support by Instruct-ERIC (to M.L. and M.W.) is acknowledged. M.W. and M.L. acknowledge project INFRAIA-02-2020 PANACEA (H2020, contract no. 101008500). M.L. acknowledges the Fondazione CR Firenze for funding. This work has been supported BioExcel, grant numbers 675728 and 823830, funded by the Horizon 2020 program of the European Commission. The NRS strains were provided by the Network on Antimicrobial Resistance in *Staphylococcus aureus* (NARSA) for distribution by BEI Resources, NIAID, NIH. The authors also wish to acknowledge the help and expertise of the University of Maryland Core Genome Sequencing Facility, Micromyx LLC, Kalamazoo, MI, NeoSome Life Sciences, Billerica MA. The authors would like to thank the following scientists for their work on clovibactin at NovoBiotic Pharmaceuticals, LLC, Alysha Desrosiers, William Millett, Kelly Demeo, Ashley Zullo, and Cintia Felix. The plasmid pIJ12738 was a gift from the John Innes Centre. The authors further thank Dr. Andrei Gurinov (Utrecht University) for assistance during the DNP-ssNMR experiments and Marc Sylvester (University of Bonn) for the mass spectrometry support.

AUTHOR CONTRIBUTIONS

K.L., T.S., D.H., L.L.L., and M.W. initiated the study. R.S., A.J.P., M.G.N.D., A.N., R.K., M.B., M.L., and M.W. did NMR experiments. A.N. isolated clovibactin. K.C.L., T.H., A.M.K., and S.D.B. did mode of action studies. R.S. and F.G. did fluorescence microscopy. A.M.K. and U.K. did single-molecule mobility measurements in supported bilayers. S.M. and W.H.R. did HS-AFM studies. A.L.S. performed the fermentations, gene knockout work, and isolated the DNA for sequencing. C.A. performed susceptibility and cytotoxicity assays. C.J.S. sequenced and annotated the genome. R.S. and M.W. did calorimetric studies. Y.L. provided research agents. R.S., M.G.N.D., and E.B. prepared ssNMR samples and lipid II. F.L., B.J.A.V., R.V.H., A.M.J.J.B., and M.W. did structure calculations. All authors contributed to data analysis and writing of the manuscript.

DECLARATION OF INTERESTS

The following authors, A.J.P., C.A., A.N., A.L.S., L.L.L., D.H., and K.L., declare competing financial interests because they are employees and consultants of NovoBiotic Pharmaceuticals. A patent US 11,203,616 B2 was issued on 12/21/2021 and describes the use of clovibactin (Novo29) and as an antibiotic, as well as the pharmaceutical composition and antibiotic use of derivatives.

Received: October 10, 2022
Revised: June 1, 2023
Accepted: July 28, 2023
Published: August 22, 2023

REFERENCES

1. Homma, T., Nuxoll, A., Gandt, A.B., Ebner, P., Engels, I., Schneider, T., Götz, F., Lewis, K., and Conlon, B.P. (2016). Dual targeting of cell wall precursors by teixobactin leads to cell lysis. Antimicrob. Agents Chemother. *60*, 6510–6517. https://doi.org/10.1128/AAC.01050-16.
2. Mordoch, S.S., Granot, D., Lebendiker, M., and Schuldiner, S. (1999). Scanning cysteine accessibility of EmrE, an H+-coupled multidrug transporter from Escherichia coli, reveals a hydrophobic pathway for solutes. J. Biol. Chem. *274*, 19480–19486.
3. Miethke, M., Pieroni, M., Weber, T., Brönstrup, M., Hammann, P., Halby, L., Arimondo, P.B., Glaser, P., Aigle, B., Bode, H.B., et al. (2021). Towards the sustainable discovery and development of new antibiotics. Nat. Rev. Chem. *5*, 726–749. https://doi.org/10.1038/s41570-021-00313-1.
4. Cook, M.A., and Wright, G.D. (2022). The past, present, and future of antibiotics. Sci. Transl. Med. *14*, eabo7793. https://doi.org/10.1126/scitranslmed.abo7793.
5. Lewis, K. (2020). The science of antibiotic discovery. Cell *181*, 29–45. https://doi.org/10.1016/j.cell.2020.02.056.
6. Lewis, K. (2013). Platforms for antibiotic discovery. Nat. Rev. Drug Discov. *12*, 371–387. https://doi.org/10.1038/nrd3975.
7. Wilson, M.C., Mori, T., Rückert, C., Uria, A.R., Helf, M.J., Takada, K., Gernert, C., Steffens, U.A.E., Heycke, N., Schmitt, S., et al. (2014). An environmental bacterial taxon with a large and distinct metabolic repertoire. Nature *506*, 58–62. https://doi.org/10.1038/nature12959.
8. Nichols, D., Cahoon, N., Trakhtenberg, E.M., Pham, L., Mehta, A., Belanger, A., Kanigan, T., Lewis, K., and Epstein, S.S. (2010). Use of ichip for high-throughput in situ cultivation of "uncultivable" microbial species. Appl. Environ. Microbiol. *76*, 2445–2450. https://doi.org/10.1128/AEM.01754-09.
9. Ling, L.L., Schneider, T., Peoples, A.J., Spoering, A.L., Engels, I., Conlon, B.P., Mueller, A., Schäberle, T.F., Hughes, D.E., Epstein, S., et al. (2015). A new antibiotic kills pathogens without detectable resistance. Nature *517*, 455–459. https://doi.org/10.1038/nature14098.
10. Shukla, R., Lavore, F., Maity, S., Derks, M.G.N., Jones, C.R., Vermeulen, B.J.A., Melcrová, A., Morris, M.A., Becker, L.M., Wang, X., et al. (2022). Teixobactin kills bacteria by a two-pronged attack on the cell envelope. Nature *608*, 390–396. https://doi.org/10.1038/s41586-022-05019-y.
11. Gavrish, E., Sit, C.S., Cao, S., Kandror, O., Spoering, A., Peoples, A., Ling, L., Fetterman, A., Hughes, D., Bissell, A., et al. (2014). Lassomycin, a ribosomally synthesized cyclic peptide, kills *Mycobacterium tuberculosis* by targeting the ATP-dependent protease ClpC1P1P2. Chem. Biol. *21*, 509–518. https://doi.org/10.1016/j.chembiol.2014.01.014.
12. Quigley, J., Peoples, A., Sarybaeva, A., Hughes, D., Ghiglieri, M., Achorn, C., Desrosiers, A., Felix, C., Liang, L., Malveira, S., et al. (2020). Novel antimicrobials from uncultured bacteria acting against Mycobacterium tuberculosis. mBio *11*. e01516–e01520. https://doi.org/10.1128/mBio.01516-20.

13. Buerger, S., Spoering, A., Gavrish, E., Leslin, C., Ling, L., and Epstein, S.S. (2012). Microbial scout hypothesis, stochastic exit from dormancy, and the nature of slow growers. Appl. Environ. Microbiol. *78*, 3221–3228. https://doi.org/10.1128/AEM.07307-11.

14. Buerger, S., Spoering, A., Gavrish, E., Leslin, C., Ling, L., and Epstein, S.S. (2012). Microbial scout hypothesis and microbial discovery. Appl. Environ. Microbiol. *78*, 3229–3233. https://doi.org/10.1128/AEM.07308-11.

15. Fage, C.D., Lathouwers, T., Vanmeert, M., Gao, L.J., Vrancken, K., Lammens, E.M., Weir, A.N.M., Degroote, R., Cuppens, H., Kosol, S., et al. (2020). The kalimantacin polyketide antibiotics inhibit fatty acid biosynthesis in Staphylococcus aureus by targeting the enoyl-acyl carrier protein Binding Site of FabI. Angew. Chem. Int. Ed. Engl. *59*, 10549–10556. https://doi.org/10.1002/anie.201915407.

16. Mattheus, W., Gao, L.-J., Herdewijn, P., Landuyt, B., Verhaegen, J., Maschelein, J., Volckaert, G., and Lavigne, R. (2010). Isolation and purification of a new Kalimantacin/Batumin-related polyketide antibiotic and elucidation of its biosynthesis gene cluster. Chem. Biol. *17*, 149–159. https://doi.org/10.1016/j.chembiol.2010.01.014.

17. Fernández-Martínez, L.T., and Bibb, M.J. (2014). Use of the meganuclease I-SceI of Saccharomyces cerevisiae to select for gene deletions in actinomycetes. Sci. Rep. *4*, 7100. https://doi.org/10.1038/srep07100.

18. Hsu, S.-T.D., Breukink, E., Tischenko, E., Lutters, M.A.G., de Kruijff, B., Kaptein, R., Bonvin, A.M.J.J., and van Nuland, N.A.J. (2004). The nisin–lipid II complex reveals a pyrophosphate cage that provides a blueprint for novel antibiotics. Nat. Struct. Mol. Biol. *11*, 963–967. https://doi.org/10.1038/nsmb830.

19. Blin, K., Shaw, S., Steinke, K., Villebro, R., Ziemert, N., Lee, S.Y., Medema, M.H., and Weber, T. (2019). antiSMASH 5.0: updates to the secondary metabolite genome mining pipeline. Nucleic Acids Res. *47*, W81–W87. https://doi.org/10.1093/nar/gkz310.

20. Lebreton, F., Manson, A.L., Saavedra, J.T., Straub, T.J., Earl, A.M., and Gilmore, M.S. (2017). Tracing the enterococci from Paleozoic origins to the hospital. Cell *169*, 849–861.e13. https://doi.org/10.1016/j.cell.2017.04.027.

21. Strahl, H., and Hamoen, L.W. (2010). Membrane potential is important for bacterial cell division. Proc. Natl. Acad. Sci. USA *107*, 12281–12286. https://doi.org/10.1073/pnas.1005485107.

22. Silver, L.L. (2007). Multi-targeting by monotherapeutic antibacterials. Nat. Rev. Drug Discov. *6*, 41–55.

23. Harms, H., Klöckner, A., Schrör, J., Josten, M., Kehraus, S., Crüsemann, M., Hanke, W., Schneider, T., Schäberle, T.F., and König, G.M. (2018). Antimicrobial Dialkylresorcins from marine-derived microorganisms: insights into their mode of action and putative ecological relevance. Planta Med. *84*, 1363–1371. https://doi.org/10.1055/a-0653-7451.

24. Wirtz, D.A., Ludwig, K.C., Arts, M., Marx, C.E., Krannich, S., Barac, P., Kehraus, S., Josten, M., Henrichfreise, B., Müller, A., et al. (2021). Biosynthesis and mechanism of action of the cell wall targeting antibiotic hypeptin. Angew. Chem. Int. Ed. Engl. *60*, 13579–13586. https://doi.org/10.1002/anie.202102224.

25. Medeiros-Silva, J., Jekhmane, S., Paioni, A.L., Gawarecka, K., Baldus, M., Swiezewska, E., Breukink, E., and Weingarth, M. (2018). High-resolution NMR studies of antibiotics in cellular membranes. Nat. Commun. *9*, 3963. https://doi.org/10.1038/s41467-018-06314-x.

26. Hong, M. (2006). Solid-state NMR studies of the structure, dynamics, and assembly of β-sheet membrane peptides and α-helical membrane proteins with antibiotic activities. Acc. Chem. Res. *39*, 176–183. https://doi.org/10.1021/ar040037e.

27. Wang, Y., and Jardetzky, O. (2002). Probability-based protein secondary structure identification using combined NMR chemical-shift data. Protein Sci. *11*, 852–861. https://doi.org/10.1110/ps.3180102.

28. Lewandowski, J.R., Sass, H.J., Grzesiek, S., Blackledge, M., and Emsley, L. (2011). Site-specific measurement of slow motions in proteins. J. Am. Chem. Soc. *133*, 16762–16765. https://doi.org/10.1021/ja206815h.

29. Jekhmane, S., Medeiros-Silva, J., Li, J., Kümmerer, F., Müller-Hermes, C., Baldus, M., Roux, B., and Weingarth, M. (2019). Shifts in the selectivity filter dynamics cause modal gating in K+ channels. Nat. Commun. *10*, 123. https://doi.org/10.1038/s41467-018-07973-6.

30. Shukla, R., Medeiros-Silva, J., Parmar, A., Vermeulen, B.J.A., Das, S., Paioni, A.L., Jekhmane, S., Lorent, J., Bonvin, A.M.J.J., Baldus, M., et al. (2020). Mode of action of teixobactins in cellular membranes. Nat. Commun. *11*, 2848. https://doi.org/10.1038/s41467-020-16600-2.

31. Doherty, T., and Hong, M. (2009). 2D 1H–31P solid-state NMR studies of the dependence of inter-bilayer water dynamics on lipid headgroup structure and membrane peptides. J. Magn. Reson. *196*, 39–47. https://doi.org/10.1016/j.jmr.2008.10.001.

32. Weingarth, M., Bodenhausen, G., and Tekely, P. (2010). Broadband magnetization transfer using moderate radio-frequency fields for NMR with very high static fields and spinning speeds. Chem. Phys. Lett. *488*, 10–16. https://doi.org/10.1016/j.cplett.2010.01.072.

33. Kodera, N., Yamamoto, D., Ishikawa, R., and Ando, T. (2010). Video imaging of walking myosin V by high-speed atomic force microscopy. Nature *468*, 72–76. https://doi.org/10.1038/nature09450.

34. Maity, S., Ottelé, J., Santiago, G.M., Frederix, P.W.J.M., Kroon, P., Markovitch, O., Stuart, M.C.A., Marrink, S.J., Otto, S., and Roos, W.H. (2020). Caught in the act: mechanistic insight into supramolecular polymerization-driven self-replication from real-time visualization. J. Am. Chem. Soc. *142*, 13709–13717. https://doi.org/10.1021/jacs.0c02635.

35. Münch, D., and Sahl, H.-G. (2015). Structural variations of the cell wall precursor lipid II in Gram-positive bacteria — impact on binding and efficacy of antimicrobial peptides. Biochim. Biophys. Acta *1848*, 3062–3071. https://doi.org/10.1016/j.bbamem.2015.04.014.

36. Baldus, M., and Meier, B.H. (1996). Total correlation spectroscopy in the solid state. The use of scalar couplings to determine the through-bond connectivity. J. Magn. Reson. A *121*, 65–69. https://doi.org/10.1006/jmra.1996.0137.

37. van Zundert, G.C.P., Rodrigues, J.P.G.L.M., Trellet, M., Schmitz, C., Kastritis, P.L., Karaca, E., Melquiond, A.S.J., van Dijk, M., de Vries, S.J., and Bonvin, A.M.J.J. (2016). The HADDOCK2.2 web server: user-friendly integrative modeling of biomolecular complexes. J. Mol. Biol. *428*, 720–725. https://doi.org/10.1016/j.jmb.2015.09.014.

38. Heinig, M., and Frishman, D. (2004). Stride: a web server for secondary structure assignment from known atomic coordinates of proteins. Nucleic Acids Res. *32*, W500–W502. https://doi.org/10.1093/nar/gkh429.

39. Shahsavari, N., Wang, B., Imai, Y., Mori, M., Son, S., Liang, L., Böhringer, N., Manuse, S., Gates, M.F., Morrissette, M., et al. (2022). A silent operon of *Photorhabdus luminescens* encodes a prodrug mimic of GTP. mBio *13*, e0070022. https://doi.org/10.1128/mbio.00700-22.

40. Mahapatra, S., Scherman, H., Brennan, P.J., and Crick, D.C. (2005). N glycolylation of the nucleotide precursors of peptidoglycan biosynthesis of Mycobacterium spp. is altered by drug treatment. J. Bacteriol. *187*, 2341–2347. https://doi.org/10.1128/JB.187.7.2341-2347.2005.

41. Sahl, H.G., and Brandis, H. (1981). Production, purification and chemical properties of an antistaphylococcal agent produced by Staphylococcus epidermidis. J. Gen. Microbiol. *127*, 377–384. https://doi.org/10.1099/00221287-127-2-377.

42. Mallozzi, M., Bozue, J., Giorno, R., Moody, K.-S., Slack, A., Cote, C., Qiu, D., Wang, R., McKenney, P., Lai, E.-M., et al. (2008). Characterization of aBacillus anthracisspore coat-surface protein that influences coat-surface morphology. FEMS Microbiol. Lett. *289*, 110–117. https://doi.org/10.1111/j.1574-6968.2008.01380.x.

43. Kunst, F., Ogasawara, N., Moszer, I., Albertini, A.M., Alloni, G., Azevedo, V., Bertero, M.G., Bessières, P., Bolotin, A., Borchert, S., et al. (1997). The complete genome sequence of the Gram-positive bacterium Bacillus subtilis. Nature *390*, 249–256. https://doi.org/10.1038/36786.

44. Mohan, A., Padiadpu, J., Baloni, P., and Chandra, N. (2015). Complete genome sequences of a Mycobacterium smegmatis laboratory strain

(MC2155) and isoniazid-resistant (4XR1/R2) mutant strains. Genome Announc. *3*. e01520–e01514. https://doi.org/10.1128/genomeA.01520-14.

45. Larsen, M.H., Biermann, K., Chen, B., Hsu, T., Sambandamurthy, V.K., Lackner, A.A., Aye, P.P., Didier, P., Huang, D., Shao, L., et al. (2009). Efficacy and safety of live attenuated persistent and rapidly cleared Mycobacterium tuberculosis vaccine candidates in non-human primates. Vaccine *27*, 4709–4717. https://doi.org/10.1016/j.vaccine.2009.05.050.
46. Ling, L.L., Xian, J., Ali, S., Geng, B., Fan, J., Mills, D.M., Arvanites, A.C., Orgueira, H., Ashwell, M.A., Carmel, G., et al. (2004). Identification and characterization of inhibitors of bacterial enoyl-acyl carrier protein reductase. Antimicrob. Agents Chemother *48*, 1541–1547. https://doi.org/10.1128/AAC.48.5.1541-1547.2004.
47. Arthur, M., Molinas, C., Depardieu, F., and Courvalin, P. (1993). Characterization of Tn1546, a Tn3-related transposon conferring glycopeptide resistance by synthesis of depsipeptide peptidoglycan precursors in Enterococcus faecium BM4147. J. Bacteriol. *175*, 117–127. https://doi.org/10.1128/jb.175.1.117-127.1993.
48. Cai, X., Lucini Paioni, A., Adler, A., Yao, R., Zhang, W., Beriashvili, D., Safeer, A., Gurinov, A., Rockenbauer, A., Song, Y., et al. (2021). Highly efficient trityl-nitroxide biradicals for biomolecular high-field dynamic nuclear polarization. Chemistry *27*, 12758–12762. https://doi.org/10.1002/chem.202102253.
49. Schneider, C.A., Rasband, W.S., and Eliceiri, K.W. (2012). NIH Image to ImageJ: 25 years of image analysis. Nat. Methods *9*, 671–675. https://doi.org/10.1038/nmeth.2089.
50. Cokol-Cakmak, M., and Cokol, M. (2019). Miniaturized checkerboard assays to measure antibiotic interactions. Methods Mol. Biol. *1939*, 3–9. https://doi.org/10.1007/978-1-4939-9089-4_1.
51. Kamigiri, K., Suzuki, Y., Shibazaki, M., Morioka, M., Suzuki, K.-I., Tokunaga, T., Setiawan, B., and Rantiatmodjo, R.M. (1996). Kalimantacins A, B and C, Novel antibiotics fromAlealigenes sp. YL-02632S. I. Taxonomy, fermentation, isolation and biological propertie. J. Antibiot. (Tokyo) *49*, 136–139. https://doi.org/10.7164/antibiotics.49.136.
52. Kohlrausch, U., and Höltje, J.V. (1991). Analysis of murein and murein precursors during antibiotic-induced lysis of Escherichia coli. J. Bacteriol. *173*, 3425–3431. https://doi.org/10.1128/jb.173.11.3425-3431.1991.
53. Schneider, T., Gries, K., Josten, M., Wiedemann, I., Pelzer, S., Labischinski, H., and Sahl, H.G. (2009). The lipopeptide antibiotic Friulimicin B inhibits cell wall biosynthesis through complex formation with bactoprenol phosphate. Antimicrob. Agents Chemother. *53*, 1610–1618. https://doi.org/10.1128/AAC.01040-08.
54. Tan, S., Ludwig, K.C., Müller, A., Schneider, T., and Nodwell, J.R. (2019). The lasso peptide Siamycin-I targets lipid II at the Gram-positive cell surface. ACS Chem. Biol. *14*, 966–974. https://doi.org/10.1021/acschembio.9b00157.
55. Umbreit, J.N., and Strominger, J.L. (1972). Isolation of the lipid intermediate in peptidoglycan biosynthesis from Escherichia coli. J. Bacteriol. *112*, 1306–1309. https://doi.org/10.1128/jb.112.3.1306-1309.1972.
56. Schneider, T., Kruse, T., Wimmer, R., Wiedemann, I., Sass, V., Pag, U., Jansen, A., Nielsen, A.K., Mygind, P.H., Raventós, D.S., et al. (2010). Plectasin, a fungal defensin, targets the bacterial cell wall precursor Lipid II. Science *328*, 1168–1172. https://doi.org/10.1126/science.1185723.
57. Rouser, G., Fkeischer, S., and Yamamoto, A. (1970). Two dimensional thin layer chromatographic separation of polar lipids and determination of phospholipids by phosphorus analysis of spots. Lipids *5*, 494–496. https://doi.org/10.1007/BF02531316.
58. Brötz, H., Bierbaum, G., Leopold, K., Reynolds, P.E., and Sahl, H.-G. (1998). The lantibiotic mersacidin inhibits peptidoglycan synthesis by targeting lipid II. Antimicrob. Agents Chemother. *42*, 154–160. https://doi.org/10.1128/AAC.42.1.154.
59. Rick, P.D., Hubbard, G.L., Kitaoka, M., Nagaki, H., Kinoshita, T., Dowd, S., Simplaceanu, V., and Ho, C. (1998). Characterization of the lipid-carrier involved in the synthesis of enterobacterial common antigen (ECA) and identification of a novel phosphoglyceride in a mutant of Salmonella typhimurium defective in ECA synthesis. Glycobiology *8*, 557–567. https://doi.org/10.1093/glycob/8.6.557.
60. Schneider, T., Senn, M.M., Berger-Bächi, B., Tossi, A., Sahl, H.G., and Wiedemann, I. (2004). In vitro assembly of a complete, pentaglycine interpeptide bridge containing cell wall precursor (lipid II-Gly5) of Staphylococcus aureus. Mol. Microbiol. *53*, 675–685. https://doi.org/10.1111/j.1365-2958.2004.04149.x.
61. Kim, D., Langmead, B., and Salzberg, S.L. (2015). HISAT: a fast spliced aligner with low memory requirements. Nat. Methods *12*, 357–360. https://doi.org/10.1038/nmeth.3317.
62. Okonechnikov, K., Conesa, A., and García-Alcalde, F. (2016). Qualimap 2: advanced multi-sample quality control for high-throughput sequencing data. Bioinformatics *32*, 292–294. https://doi.org/10.1093/bioinformatics/btv566.
63. Love, M.I., Huber, W., and Anders, S. (2014). Moderated estimation of fold change and dispersion for RNA-seq data with DESeq2. Genome Biol. *15*, 550. https://doi.org/10.1186/s13059-014-0550-8.
64. Zhang, Y., Parmigiani, G., and Johnson, W.E. (2020). ComBat-seq: batch effect adjustment for RNA-seq count data. NAR Genom. Bioinform. *2*, lqaa078. https://doi.org/10.1093/nargab/lqaa078.
65. Ruland, J.A., Krüger, A.M., Dörner, K., Bhatia, R., Wirths, S., Poetes, D., Kutay, U., Siebrasse, J.P., and Kubitscheck, U. (2021). Nuclear export of the pre-60S ribosomal subunit through single nuclear pores observed in real time. Nat. Commun. *12*, 6211. https://doi.org/10.1038/s41467-021-26323-7.
66. Schindelin, J., Arganda-Carreras, I., Frise, E., Kaynig, V., Longair, M., Pietzsch, T., Preibisch, S., Rueden, C., Saalfeld, S., Schmid, B., et al. (2012). Fiji: an open-source platform for biological-image analysis. Nat. Methods *9*, 676–682. https://doi.org/10.1038/nmeth.2019.
67. Tinevez, J.-Y., Perry, N., Schindelin, J., Hoopes, G.M., Reynolds, G.D., Laplantine, E., Bednarek, S.Y., Shorte, S.L., and Eliceiri, K.W. (2017). TrackMate: an open and extensible platform for single-particle tracking. Methods *115*, 80–90. https://doi.org/10.1016/j.ymeth.2016.09.016.
68. Breukink, E., van Heusden, H.E., Vollmerhaus, P.J., Swiezewska, E., Brunner, L., Walker, S., Heck, A.J.R., and de Kruijff, B. (2003). Lipid II is an intrinsic component of the pore induced by nisin in bacterial membranes. J. Biol. Chem. *278*, 19898–19903. https://doi.org/10.1074/jbc.M301463200.
69. Danilov, L.L., Druzhinina, T.N., Kalinchuk, N.A., Maltsev, S.D., and Shibaev, V.N. (1989). Polyprenyl phosphates: synthesis and structure-activity relationship for a biosynthetic system of Salmonella anatum O-specific polysaccharide. Chem. Phys. Lipids *51*, 191–203. https://doi.org/10.1016/0009-3084(89)90006-6.
70. Kohlrausch, U. (1991). One-step purification procedure for UDP-N-acetylmuramyl-peptide murein precursors from Bacillus cereus. FEMS Microbiol. Lett. *78*, 253–257. https://doi.org/10.1016/0378-1097(91)90166-8.
71. Weingarth, M., Bodenhausen, G., and Tekely, P. (2009). Low-power decoupling at high spinning frequencies in high static fields. J. Magn. Reson. *199*, 238–241. https://doi.org/10.1016/j.jmr.2009.04.015.
72. Weingarth, M., Demco, D.E., Bodenhausen, G., and Tekely, P. (2009). Improved magnetization transfer in solid-state NMR with fast magic angle spinning. Chem. Phys. Lett. *469*, 342–348. https://doi.org/10.1016/j.cplett.2008.12.084.
73. Etzkorn, M., Böckmann, A., Lange, A., and Baldus, M. (2004). Probing molecular interfaces using 2D magic-angle-spinning NMR on protein mixtures with different uniform labeling. J. Am. Chem. Soc. *126*, 14746–14751. https://doi.org/10.1021/ja0479181.
74. Medeiros-Silva, J., Mance, D., Daniëls, M., Jekhmane, S., Houben, K., Baldus, M., and Weingarth, M. (2016). H-detected solid-state NMR studies of water-inaccessible proteins in vitro and in situ. Angew. Chem. Int. Ed. Engl. *55*, 13606–13610. 1. https://doi.org/10.1002/anie.201606594.

STAR★METHODS

KEY RESOURCES TABLE

REAGENT or RESOURCE	SOURCE	IDENTIFIER
Bacterial and virus strains		
Staphylococcus simulans 22 (formerly *S. cohnii* 22)	Sahl and Brandis[41]	N/A
Staphylococcus aureus	NCTC	NCTC 8325-4
Staphylococcus aureus	ATCC	ATCC 29213
Staphylococcus aureus	ATCC	ATCC 700699
Staphylococcus aureus	ATCC	ATCC 33591
Staphylococcus aureus	NARSA (BEI Resources)	NRS71
Staphylococcus aureus	NARSA (BEI Resources)	NRS108
Staphylococcus aureus Mu50	NARSA (BEI Resources)	NRS1
Staphylococcus epidermidis	ATCC	ATCC 35982
Staphylococcus epidermidis	NARSA (BEI Resources)	NRS8
Staphylococcus haemolyticus	NARSA (BEI Resources)	NRS9
Staphylococcus haemolyticus	NARSA (BEI Resources)	NRS69
Enterococcus faecalis	ATCC	ATCC 51299
Streptococcus pneumoniae	ATCC	ATCC 10813
Streptococcus pyogenes	ATCC	ATCC 19615
Staphylococcus warneri	NARSA (BEI Resources)	NRS138
Escherichia coli K12 MG1655	ATCC	ATCC 700926
Pseudomonas aeruginosa PAO-1	ATCC	ATCC 47085
Bacillus anthracis Sterne	Mallozzi et al.[42] PMID: 19054101	*Bacillus anthracis* Sterne
Bacillus subtilis trpC2 1A1	Kunst et al.[43] PMID: 9384377.	168
Mycobacterium smegmatis MC^2 155	Mohan et al.[44]	MC^2 155
M. tuberculosis ΔlysA ΔpanCD	Larsen et al.[45]	MC^2 6020
Escherichia coli AB1157 (EGSC); asmB1 delta-tolC::kan	Ling et al.[46] PMID: 15105103; PMCID: PMC400533.	WO153
Enterococcus faecium BM4147	Arthur et al.[47] PMID: 8380148; PMCID: PMC196104.	BM4147
Eleftheria terrae ssp. carolina	This paper	P9846
Eleftheria terrae ssp. carolina Δbat1	This paper	P9846m01
Biological samples		
Laurus nobilis	Local supermarket	N/A
Chemicals, peptides, and recombinant proteins		
SNAPol-1	Cai et al.[48]	N/A
[U-^{13}C]-D-glucose	Merck	Cat#389374; CAS: 110187-42-3
[^{15}N]-NH_4Cl	Cortecnet	Cat#CN80P10; CAS: 39466-62-1
$DiSC_2(5)$	Merck	Cat#173754; CAS: 514-73-8
UDP-GlcNAc	Biosynth	Cat#MU07955; CAS: 91183-98-1
SYTOX™ green	Thermofisher	Cat#S7020
glucosamine hydrochloride, D-[6-^{3}H(N)]	Perkin Elmer	NET190A250uc
leucine, L-[3,4,5-^{3}H(N)]	Perkin Elmer	NET460250UC
uridine, [5-^{3}H]	Perkin Elmer	NET174250UC
thymidine, [methyl-^{3}H]	Perkin Elmer	NET027X250UC
D-glucose (U-^{13}C6, 99%)	Cambridge Isotope Laboratories	CLM-1396-10
Celtone base powder (^{15}N, 98%+)	Cambridge Isotope Laboratories	CGM-1030P-N-1
Celtone base powder (^{13}C, 98%+)	Cambridge Isotope Laboratories	CGM-1030P-C-1

(*Continued on next page*)

Continued

REAGENT or RESOURCE	SOURCE	IDENTIFIER
Celtone base powder (^{13}C, 98%+; ^{15}N, 98%+)	Cambridge Isotope Laboratories	CGM-1030P-CN-1
L-PROLINE (^{15}N, 98%)	Cambridge Isotope Laboratories	NLM-835-0.5
L-PROLINE (1-^{13}C, 99%)	Cambridge Isotope Laboratories	CLM-510-0.25
L-PROLINE (^{13}C5, 99%; ^{15}N, 99%)	Cambridge Isotope Laboratories	CNLM-436-H-0.5
Critical commercial assays		
CellTiter 96® AQueous One Solution Cell Proliferation Assay	VWR	G3580
Deposited data		
Raw and analyzed data	This paper	GEO: GSE228489
NMR assignments	This paper	BMRB: 52013, 51629, and 51630
Experimental solid-state NMR raw data	This paper	Zenodo (https://doi.org/10.5281/zenodo.7075976)
Experimental models: Cell lines		
NIH/3T3	ATCC	CRL-1658
HepG2	ATCC	HB-8065
Oligonucleotides		
Primer: bat1kofrag1F agactaGGATCC gacgggccttacgcagg	This paper	N/A
Primer: bat1kofrag1R agactGGTACCact ccacagcagtgttgaaggt	This paper	N/A
Primer: bat1kofrag2F: agactaGGATCC ctgcgggtggaccccgt	This paper	N/A
Primer: bat1kofrag2R acagtaTCTAGAg cgcacactccctactcggtc	This paper	N/A
Primer: Bat1downstream gcgctggccctcggaaag	This paper	N/A
Primer: Bat2upstream gcgccgcttggacacttat	This paper	N/A
Recombinant DNA		
Suicide vector backbone for pBat1ko	Fernández-Martínez and Bibb, 2014	pIJ12738
Plasmid: for the interruption of bat1: pBat1ko	This paper	pBat1ko
Software and algorithms		
AntiSMASH 5.1.1	https://academic.oup.com/nar/article/47/W1/W81/5481154 (https://doi.org/10.1093/nar/gkz310)	https://antismash.secondarymetabolites.org/#!/start
Igor Pro 6	Kodera et al.[33]	N/A
ImageJ	Schneider et al.[49]	https://imagej.nih.gov/ij/
HADDOCKv2.4	van Zundert et al.[37]	https://wenmr.science.uu.nl/haddock2.4/
Other		
^{13}C,^{15}N High Performance OD2 Media solution for *E. coli*	Silantes	N/A
Cary Eclipse fluorescence spectrometer	Agilent	Cat#110601402
		FL0904M005

RESOURCE AVAILABILITY

Lead contact

Further information and requests for resources and reagents should be directed to and will be fulfilled by the lead contact, Markus Weingarth (m.h.weingarth@uu.nl).

Materials availability

Clovibactin, or its producing strain, will be made available to researchers under an MTA agreement.

Data and code availability

- The NMR assignments of unbound clovibactin and the clovibactin – lipid II complex have been deposited in the BMRB database (accession numbers BMRB: 52013, 51629, and 51630) and are publicly available as of the date of publication.
- Experimental solid-state NMR raw data have been deposited in an open repository (https://doi.org/10.5281/zenodo.7075976) and are publicly available as of the date of publication.
- All RNA-Seq Illumina read files as well as the batch-corrected counts have been deposited in NCBI's Gene Expression Omnibus and are accessible under accession number GEO: GSE228489 and are publicly available as of the date of publication.
- This paper does not report original code.
- Any additional information required to reanalyse the data reported in this paper is available from the lead contact upon request.

EXPERIMENTAL MODEL AND SUBJECT DETAILS

Bacterial strains

P9846 and P9846m01 were propagated on SMS agar (0.125 g casein, 0.1 g potato starch, 1 g casamino acids, 20 g bacto-agar in 1 L of water). Colonies from both strains were harvested from agar plates and stored in 15% glycerol at -80°C.

NRS strains were purchased from the Network on Antimicrobial Resistance in *Staphylococcus aureus* (NARSA) for distribution by BEI Resources, NIAID, NIH. ATCC strains were purchased from ATCC. *S. aureus* NCTC 8325-4, *B. subtilis* trpC2 A1A,[43] *M. smegmatis* MC^2 155,[45,44] *M. tuberculosis* MC^2 6020 were kindly provided by Kim Lewis, Northeastern University. *E. coli* WO153 and *E. faecium* BM4147[47] were kindly provided by T. Opperman, Microbiotix Pharmaceuticals. *B. anthracis* Sterne[42] was kindly provided by Adam Driks, Loyola University. The other bacterial strains in Table S1 were clinical isolates from the Micromyx repository. The culture medium employed for the majority of the strains was cation adjusted Mueller Hinton II. Exceptions are described below. Streptococci were grown in cation adjusted MHB II supplemented with 3% lysed horse blood. Haemophilus was grown in Haemophilus Test Media. *N. gonorrhoeae* was grown in a modified broth medium containing 15 g Oxoid Special Peptone, 1 g corn starch, 5 g NaCl, 4 g K_2HPO_4, and 1 g KH_2PO_4. It was autoclaved, centrifuged at 5,000 x g for 10 min, the supernatant was passed through a 0.45 μm filter, and IsoVitaleX supplement was added at 1% (v/v). Mycobacteria were grown in 7H9 broth and 7H10 agar. Upon receipt, bacterial isolates were streaked onto the recommended agar plates and incubated at the recommended optimal conditions for growth. Colonies were harvested from the plates, resuspended in recommended broth supplemented with 15% glycerol and stored frozen at -80°C.

S. aureus SA113 (ATCC 35556), the ΔatlA mutant, Mu50 (ATCC 700699), RN4220 (DSM 26309), and SG511 (DSM 6247) were grown aerobically at 37 °C, in cation-adjusted Mueller Hinton medium. *S. aureus* HG001 was grown in tryptic soy broth at 37 °C, aerobically. All *B. subtilis* 168 (DSM 23778) strains were grown in cation-adjusted Mueller Hinton medium at 30 °C, aerobically. *S. simulans* 22 (formerly *S. cohnii* 22),[41] was grown aerobically in TSB at 37 °C.

Cell Lines

The cell lines used were NIH/3T3 mouse NIH/Swiss embryonic fibroblast (ATCC CRL-1658), and Hep-G2 human liver hepatocellular carcinoma (ATCC HB-8065). NIH/3T3 was cultured in Dulbecco's Modified Eagle's Medium (DMEM) supplemented with 10% bovine calf serum (ATCC 30-2031) at 37°C and HepG2 was cultured in DMEM supplemented with 10% fetal bovine serum (ATCC 30-2021) at 37°C.

Mice

Six weeks old female CD-1 mice (Charles River Laboratories) were used for all animal experiments. All animal experiments were conducted according to protocols approved by the Institute of Animal Care and Usage Committee (IACUC) at NeoSome Life Sciences, LLC. Mice were randomly assigned to experimental groups.

METHOD DETAILS

Isolation of strain producing clovibactin

The isolate producing clovibactin, P9846, was isolated from a sandy soil collected in North Carolina using techniques previously described.[13,14] Briefly, 1 gram of heat-treated soil (dry heat at 65° C for 30 minutes) was mixed with 9 mL of sterile water, vortexed, and then diluted into molten SMS agar (0.125 g casein, 0.1 g potato starch, 1 g casamino acids, 20 g bacto-agar in 1 L of water). This mixture was then dispensed in 100 μL aliquots per well of a flat bottom 96-well plate. The 96-well plates were incubated for 16 weeks at room temperature in a humidified chamber and observations of growth were made over time. The isolate P9846 grew to a size detectable under a dissecting microscope (50X magnification) at week 12 of the incubation.

Isolates from long-term incubation experiments were sub-cultured from their original incubation plates to individual plates of SMSR4 (0.125 g casein, 0.1 g potato starch, 1.5 g casamino acids, 1 g glucose, 0.1 g yeast extract, 0.3 g proline, 1 g $MgCl_2$-6H2O, 0.4 g $CaCl_2$- $2H_2O$, 0.02 g K_2SO_4, 0.56 g TES free acid (2-[[1,3-dihydroxy-2-(hydroxymethyl) propan-2-yl]amino]ethanesulfonic acid) and 20 g bacto-agar in 1 L of water agar). Monocultures of isolates were grown in a seed medium (15 g glucose, 10 g malt extract, 10 g soluble starch, 2.5 g yeast extract, 5 g casamino acids, and 0.2 g $CaCl_2$-$2H_2O$ per 1 litre of deionized H_2O, pH 7.0) to promote biomass production. Grown cultures were diluted 1:20 into 4 different fermentation broths. After 11 days of agitation at 28°C, the fermentations were dried and resuspended in an equal volume of 100% DMSO. Then 5 μL of extracts were spotted onto a lawn of growing *S. aureus* NCTC8325-4 cells in Mueller Hinton agar (MHA) plates. After 20 hours of incubation at 37°C, visible clearing zones indicated antibacterial activity. The extract from P9846 produced a large clearing zone. Although it produced antibacterial activity under several fermentation media, the best activity (that is, largest clearing zone) was seen with R4 fermentation broth (10 g glucose, 1 g yeast extract, 0.1 g casamino acids, 3 g proline, 10 g $MgCl_2$-$6H_2O$, 4 g $CaCl_2$-$2H_2O$, 0.2 g K_2SO_4, 5.6 g TES free acid (2-[[1,3-dihydroxy-2-(hydroxymethyl) propan-2-yl]amino]ethanesulfonic acid) per 1 litre of deionized H_2O, pH adjusted to 7.0 using KOH).

Clovibactin Isolation Procedure

n-Butanol (0.5V) was added to fermentation broth. The mixture was shaken vigorously, then left over night at room temperature until 2 distinct phases developed. The butanol phase was dried to completeness on a Buchi rotary evaporator. The resulting residue was reconstituted in a solution of 25% acetonitrile in water with 0.1% trifluoroacetic acid (~240 mL). This concentrated extract was centrifuged, and the supernatant decanted to remove any undissolved material. The supernatant was divided into 6 equal portions (~40 mL each) and successively purified on a preconditioned C18 flash chromatography column (Biotage, Sfar C18 60g, gradient of 25% - 100% acetonitrile in water (w/0.1% TFA), 50 mL/min). The compound of interest (clovibactin) was found at an adequate level of purity in two fractions as verified by mass spectrometry. The fractions containing clovibactin were concentrated under reduced pressure and lyophilized to yield approximately 125 mg from 6 L of fermentation.

Clovibactin Mass Spectrometry

Clovibactin was obtained as a white amorphous powder and its molecular formula ($C_{43}H_{70}N_{10}O_{11}$) was determined by LC-MS (*m/z* of 903.5291 $[M+H]^+$, calculated 903.5298). This is consistent with ^1H and ^{13}C NMR data. Furthermore, ^{13}C and ^{15}N labeled clovibactin had an observed mass of 956.6472 $[M+H]^+$ (calculated 956.6460).

Clovibactin 1D and 2D solution NMR Experiments

About 10 mg of Clovibactin was dissolved in ~600 μL of DMSO-*d*6. The following NMR experiments were performed on this sample: ^1H, ^{13}C, ^1H-^1H COSY, ^1H-^1H NOESY, ^1H-^1H TOCSY, ^1H-^{13}C HSQC, ^1H-^{13}C HMBC, ^1H-^{15}N HSQC.

Whole genome sequencing of P9846

Isolated gDNA was sequenced on a multiplexed PacBio Sequel II SMRT Cell 8M (Pacific Biosciences) using Sequel II 2.0 chemistry at the University of Maryland Core Genome Sequencing Facility yielding 836,139 total reads for this sample with a mean read length of 11,416 bp. Reads were assembled with SMRT8.0.0_HGAP4 (N50 = 5,455,962). The completed genome for P9846 contained a single circular chromosome and 3 extrachromosomal contigs (5.5 Mb chromosome, 7.0 Mb total) with 69% GC content. Our data has been deposited on NCBI Genbank under the BioProject PRJNA882350, BioSample SAMN30932845 with Accession numbers CP106950-CP106953.

Biosynthetic analysis of P9846 genome

Assembled contigs were concatenated into a single nucleotide FASTA file and analyzed by AntiSMASH (https://antismash.secondarymetabolites.org/#!/start) version 5.1.1 using relaxed detection strictness and all extra features enabled. 10 putative biosynthetic gene clusters (BGCs) were identified on the chromosome, as well as 4 and 5 on two of the three extrachromosomal contigs for a total of 19 BGCs. Of these, two were found to have high similarity to known compounds in the Minimum Information about a Biosynthetic Gene cluster (MIBiG) database, the PKS compounds SGR-polycyclic tetramate macrolactam and malleilactone.

Annotation of clovibactin biosynthetic gene cluster

The BGC responsible for cyclic peptide clovibactin was identified in the extrachromosomal genetic material where the majority of the NRPS BGCs are located. Eight complete NRPS modules corresponding to the amino acids found in the compound were identified and predictions of adenylation domain specificity from AntiSMASH were checked against Non-Ribosomal Peptide Synthase Substrate Predictor (NRPSsp, http://www.nrpssp.com/). Presence of dual-function condensation domains were used to identify sites of epimerization. Dioxygenase function was assigned based on homology to *cucE* from cupriachelin biosynthesis (MIBiG BGC0000330). The annotated sequence for clovibactin has been deposited into the MIBiG repository under the accession number BGC0002755.

Determination of MICs

MIC values were determined using a broth microdilution method as recommended by the CLSI. The test medium for most species was cation-adjusted Mueller-Hinton broth (MHB). The same test medium was supplemented with 3% lysed horse blood (Cleveland Scientific, Bath, OH.) for growing Streptococci. *Haemophilus* Test Medium was used for *H. influenzae* (Teknova, Hollister, CA, or HTM; Remel; Lot No. 903401), Middlebrook 7H9 broth (Difco) was used for mycobacteria. For *N. gonorrhoeae*, a modified broth medium described by the ATCC was used. The medium contained 15 g Oxoid Special Peptone (Oxoid, Hampshire, UK; Lot No. 1280296), 1 g corn starch (Ward's Science; Rochester, NY; Lot No. AD-13344-14), 5 g NaCl (VWR, Radnor, PA; Lot No. 57897), 4 g K_2HPO_4 (Sigma, St. Louis, MO; Lot No. 052K0147), and 1 g KH_2PO_4 (Sigma; Lot No. SLBC1921V). After autoclaving, the medium was centrifuged at 5,000 x g for 10 min, the supernatant was passed through a 0.45 μm filter, and IsoVitaleX supplement (BD; Lot No. 6309687) was added at 1% (v/v). Two-dimensional checkerboards were set up according to standard protocol.[50]

All test media were supplemented with 0.002% polysorbate (Tween) 80 to prevent drug binding to plastic surfaces, and cell concentration was adjusted to approximately $5X10^5$ cells/mL. After 20 hours of incubation at 37°C (2 days for *M. smegmatis*, 7 days for *M. tuberculosis*), the MIC was defined as the lowest concentration of antibiotic with no visible growth.

Fetal bovine serum (ATCC) was added to MHB (1:10) to test the effect of serum for *S. aureus* NCTC 8325-4 and *S. aureus* ATCC 29213.

Experiments were performed with three biological replicates.

Mammalian cytotoxicity

The CellTiter 96® AQueous One Solution Cell Proliferation Assay (Promega) was used to determine the cytotoxicity of clovibactin on NIH 3T3 mouse embryonic fibroblast (ATCC CRL-1658, in Dulbecco's Modified Eagle's medium supplemented with 10% bovine calf serum), and HepG2 cells (ATCC HB-8065™, in Dulbecco's Modified Eagle's medium supplemented with 10% fetal bovine serum). Exponentially growing cells were seeded into a 96-well flat bottom plate and incubated at 37°C. After 24 hours, the medium was replaced with fresh medium containing test compounds (0.5 μL of a two-fold serial dilution in DMSO to 99.5 μL of media, tested up to 100 μg/mL clovibactin). After 72 hours of incubation at 37°C, reporter solution was added to the cells and after 2 hours, the OD_{490} was measured using a Spectramax Plus Spectrophotometer. Experiments were performed with three biological replicates.

Minimum bactericidal concentration (MBC)

Cells from the wells from an MIC microbroth plate for *S. aureus* NCTC8325-4 and *S. aureus* ATCC29213 that had been incubated for 20 hours at 37°C were pelleted. An aliquot of the initial inoculum for the MIC plate was similarly processed. The cells were resuspended in fresh media, plated onto MHA, and the colonies enumerated after incubating for 24 hours at 37°C. The MBC is defined as the first drug dilution which resulted in a 99.9% decrease from the initial bacterial titer of the starting inoculum. Experiments were performed with three biological replicates.

Time-kill curves

Macrobroth MIC was determined for *S. aureus* ATCC 29213 in MHB II supplemented with 0.002% polysorbate 80 as 1 mL culture in polystyrene culture tubes after 20 hours of incubation at 37°C with aeration at 225 rpm. The MIC was 16 μg/mL for chloramphenicol, 1 μg/mL for vancomycin and 2 μg/mL for clovibactin under these conditions. To conduct time dependent killing, exponentially growing *S. aureus* ATCC 29213 cells were challenged with antibiotics at 37°C with aeration at 225 rpm -chloramphenicol (5xMIC, 80 μg/mL), vancomycin (10xMIC, 10 μg/mL), clovibactin (1XMIC, 2 μg/mL) or clovibactin (5xMIC, 10 μg/mL) in culture tubes at 37°C and 225 rpm. At intervals, 100 μL aliquots were removed, and 100 μL of ten-fold serially diluted suspensions were plated on MHA plates. Colonies were counted after 20 hours of incubation at 37°C, and CFU/mL was calculated. For time-dependent killings of *S. aureus* SA113 and the corresponding Δ*atlA* mutant exponentially growing cultures were challenged with 2× MIC of each antibiotic. Aliquots were collected at defined time points and 30 μL of serially diluted suspensions in PBS (pH 7.4) were plated on MHA plates. Colony counts were determined after overnight incubation at 37°C. Experiments were performed with three biological replicates.

Macromolecular synthesis assay

S. aureus NCTC 8325-4 cells were cultured in minimal medium (0.02 M Hepes, 0.002 M $MgSO_4$, 0.0001 M $CaCl_2$, 0.4% succinic acid, 0.043 M NaCl, 0.5% $(NH_4)_2$ SO_4) supplemented with 5% Tryptic Soy Broth (TSB). Cells were pelleted and resuspended into fresh minimal medium supplemented with 5% TSB containing test compounds and radioactive precursors to a density of 10^8 cells/mL. The radioactive precursors were glucosamine hydrochloride, D-[6-3H(N)] (1 mCi/mL), leucine, L-[3,4,5-3H(N)] (1 mCi/mL), uridine, [5-3H] (1 mCi/mL), or thymidine, [methyl-3H] (0.25 mCi/mL) to measure cell wall, protein, RNA, and DNA synthesis, respectively. After 20 minutes of incubation at 37°C, aliquots were removed, added to ice cold 25% trichloroacetic acid (TCA), and filtered using Multiscreen Filter plates (Millipore Cat. MSDVN6B50). The filters were washed twice with ice cold 25% TCA, twice with ice cold water, dried and counted with scintillation fluid using Perkin Elmer MicroBeta TriLux Microplate Scintillation and Luminescence counter. Experiments were performed with two biological replicates.

Resistance studies

No spontaneous resistant mutants of *S. aureus* ATCC29213 were obtained when plating 1.2X10^{10} cells on agar media with 4xMIC clovibactin. No colonies grew up after 3 days of incubation at 37°C.

Single dose PK in mice

In a separate tolerance study, mice tolerated a single dose of clovibactin administered as an IV bolus at 10 mg/kg, 20 mg/kg or 40 mg/kg. Clovibactin was then tested in a PK study to evaluate the systemic exposure and blood residence time of the compound. CD-1 female mice (n=3 per timepoint) were administered a single dose of compound at 28 mg/kg IV bolus. Blood was drawn at different times and clovibactin plasma levels determined by LC-MSMS. PK parameters were determined using the software package Watson LIMS.

Neutropenic mouse thigh infection study

Clovibactin was evaluated in a neutropenic mouse thigh infection model. Female CD-1 mice (n=4 per group) received two doses of cyclophosphamide 4 days (150mg/kg), and 1 day (100 mg/kg) prior to infection. *S. aureus* ATCC 33591 (MRSA) was injected into the thighs. The infection controls demonstrated a bioload of 6.07 $\log_{10}$ CFUs/ gram of thigh at the time of treatment (2 hours). Clovibactin was delivered as two IV doses (2 and 4 hours post infection).

Producing ^{13}C -^{15}N labeled clovibactin

P9846 makes multiple antibacterial compounds. Under the typical fermentation conditions (R4 broth) clovibactin is made in sufficient quantities. However, under labelling conditions we found that a known antibiotic, kalimantacin,[51] was produced in large amounts and interfered with clovibactin purification. Using the whole genome sequence, we identified the BGC with 55% identity to the kalimantacin gene.[16] Production of kalimantacin was reduced below detectable levels by interrupting the bat genes and generating the strain P9846m01. The bat genes were interrupted using homologous recombination previously described.[17] Following procedures from Martinez et al. ~500 bp fragments from upstream and downstream of the P9846 bat1 gene were made by pcr (see 'key resources table' for the primers). Fragments were digested with XbaI or KpnI and BamHI (New England Biolabs) and cloned into plasmid pIJ12738 digested with XbaI and KpnI. This created a 4605 bp plasmid, pBat1ko. pBat1ko was transformed into mobilization strain ET12567. Using conjugation conditions, the pIJ12738 was transferred into P9846 and selected with 50 ug/ml apramycin on SMSR4 agar. The insertion in mutant, P9846m01 was confirmed using pcr with primers bat1downstream and bat1upstream (see 'key resources table' for the primers). Disruption was further confirmed by fermentation in R4 medium and subsequent loss of kalimantacin derived active zones against a lawn of *S. aureus* followed by a lack of detectable kalimantacin by LC-MS in the appropriate fraction.

To label clovibactin, P9846m01 was grown from a frozen stock on SMSR4 agar supplemented with 50 ug/ml apramycin for 48 hours at room temperature. Biomass was scraped into 20ml flask of Celtone-R4 broth (10 g D-glucose; Cambridge Isotope Laboratories (CLM) #CLM-1396-5, 1 g Celtone base powder; CLM #CGM-1030P-CN-1, 0.5 g L-proline; CLM #CNLM-436-H-0.5, 10 g MgCl2-6H2O, 4 g CaCl2- 2H2O, 0.2 g K2SO4, 5.6 g TES free acid (2-[[1,3-dihydroxy-2-(hydroxymethyl) propan-2-yl]amino]ethanesulfonic acid) per 1 liter of deionized H2O, pH 7 C). After 3 days of incubation with shaking at 28°C the culture was split between 2 flasks of 500ml Celtone-R4 broth. This culture was incubated with shaking at 28°C for 6 days. ^{13}C and ^{15}N labeled clovibactin was isolated in a similar manner as above, yielding 5.7 mg of ^{13}C^{15}N - labeled clovibactin from a 1 L fermentation.

β-galactosidase reporter assays

B. subtilis β-galactosidase reporter assays were performed as previously described.[23] In short, reporter strains were grown in MHB containing 5 μg/ml chloramphenicol at 30 °C to an OD_{600} of 0.5. Subsequently, cells were poured at 1x10^7 CFU/ml in MHA plates supplemented with 5 μg/ml chloramphenicol, 75 μg/ml (cell wall reporter), 125 μg/ml (DNA reporter), and 250 μg/ml (RNA and protein reporters) X-gal, respectively. After solidification of the plates, 6 μg of clovibactin and control antibiotics selectively inducing the promotors were spotted (6 μg vancomycin for cell wall, 0.3 μg ciprofloxacin for DNA, 6 μg rifampicin for RNA, 3 μg clindamycin for protein). Results were documented after incubation overnight at 30°C.

Quantification of intracellular UDP-N-acetylmuramic acid-pentapeptide

To analyze the cytoplasmic nucleotide pool we adapted the protocol of Kohlrausch and Höltje.[52] *S. aureus* SG511 was grown in 20 ml MHB at 37°C to an OD_{600} of 0.6 and incubated with 130 μg/ml chloramphenicol for 15 min. Clovibactin was added at 0.5×, 1×, 2.5×, and 5×MIC and incubated for another 30 min. Vancomycin (5× MIC) was used as positive control. Extraction and analysis of nucleotide-linked peptidoglycan precursors was performed as described previously.[53] Corresponding fractions were confirmed by mass spectrometry.

Luciferase reporter antagonization assays

B. subtilis luciferase reporter assays were conducted as previously described.[54,55] Briefly, luciferase reporters were grown in MHB containing 5 μg/ml chloramphenicol at 30°C to an OD_{600} of 0.5. Cells were added to 96-well white wall chimney plates containing serially diluted antibiotics. For antagonization assays, purified cell wall lipid intermediates (C_{55}PP, lipid I, lipid II, lipid III_{WTA}) and phospholipids (phosphatidylglycerol [PG], phosphatidylcholine [PC], cardiolipin [CL]) were added in 0.5 to 4-fold molar excess with

respect to clovibactin (0.5× MIC) and were pre-incubated for 10 min prior to addition of the reporter strain. Luminescence measurements were performed at 30 °C in a microplate reader Spark 10M (Tecan). At least three independent biological replicate experiments were conducted.

Bacterial cell wall integrity assay

Bacterial cell wall integrity assays were adapted from previous work (Schneider et al.[56]) *B. subtilis* 168 cultures were grown in MHB at 30 °C to an OD_{600} of 0.3. Subsequently, cells were treated with were treated with clovibactin, teixobactin, hypeptin and vancomycin (0.25x MIC each) and 32 μg/ml clindamycin, or DMSO for 30 min. Cells were immediately fixed in a 1 ml 1:3 (v:v) mixture of acetic acid and methanol and immobilized on thin 1% w/v agarose slides. Imagaing was performed by phase contrast microscopy on a Zeiss AxioObserver Z1 equipped with an HCP 120 C lamp, an αPlan-APOCHROMAT 100×/1.46 oil objective and an AxioCam MRm camera and further processed with Zen 2 (Zeiss) and analyzed and postprocessed using ImageJ v1.52p.[49] Semi-quantitative analysis of cell phenotypes was performed manually, and statistical significance was carried out with GraphPad Prism 9.0.0 using unpaired two-tailed Student's *t*-test and a 95% confidence interval.

MIC-type antagonization assays

Antagonization of the antibiotic activity of clovibactin by potential target molecules was performed by an MIC-based setup in microtiter plates. Clovibactin (8× MIC) was mixed with HPLC-purified antagonists (C_{55}PP, lipid I, lipid II, lipid III_{WTA} and DOPG) in 0.5 to 4-fold molar excess with respect to the antibiotic. *S. aureus* SG511 ($5x10^5$ CFU/ml) was added and samples were examined for visible bacterial growth after incubation at 37°C overnight. Experiments were performed with at least three biological replicates.

Synthesis and purification of lipid intermediates

Large scale synthesis and purification of the PGN precursors lipid I and lipid II were performed as previously described.[9] UDP-N-acetyl-muramic acid pentapeptide (UDP-MurNAc-pp) was purified according to the protocol elaborated by Kohlrausch and Höltje.[52] Undecaprenyl phosphate (C_{55}P) and undecaprenyl diphosphate (C_{55}PP) were purchased from Larodan Fine Chemicals AB (Malmö, Sweden). The phospholipids 1,2-dioleoyl-*sn*-glycero-3- phosphocholine (DOPC), 1,2-dioleoyl-*sn*-glycero-3-phosphoglycerol (DOPG) and 1′,3′-bis[1,2-distearoyl-*sn*-glycero-3-phospho]-glycerol (DOCL, cardiolipin) were purchased from Avanti Polar Lipids (Alabaster, AL, USA). The concentration of purified PGN and wall teichoic acid precursors was quantified on the basis of their phosphate content as described.[57]

In vitro lipid II synthesis with isolated membranes

In vitro lipid II synthesis was performed using membranes of *M. luteus* as previously described.[55,58] Briefly, synthesis was assayed by incubating membrane preparations (200 μg protein) with 5 nmol C_{55}P, 50 nmol UDP-MurNAc-pentapeptide, 50 nmol UDP-N-acetyl-glucosamine (UDP-GlcNAc) in 60 mM Tris-HCl, 5 mM $MgCl_2$, and 0.5 % Triton X-100, at pH 7.5 in a total volume of 50 μl at 30°C for 1 h. C_{55}P-containing products were extracted with an equal volume of *n*-butanol/pyridine acetate, pH 4.2 (2:1, v/v) and analyzed by thin layer chromatography (TLC) using chloroform/methanol/water/ammonia (88:48:10:1, v/v/v/v) as the solvent[59] and phosphomolybdic acid staining (Schneider et al.[60]). The quantitative analysis of lipids extracted to the butanol phase was carried out by phosphorimaging in a StormTM imaging system (GE Healthcare) or PMA staining and analysis performed using Image Quant TL. Clovibactin was added in molar ratios of 0.5 to 4 with regard to C_{55}P.

In vitro PGN synthesis reactions using purified proteins and substrates

To determine the enzymatic activity of MraY-His_6 the assay was carried out in a total volume of 50 μl containing 5 nmol C_{55}P, 25 nmol of UDP-MurNAc-pp in 100 mM Tris-HCl, 10 mM $MgCl_2$, at pH 7.5, and 0.6% Triton X-100. The reaction was initiated by the addition of 2 μg of MraY-His_6 and incubated for 1.5 hours at 30°C.

The *in vitro* MurG reaction was performed in a 30 μL reaction containing 2 nmol of purified lipid I and 25 nmol of UDP-N-acetyl glucosamine (UDP-GlcNAc) in 200 mM Tris-HCl, 5.7 mM $MgCl_2$, at pH 7.5, and 0.8% Triton X-100 with 2 μg of purified, recombinant MurG-His_6 enzyme. Reaction mixtures were incubated for 30 min at 30°C.

The PBP2 activity assay was performed in a 50 μL reaction containing 2 nmol of purified lipid II, in 20 mM MES, 2 mM $MgCl_2$, and 2 mM $CaCl_2$, at pH 5.5 with 2 μg of purified, recombinant PBP2-His_6 enzyme. Reaction mixtures were incubated for 2 h at 30 °C.

Dephosphorylation of C_{55}PP was determined using purified YbjG-His_6 enzyme (SA0415). A total of 20 nmol of C_{55}PP was incubated with 3 μg of YbjG-His_6 in 20 mM Tris-HCl, 150 mM NaCl, and 0.8% Triton X-100 at pH 7.5 in 50 μL for 30 min at 30°C.

In all *in vitro* assays, clovibactin was added in molar ratios from 0.5 to 2 (and to 4 for MraY and MurG) with respect to the respective substrate. C_{55}P-containing products were extracted, analyzed by TLC and quantified as described above. The quantitative analysis of lipids extracted to the *n*-butanol phase was carried out using ImageJ v1.53p software (National Institutes of Health).[49] Experiments were performed at least in triplicates.

Complex formation clovibactin

Binding of clovibactin to C_{55}PP, lipid I, lipid II, lipid III_{WTA} and DOPG was analyzed by incubating 2 nmol (lipid I, lipid II, lipid III_{WTA}) or 5 nmol (C_{55}PP and DOPG) with 8-fold molar excess of clovibactin in 50 mM Tris-HCl, at pH 7.5 for 30 min at room temperature.

Complex formation was analyzed by extracting unbound precursors from the reaction mixture followed by TLC analysis as described above. Experiments were performed with biological replicates.

Lysis assay

Analysis of lysis was conducted with MHB-grown exponential phase cells (OD_{600} of 0.5) of *S. aureus* SA113 and the AtlA-deficient mutant *S. aureus* SA113 Δ*atlA*, that were treated with clovibactin, teixobactin, and vancomycin at concentrations of 0.5×, 1×, 2×, and 5×MIC and optical density (OD_{600}) was measured after 24 hours. The final OD_{600} was expressed as the relative absorbance to initial values of each strain. Experiments were performed with three biological replicates. For qualitative analysis exponential phase cells were adjusted to an OD_{600} of 1 and treated with antibiotics at 2× MIC. After 24 hours, cell turbidity was photographed in microtiter plates.

Zymographic analysis

S. aureus SA113 was grown in 100 mL MHB until an OD_{600} of 0.5. The culture was then split into 10 mL aliquots. Each aliquot was treated with the respective antibiotic (5× MIC) for 30 min. The cells were harvested by centrifugation (4,500 × *g*, 15 min). Supernatants were concentrated to 200 μL using VivaSpin6 colums (Sartorius, MWCO 10,000 kDa, 4,000 × *g*), and then to 50 μL using VivaSpin500 column (Sartorius, MWCO 3,000 kDa, 12,000 × *g*) and were run in a 4-12% sodium dodecyl sulfate (SDS)-polyacrylamide gel containing pasteurized *S. aureus* RN4220 cells. To remove SDS, the gel was washed 6 times for 10 min with deionized water and incubated in freshly prepared renaturation buffer (50 mM Tris-HCl, pH 7.5, 10 mM $CaCl_2$, 10 mM $MgCl_2$, 0.1% v/v Triton X-100, pH 7.5) for 16 h at 37°C. To visualize clear bands, representing cell lysis, the gel was stained with 0.1% w/v methylene blue. The assay was repeated three times, with a representative experiment shown.

MinD delocalization studies

B. subtilis 1981 *erm spc minD*:*ermC amyE*::P_{xyl}-*gfp-minD*, a strain with a *gfp-minD* fusion under control of the P_{xyl} promotor (kindly provided by H. Strahl, Newcastle), was grown in MHB supplemented with 0.1 % w/v xylose and 50 μg/ml spectinomycin at 30 °C to an OD_{600} of 0.6. Imaging was carried out within 2, 5, and 30 min after addition of antibiotic at 2× and 10× MIC. The proton ionophore carbonyl cyanide *m*-chlorophenylhydrazone (CCCP, 100 μM) was used as positive control and imaging was carried out within 2 min. Samples were immobilized on microscope slides covered with 1 % w/v agarose. Fluorescence microscopy and analysis was performed using the same microscope and software as described for phase contrast microscopy.

Fluorescence labeling and fluorescence microscopy

Clovibactin was dissolved in anhydrous DMF (5 mg/ml) and BODIPY™ FL succimidyl ester (Invitrogen) was dissolved in DMSO (10 mg/ml). For labeling, 1 vol of BODIPY™ FL was added to 0.5 vols of DIPEA and 5 vols clovibactin solution and incubated at room temperature with gentle agitation. After 2 hours, ice-cold diethylether was added to the reaction mixture leading to precipitation of clovibactin. After centrifugation, the supernatant was carefully aspirated, and the pellet was dissolved in anhydrous DMF. Separation of labeled and non-labeled clovibactin was achieved by HPLC purification on a Poroshell 120 EC-C18, 2.7 μm, 3 × 150 mm column (Agilent), column temperature 50 °C, with a gradient of (A) 79.9% H_2O + 20% acetonitrile (MeCN) + 0.1% trifluoroacetic acid (TFA) and (B) 49.9% H_2O + 50% MeCN + 0.1% TFA: 0 min, %B = 0, 10 min, %B = 60, 34 min, %B = 80. Clovibactin-FL was collected and confirmed by LC-MS.

To study localization of clovibactin in *S. aureus*, cultures were grown in MHB at 37°C until an OD_{600} of 0.5 and were pre-incubated for 10 min with teixobactin (2× MIC). Cells were then washed four times with MHB prior to 10 min incubation with a 1:3 mixture of unlabeled and labeled clovibactin (2× MIC). To visualize cell membranes, nile red was added to a final concentration of 1 μg/ml. Subsequently, cells were washed four times in phosphate-buffered saline (PBS) and mounted on microscope slides covered with a thin film of 1% v/v agarose. At least $n \geq 30$ cells per replicate were used for calculations for each condition from three biologically independent experiments.

Images were acquired using Zeiss AxioObserver Z1 equipped with an HXP 120 C lamp, an αPlan-APOCHROMAT 100×/1.46 oil objective and an AxioCam MRm camera. Standard filter sets were used for BODIPY™ FL (450–490 nm excitation and 500–500 nm emission). Images were further processed with Zen 2 (Zeiss) and analyzed and postprocessed using ImageJ v1.52p[49] and GraphPad Prism version 9.0.0 for Windows.

Transcriptomics

S. aureus HG001 cells were grown overnight in TSB medium at 37 °C. The cultures were diluted to 2% in fresh TSB medium and incubated at 37 °C until they reached an OD_{600} 0.5. Cells were challenged with subinhibitory concentration of teixobactin and clovibactin (0.25x MIC) or left untreated and incubated for 1 h under the same conditions. The chosen concentration depends on the growth inhibition without evident lysis of the cells. Afterwards, 20 ml of cultures were harvested (8000 x *g*, 5 min, RT), the pellets were resuspended in 1 ml RNA protect buffer (New England Biolabs, Frankfurt am Main, Germany) and incubated for 5 min at RT. After removal of the buffer by centrifugation (8000 x *g*, 5 min, RT), the cells were lysed in 200 μl Tris-EDTA buffer containing 25 μg lysostaphin and incubated at 37 °C for 30 min. RNA was isolated using the Monarch total RNA miniprep kit (New England Biolabs)

following the manufacturer's instructions and stored at -80 °C. Quality and quantity of total RNA were determined by NanoDrop™ (Thermo Scientific, USA) and by agarose gel electrophoresis. The RNA extraction was performed with 3 biological replicates.

RNA-Seq data assessment and analysis

Sequencing statistics including the quality per base and adapter content assessment of the resulting transcriptome sequencing data were conducted with FastQC v0.11.8 (https://www.bioinformatics.babraham.ac.uk/projects/fastqc/). All reads mappings were performed against the strain *S. aureus* HG001 *(RefSeq ID: NZ_CP018205.1)*. The mappings of all samples were conducted with HISAT2 v2.1.0.[61] As parameters spliced alignment of reads was disabled and strand-specific information was set to reverse complemented (HISAT2 parameter –no-spliced-alignment and –rna-strandness "R"). The resulting mapping files in SAM format were converted to BAM format using SAMtools v1.9. Mapping statistics, including strand specificity estimation and percentage of mapped reads, were conducted with the RNA-Seq module of QualiMap2 v2.2.2-a.[62] Gene counts for all samples were computed with featureCounts v1.6.4, where the selected feature type was set to transcript records (featureCounts parameter -t transcript). A quality check for ribosomal rRNA was performed with a self-written script based on the absolute counts of annotated rRNAs. To assess variability of the replicates, a principal component analysis (PCA) was conducted with the DESeq2 package v1.28.1.[63]

Normalization and differential gene expression

For batch correction between the first batch of samples (teixobactin + untreated) and the second batch of samples (clovibactin + untreated) ComBat-seq[64] was applied to a slightly larger data set with the batch and group parameters set. For the computation of genes differentially expressed between the treated and the untreated samples, DESeq2 v1.20.0 was applied to the absolute gene counts as computed with featureCounts. For differences between the two treated samples and the untreated samples, genes with an adjusted p-value (FDR) < 0.05 and absolute $\log_2$ fold change (FC) > 1 were reported as differentially expressed. All RNA-Seq Illumina read files as well as the batch-corrected counts have been deposited in NCBI's Gene Expression Omnibus and are accessible under accession number GSE228489.

Analysis of single molecule mobility in supported lipid bilayers

Lipid II-Atto565 was obtained by labeling of lipid II with a 10-fold excess of Atto565-NHS ester (Sigma-Aldrich, Taufkirchen, Germany) in presence of 0.6 vol% diisopropylethylamine (Sigma-Aldrich, Taufkirchen, Germany). The reaction was carried out in water-free chloroform for 2 hours at room temperature. Lipid II-Atto565 was purified via thin layer chromatography.Supported bilayers were formed by DOPC 0.2 mol% lipid II/lipid II-Atto565.

The required lipid composition was prepared in chloroform to reach a lipid concentration of 1.3 mM. Then, chloroform was removed in a nitrogen stream and the dried lipid film was solved in HEPES/Triton buffer (20 mM HEPES, 150 mM NaCl, 20 mM Triton X-100, pH 7,4) in order to reach a lipid concentration of 5 mM. The stock solution was divided into 20 μL aliquots and stored at -20°C. To enable the preparation of planar lipid bilayers on coverslips, a suspension containing very small unilamellar vesicles (VSUV) was prepared by addition of 200 μL HEPES buffer (20 mM HEPES, 150 mM NaCl) and 200 μL of a 4 mM heptakis(2,6-di-O-methyl)-ß-cyclodextrin to each of the aliquoted lipid-detergent solutions. Finally, the vial was vortexed for 2 minutes.

In order to increase the hydrophilicity of the glass support, coverslips with a diameter of 18 mm were placed for at least 1 hour in freshly prepared Piranha-solution (one-part H_2O_2 30% and three parts H_2SO_4). Then, the coverslips were washed with milliQ water, dried in a nitrogen stream and inserted into custom-built sample chambers. The VSUV suspension resulting from one aliquot was immediately added on top of the cleaned coverslip. After an incubation time of 6 minutes, unfused vesicles were removed by washing of the coverslip with HEPES buffer. During the washing steps care was taken to not dry out the lipid bilayer. Bilayers were kept in HEPES buffer and the respective amounts of teixobactin and clovibactin were added from stock solutions in DMSO to freshly prepared bilayers.

After an incubation time of 30 minutes the samples were imaged using a custom-built setup enabling single-molecule microscopy.[65] An α-plan-apochromat 63x/1.46 objective (Zeiss) and a sCMOS camera (Prime BSI, Teledyne Photometrics, Tucson, AZ, USA) were used for data acquisition resulting in a pixel size of 103.2 nm. Images were acquired with a field of view of 30.96 μm x 30.96 μm and a single frame integration time of 10 ms. Excitation of Atto565 was performed using a DPL 561 nm laser (Hübner Photonics GmbH, Kassel, Germany). For every sample 27 movies consisting of 1000 frames were acquired at different sample locations. For every experimental condition three independently prepared samples were measured. Single-particle tracking was performed with the ImageJ 1.52p[66] plugin TrackMate[67] after background subtraction using a rolling ball radius of 50. For spot detection, the LoG-based detector was used, the parameter "estimated blob diameter" was set to 0.75 μm, the threshold was set to 2.2. Tracking was performed by the "Simple LAP Tracker". Gap-closing was allowed with a maximum closing distance of 1 μm and a maximum frame gap of two frames. A maximum linking distance of 1 μm was chosen. From the resulting tracking data, the mean square displacement as function of time was determined and plotted with the Software OriginPro 2021b (OriginLab Co., Northhampton, MA, USA). A linear fit was performed and according to the Einstein equation for two-dimensional diffusion, the diffusion coefficient of lipid II-Atto565 molecules was determined by dividing the slope of the linear fit by 4.

Synthesis and purification of isotopically labelled Lipid II

Lipid II was produced according to published methods[68] based on enzymatic lipid reconstitution using the lipid II precursors UDP-GlcNAc, UDP-MurNAc-pentapeptide and polyisoprenolphosphate as substrates.[68] Lysine-form UDP-MurNAc-pentapeptide was extracted from *Staphylococcus simulans* 22. ^{13}C,^{15}N-labelled UDP-GlcNAc and UDP-MurNAc-pentapeptide (lysine form) were extracted from *S. simulans* 22 grown in [^{13}C/^{15}N]-labelled rich medium (Silantes) and supplemented with [U-^{13}C]-D-glucose and [^{15}N]-NH_4Cl. Polyisoprenolphosphate was synthesized via phosphorylation of polyisoprenol obtained from *Laurus nobilis*.[69] The head-group precursors were extracted from bacteria and polyisoprenol was extracted from leaves as described.[70] After synthesis, lipid II was extracted with 2:1 BuOH:(Pyr/Acetate, 6 M) and then purified with a DEAE cellulose resin using a salt gradient of 0 - 600 mM NH_4HCO_3 with 2:3:1 $CHCl_3$:MeOH:[H_2O+salt]. Fractions containing pure lipid II were pooled, dried, and dissolved in 2:1 chloroform/methanol. Lipid II concentration was estimated through an inorganic phosphate determination.[57]

Solid-state NMR sample preparation

Multi-lamellar vesicles (MLVs) of DOPC doped with 4 mol% lysine-lipid II in buffer (30mM Citrate, 300mM NaCl, pH 5.5) were collected by centrifugation (60,000×*g*) and loaded into ssNMR rotors. For 3.2 mm rotors, we used 800 nmol of clovibactin with unlabelled lipid II, while we used 400 nmol with labelled lipid II. For 1.3 mm rotors, samples contained 200 nmol of antibiotic for unlabelled lipid II.

Solid-state NMR spectroscopy

^{1}H-detected ssNMR experiments were performed at 60 kHz magic angle spinning (MAS) using magnetic fields of 700, 950, and 1200 MHz (^{1}H frequency) with dipolar transfer steps and using low-power PISSARRO[71] decoupling in all dimensions. See Tables S2 and S3 for NMR assignments. ^{1}H-detected ^{15}N T_{1rho} relaxation experiments[28,29] were acquired with a ^{15}N spin lock-field of 18 kHz and spin-lock durations of 0, 10, 20, 40, 70, and 100 ms. T_{1rho} trajectories were fit to single exponentials. 2D CC experiments were acquired with PARIS[72] or PARISxy[32] recoupling (m=1) at 950 or 1200 MHz magnetic field and 15 to 18 kHz MAS. To probe interfacial contacts between ^{13}C,^{15}N-clovibactin and ^{13}C,^{15}N-lipid II, we used CC magnetization transfer times of 50, 150, and 300 ms. 2D NCα and NCO experiments were acquired at 800 MHz, 15 kHz MAS, and with 5 to 7 ms N to C cross-polarization transfer time. To characterize lipid II-bound clovibactin, we used CC magnetization transfer times of 50 and 300 ms. The scalar 2D CC TOBSY[36] experiment was acquired at 700 MHz using 8 kHz MAS with 6 ms CC mixing time. The mobility-edited[31] H(H)C experiment was measured at 700 and 1200 MHz with 16.5 kHz MAS at about 30 °C temperature using a T_2 relaxation filter of 2.5 ms. 1D MAS ^{31}P experiments were acquired at 500 MHz magnetic field and 12 kHz MAS. 2D HP experiments were acquired at 800 MHz and 60 kHz MAS using 1 and 2 ms ^{1}H to ^{31}P cross-polarization contact time.

For dynamic nuclear polarization (DNP) ssNMR measurements at 800 MHz magnetic field, an equimolar mixture of ^{13}C-labelled and ^{15}N-labelled clovibactin was added to liposomes (4 % lipid II). Prior to the measurements, the DNP samples were suspended in 60% glycerol-d8, 35% buffer solution (30mM citrate, 300 mM NaCl, pH-5.5), and 5% 15 mM SNAPol-1.[48] Intermolecular magnetization transfer was established with the NHHC pulse sequence,[73] using short (100 μs) cross-polarization transfer steps and an intermediate (300 μs) proton-proton magnetization transfer time.

- Details of 2D ssNMR experiments:

1. 2D CC PARIS experiment with ^{13}C,^{15}N-clovibactin – ^{12}C,^{14}N-lipid II

Magnetic field / MAS = 1200 MHz (^{1}H-frequency) / 18 kHz
Mixing time (CC) = 50 ms
t1 points / AQ = 452 / 5.00 ms
Recycle delay = 2.40 s
Co-added transients = 144
Experimental time = 1d 21h

2. 2D CC PARIS experiment with ^{13}C,^{15}N-clovibactin – ^{12}C,^{14}N-lipid II

Magnetic field / MAS = 1200 MHz (^{1}H-frequency) / 18 kHz
Mixing time (CC) = 300 ms
t1 points / AQ = 452 / 5.00 ms
Recycle delay = 2.40 s
Co-added transients = 224
Experimental time = 3d 5h

3. 2D CC PARISxy (m = 1) experiment with ^{13}C,^{15}N-clovibactin – ^{13}C,^{15}N-lipid II

Magnetic field / MAS = 950 MHz (^{1}H-frequency) / 15.5 kHz
Mixing time (CC) = 50 ms
t1 points / AQ = 316 / 4.40 ms
Recycle delay = 1.90 s
Co-added transients = 192
Experimental time = 1d 10h

4. 2D CC PARISxy (m = 1) experiment with $^{13}C,^{15}N$-clovibactin – $^{13}C,^{15}N$-lipid II
Magnetic field / MAS = 950 MHz (^{1}H-frequency) / 15.5 kHz
Mixing time (CC) = 300 ms
t1 points / AQ = 215 / 3.00 ms
Recycle delay = 1.84 s
Co-added transients = 1024
Experimental time = 5d 14h

5. 2D CC PARIS experiment with $^{13}C,^{15}N$-clovibactin – $^{13}C,^{15}N$-lipid II
Magnetic field / MAS = 1200 MHz (^{1}H-frequency) / 18 kHz
Mixing time (CC) = 50 ms
t1 points / AQ = 452 / 5.00 ms
Recycle delay = 2.40 s
Co-added transients = 144
Experimental time = 1d 21h

6. 2D CC PARIS experiment with $^{13}C,^{15}N$-clovibactin – $^{13}C,^{15}N$-lipid II
Magnetic field / MAS = 1200 MHz (^{1}H-frequency) / 18 kHz
Mixing time (CC) = 250 ms
t1 points / AQ = 316 / 3.50 ms
Recycle delay = 2.30 s
Co-added transients = 752
Experimental time = 7d 1h

7. 2D T_2-edited H(H)C experiment with $^{13}C,^{15}N$-clovibactin – $^{12}C,^{14}N$-lipid II
Magnetic field / MAS = 700 MHz (^{1}H-frequency) / 16.5 kHz
Mixing time (HH) = 5 ms
T_2 filter = 2.5 ms
t1 points / AQ = 60 / 2.08 ms
Recycle delay = 2.15 s
Co-added transients = 1972
Experimental time = 2d 17h

8. 2D CC TOBSY experiment with $^{13}C,^{15}N$-clovibactin – $^{13}C,^{15}N$-lipid II
Magnetic field / MAS = 950 MHz (^{1}H-frequency) / 8 kHz
Mixing time (HH) = 6 ms
t1 points / AQ = 265 / 5.38 ms
Recycle delay = 1.61 s
Co-added transients = 2304
Experimental time = 11d 16h

9. 2D NCα experiment with $^{13}C,^{15}N$-clovibactin – $^{12}C,^{14}N$-lipid II
Magnetic field / MAS = 800 MHz (^{1}H-frequency) / 15 kHz
Mixing time (NC) = 5.5 ms
t1 points / AQ = 17 / 3.6 ms
Recycle delay = 1.82 s
Co-added transients = 7168
Experimental time = 2d 17h

9. 2D NCO experiment with $^{13}C,^{15}N$-clovibactin – $^{12}C,^{14}N$-lipid II
Magnetic field / MAS = 800 MHz (^{1}H-frequency) / 15 kHz
Mixing time (NC) = 7 ms
t1 points / AQ = 25 / 4.4 ms
Recycle delay = 1.9 s
Co-added transients = 8192
Experimental time = 4d 18h

10. 2D NH experiment with $^{13}C,^{15}N$-clovibactin – $^{12}C,^{14}N$-lipid II
Magnetic field / MAS = 700 MHz (^{1}H-frequency) / 60 kHz
t1 points / AQ = 87 / 5.6 ms
Recycle delay = 0.72 s
Co-added transients = 4096
Experimental time = 5d 4h
Note = high number of co-added transients was necessary to obtain good data for the side chains of clovibactin residues 3 and 5.

11. 2D N(HH)C experiment with $^{13}C,^{15}N$-clovibactin – $^{12}C,^{14}N$-lipid II (DNP-ssNMR)
Magnetic field / MAS = 800 MHz (^{1}H-frequency) / 10.6 kHz
Mixing time (HH) = 0.3 ms
t1 points / AQ = 42 / 3.0 ms
Recycle delay = 2.8 s
Co-added transients = 3776
Experimental time = 5d 3h
12. 2D ^{1}H-^{31}P HETCOR experiment with $^{13}C,^{15}N$-clovibactin – $^{12}C,^{14}N$-lipid II
Magnetic field / MAS = 800 MHz (^{1}H-frequency) / 60 kHz
Mixing time (HP) = 2.0 ms
t1 points / AQ = 36 / 1.4 ms
Recycle delay = 1.3 s
Co-added transients = 22528
Experimental time = 12d 9h

For all 2D experiments, sign discrimination in indirect dimensions was achieved with the TPPI (time-proportional phase incrementation) method.

Fluorescence Microscopy

GUVs preparation

We used a self-assembled GUV cell, aligned with two titanium electrodes in a closed Teflon chamber (volume = 500 mL). 1 μL of 0.5 mM DOPC doped with Atto 550-labelled lipid II (0.1 mol%) was brushed on the titanium electrodes. The GUV cell was dried under vacuum. Next, the chamber was filled with 350 μL 0.1M sucrose solution, the electrodes dipped in and connected to a power supply of a sine wave (2.5V; 10 Hz; 90 minutes). Each microscopy slide (m-slide 8 well, Ibidi) was incubated with 350 μL BSA solution (1 mg/mL) for 1 hour. To detach the GUVs, the power supply was changed to square wave (2V; 2Hz; 15 minutes). The slides were washed once with water and 0.1M glucose solution. The slides were immersed in 300 μL of 0.1M glucose solution to which 50 μL of GUVs were added. These were incubated for 3 hours with 1 μM clovibactin and later observed under confocal microscope Zeiss LSM 880. GUVs were imaged using Zeiss LSM 880 with 63x/1.2NA glycerol and 100x/1.2NA oil objective lenses. The Atto 550 label appeared red upon excitation by the 560 nm laser. The brightfield was used for detection and location of the GUVs and to observe their shape. ImageJ software[66] was used for the analysis of the images.

Isothermal Titration Calorimetry

For ITC measurements, LUVs (Large unilamellar vesicles) containing Lys-lipid II were prepared by incorporating 2 mol% of Lys-lipid II in DOPC from the stock solution. The lipids were dried under a nitrogen stream and hydrated with buffer (30mM Citrate, 300mM NaCl, pH 5.5) to a lipid-phosphate concentration of 20mM determined by Rouser's method.[57] Finally, unilamellar vesicles were obtained after 10 rounds of extrusion through 200 nm membrane filters (Whatman Nuclepore, Track-Etch Membranes). ITC experiments were performed with the Affinity ITC (TA Instruments- Waters LLC, New Castle, DE, USA) to determine interaction between LUVs and clovibactin. Clovibactin was diluted in the buffer, to a final concentration of 30 μM. The samples were degassed before use. The chamber was filled with 177 μL of clovibactin, and the LUVs were titrated into the chamber at a rate of 1.96 μL/150 seconds with a constant syringe stirring rate of 125 rpm. Number of injections = 21. Experiments were performed at 37°C and analyzed using the Nano Analyze Software (TA instruments – Water LLC). All experiments were performed in duplicates. Control experiments were performed with lipid II-free DOPC LUVs. The independent model was used to determine the interaction between clovibactin and lipid II. ITC data for teixobactin was recently published.[10]

High Speed-Atomic Force Microscopy (HS-AFM) Imaging

The HS-AFM images were acquired in amplitude modulation tapping mode in liquid using a high-speed atomic force microscope (RIBM, Japan). Short cantilevers (~7 μm) with a nominal spring constant of 0.15 N/m were used (USC-F1.2-k0.15, NanoWorld, Switzerland). A minimal imaging force was applied by using a small set-point amplitude of 0.8 nm (for a 1 nm free amplitude). The HS-AFM results showing the assembly of clovibactin filaments were obtained from imaging of supported lipid bilayers on mica. The lipid bilayer was obtained by incubating LUVs containing 0.5 mg/ml of DOPC and 4 mol% lipid II (prepared as mentioned above) mixture (or 0.5 mg/ml DOPC without lipid II) on top of a freshly cleaved mica for 20-30 minutes. After the incubation period, the mica was cleaned gently using recording buffer (10 mM Tris-Cl, 100 mM NaCl, pH 8.0). Imaging was started on the lipid bilayer surface in recording buffer. Next, a concentrated clovibactin solution was added and pipetted to reach the desired final concentration in the AFM liquid chamber of 40 μl. Images were primarily processed using built-in scripts (RIBM, Japan) in Igor Pro[33] (Wavemetrics, Lake Oswego, OR, USA) and analyzed using ImageJ software. The images/movies were corrected minimally for tilt, drift, and contrast. Unless otherwise mentioned, the times reported in AFM images are relative to clovibactin addition into the imaging chamber. Reported image acquisition rate is 0.5 frames/second, and the line rate is 150 lines/second. Stated errors are standard deviation.

Permeabilization assay

S. simulans cultures were grown overnight at 37 °C in TSB. Secondary cultures were grown until the OD_{600} reached 0.5. The bacterial cells were then centrifuged at 3000x g for 5 minutes at 4 °C and washed twice with 10 mL of buffer (10 mM KPi, 100 mM KCl, 5 mM $MgSO_4$, 250 mM glucose pH=7.2). The bacterial cells were resuspended to an OD_{600} = 5 in the buffer and kept on ice until use. All permeability experiments were performed with a Cary Eclipse (FL0904M005) fluorescence spectrometer. All samples (1.0 mL) were continuously stirred in a 10×4-mm quartz cuvette and kept at 20 °C. For the assay, 10 μL of the bacterial suspension was added to 1 mL of buffer. For $DiSC_2(5)$ (excitation 650 nm, emission 670 nm, 5 nm bandwidths) ion leakage assays, 2 μL of a 0.1 mM $DiSC_2(5)$ stock in DMSO was added to the cuvette and the fluorescence was measured for 2 minutes before the addition of the antibiotic. After 5 minutes incubation, Triton-X100 (0.2 v% final) was added to completely dissipate the membrane potential. For SYTOX green (excitation at 504 nm, emission at 523 nm, 5 nm bandwidths) leakage assays, 1 μL of a 0.25 mM SYTOX green stock was added to the cuvette and the fluorescence was measured for 1 minute before the addition of the antibiotic. After a incubation time of 5 minutes, Triton-X100 (0.2 v% final) was added. We used antibiotic concentrations of 160 nM for nisin (2 x MIC), 10 μM for clovibactin (5 x MIC), and 2.5 μM for teixobactin (5 x MIC).

Structure Calculations

Parametrization of Clovibactin

Clovibactin parametrization was started from a linear peptide topology of L-amino acids. D-amino acids were generated by inverting relevant dihedral and improper torsion angles and hydroxyasparagine (Hyn) topology was based on asparagine, where -OH group parameters were derived from threonine-OH group parameters. Depsi-cycle formation between Hyn5 and Leu8 was performed as previously described for [R4,L10]-teixobactin.[30] Parameters for lipid II were taken from Hsu et al.[18]

Structure calculation protocol

We used HADDOCK version 2.4[37] for the structure calculations. An eight-body docking (four lipid II and four clovibactin molecules) was performed using ssNMR-derived distance and dihedral restraints. Five thousand models were generated in the rigid-body docking stage of HADDOCK, of which the best-scoring 500 were subjected to the flexible refinement protocol of HADDOCK. The resulting models were energy minimized. Default HADDOCK settings were used except for doubling the weight of the distance restraints during all stages of the structure calculation. The final models were further filtered based on the topological requirements (that is, the lipid tails of all lipid II molecules must point in the same direction as the membrane-exposed hydrophobic residue Leu2). This resulted in a final ensemble of 22 structural models. See Supplementary Information for detailed analysis of the calculated structural models.

In total, we used 19 unambiguous intermolecular clovibactin – clovibactin distance restraints, 4 intermolecular clovibactin – clovibactin hydrogen bonding restraints, 12 unambiguous and 4 ambiguous clovibactin - lipid II distance restraints (with the lipid II sugars), and 4 ambiguous clovibactin - lipid II PPi distance restraints. Intramolecular restraints are listed per monomers, while intermolecular clovibactin – clovibactin /interfacial clovibactin – lipid II restraints are listed per pair of interacting molecules.

- Analysis of calculated structure models

The average backbone RMSD (from the average structure) of the 22 clovibactin molecules in the complex was 2.50 ± 0.85 Å (see also Tables S4 and S5).

- NMR restraints

Intermolecular distance restraints between clovibactin molecules

All restraints based on a series of 2D $^{13}C^{13}C$ PARIS experiments (up to 300 ms $^{13}C^{13}C$ transfer) using a target distance of 7.5 Å, and lower distance margin of 5.5 Å, and a higher distance margin of 2.0 Å; i.e., format (7.5 5.5 2.0). Note that in the arrangement of four clovibactin molecules, intermolecular clovibactin-clovibactin distance restraints for the *inner* clovibactin molecules were implemented so that a restraint could be with the clovibactin molecule on either side.

Hydrogen bond restraints (intermolecular) between clovibactin molecules

Hydrogen bonding restraints in line with experimentally determined antiparallel clovibactin arrangements were applied. While two different register shifts are possible to form antiparallel β-sheets (i.e., Ser4NH could interact with Leu2CO or Ser4CO), only the variant with Leu2CO appears to agree with the intermolecular ssNMR distance restraints. Hydrogen bonding distance restraints were defined accordingly with upper and lower limits of 2.3 and 1.5 Å, respectively, i.e., format (2.0 0.5 0.3). These restraints were applied between the amino protons of depsi-cycles residues and oxygens of the PPi-group.

clovibactin A with *clovibactin B*

Leu2NH	-	Ser4CO
Leu2CO	-	Ser4NH
Ser4NH	-	Leu2CO
Ser4CO	-	Leu2NH

clovibactin C with *clovibactin D*

Phe1NH	-	Lys3CO
Phe1CO	-	Lys3NH
Lys3NH	-	Phe1CO
Lys3CO	-	Phe1NH

clovibactin C with *clovibactin D*
Similar as in ***A*** with ***B***

Interfacial distance restraints between clovibactin and lipid II

Restraints involving the pyrophosphate group. Ambiguous distance restraints were applied between the backbone amino protons of the four depsi-cycle residues (Hyn5-Leu8) with either phosphate of the pyrophosphate group using upper and lower limits of 2.4 and 1.7 Å, respectively, i.e., format (2.0 0.3 0.4). Restraints based on a 2D $^{1}H^{31}P$ experiment (Figure 5B of the manuscript).

Restraints involving the MurNAc/GlcNAc sugars

Restraints were based on a series of 2D $^{13}C^{13}C$ PARIS and PARISxy experiments with 50, 250, and 300 ms magnetization transfer. Due to the mobility of the depsi-cycle in the complex (Figures 4B and 4C of the main text), most interfacial clovibactin – lipid II restraints were weak. We therefore applied all interfacial clovibactin – lipid II CC restraints with wider boundaries (7.5 5.5 2.0), i.e., upper and lower boundaries of 9.5 and 2.0 Å, respectively. Notwithstanding the wider boundaries, the interface is well defined (1.47±0.40 Å interfacial RMSD defined by residues Ala6, Leu7, Leu8 of clovibactin, PPi and MurNAc of lipid II)

Topological restraints

Eventually, a filtering strategy was applied to constrain the conformational space of the isoprenyl tails. Structural models were only accepted if all lipid II tails pointed into the direction of the membrane-exposed side chain of Leu2 (see Figures 4I and S6). Sorting of the lipid II tails was steered by imposing soft distance restraints between the side chain of Leu2 and the lipid II isoprenyl-tails, and by imposing soft distance restraints between the isoprenyl-tails.

QUANTIFICATION AND STATISTICAL ANALYSIS

All of the statistical details for each experiment are described in the figure legends.

Supplemental figures

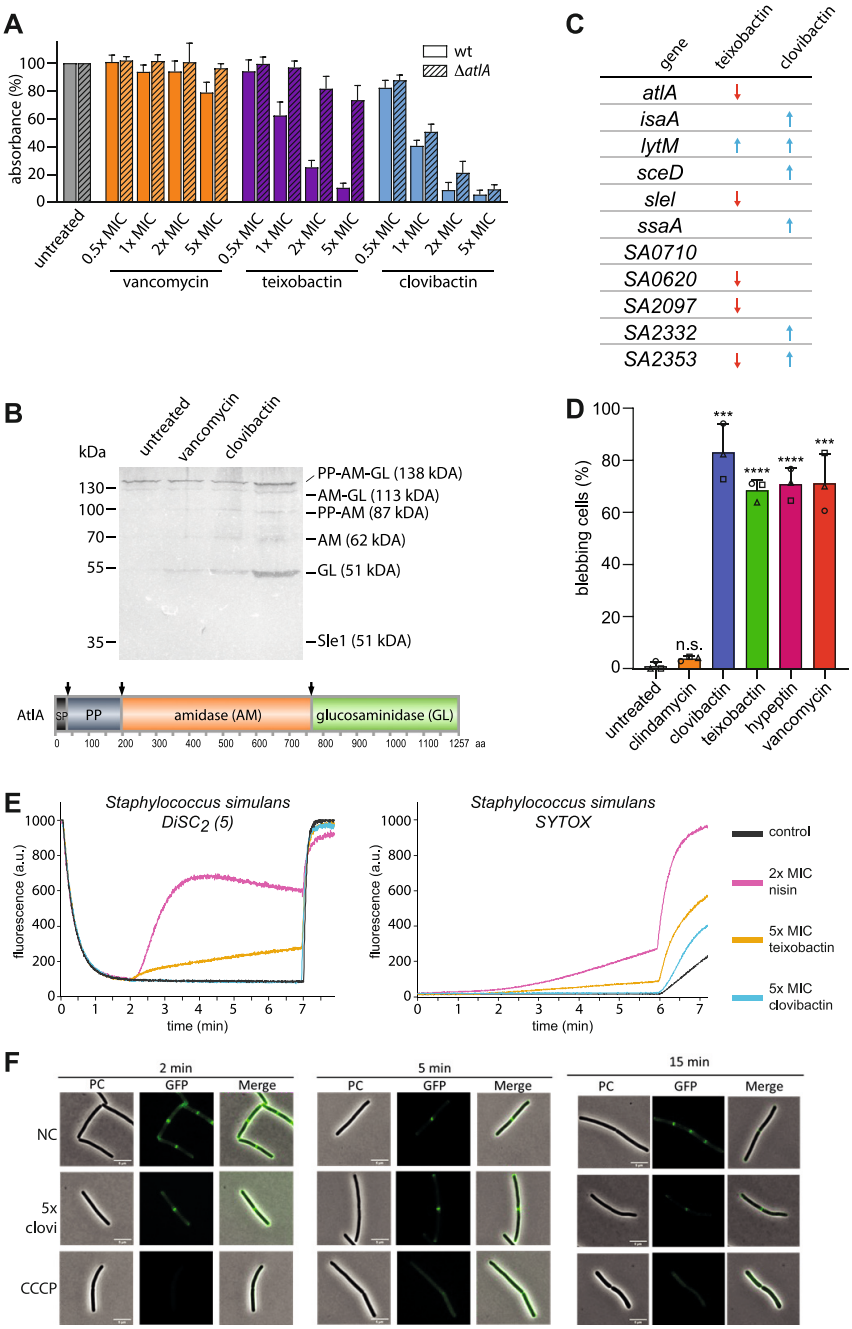

Figure S1. Clovibactin-induced lysis in *S. aureus* is AtlA independent, related to Figures 2 and 3

(A) Cells of *S. aureus* SA113 and a *ΔaltA* mutant were incubated with each compound at increasing concentrations for 24 h, as indicated. Mean values from three independent experiments are shown. Error bars represent standard deviations. Related to Figure 2C.

(B) Zymographic analysis of supernatants derived from clovibactin- and teixobactin-treated *S. aureus* cells on sodium dodecyl sulfate polyacrylamide gel electrophoresis (SDS-PAGE) gel containing heat-killed *S. aureus* RN4220 as a substrate. The dark bands indicate the clear zone in the SDS-PAGE gel. AtlA is visible in multiple bands representing the precursor protein (Pro-AtlA) that is cleaved to generate intermediates as depicted in the scheme.

(C) Differential regulation of WalRK-controlled genes in clovibactin- and teixobactin-treated *S. aureus* HG001 (0.25 × MIC) by RNA sequencing; downregulated (red) and upregulated (blue).

(legend on next page)

(D) Cell wall active antibiotics teixobactin, hypeptin, vancomycin, and protein synthesis inhibitor clindamycin were used as controls. Scale bars, 2 μm. Error bars represent standard deviation. At least n ≥ 30 cells per replicate were evaluated for each condition from three biologically independent experiments. Significance was determined by unpaired two-tailed Student's t test with a 95% confidence interval. ****p < 0.0001, ***p < 0.0004, n.s., not significant (p = 0.0558). Related to Figure 3C of the manuscript.

(E) Permeabilization assay with $DiSC_2$ (5) and SYTOX reporter dyes for *Staphylococcus simulans* with nisin, teixobactin, clovibactin, and untreated cells. Although nisin and teixobactin compromise the membrane integrity, clovibactin shows no permeabilizing activity for either of the two reporters.

(F) GFP-MinD cells of *B. subtilis* were treated with clovibactin (5 × MIC). The ionophore carbonyl cyanide *m*-chlorophenylhydrazone (CCCP) was used as a positive control. Scale bars, 5 μm. The shown data are representative of two independent experiments for each SYTOX and $DiSC_2$ (5).

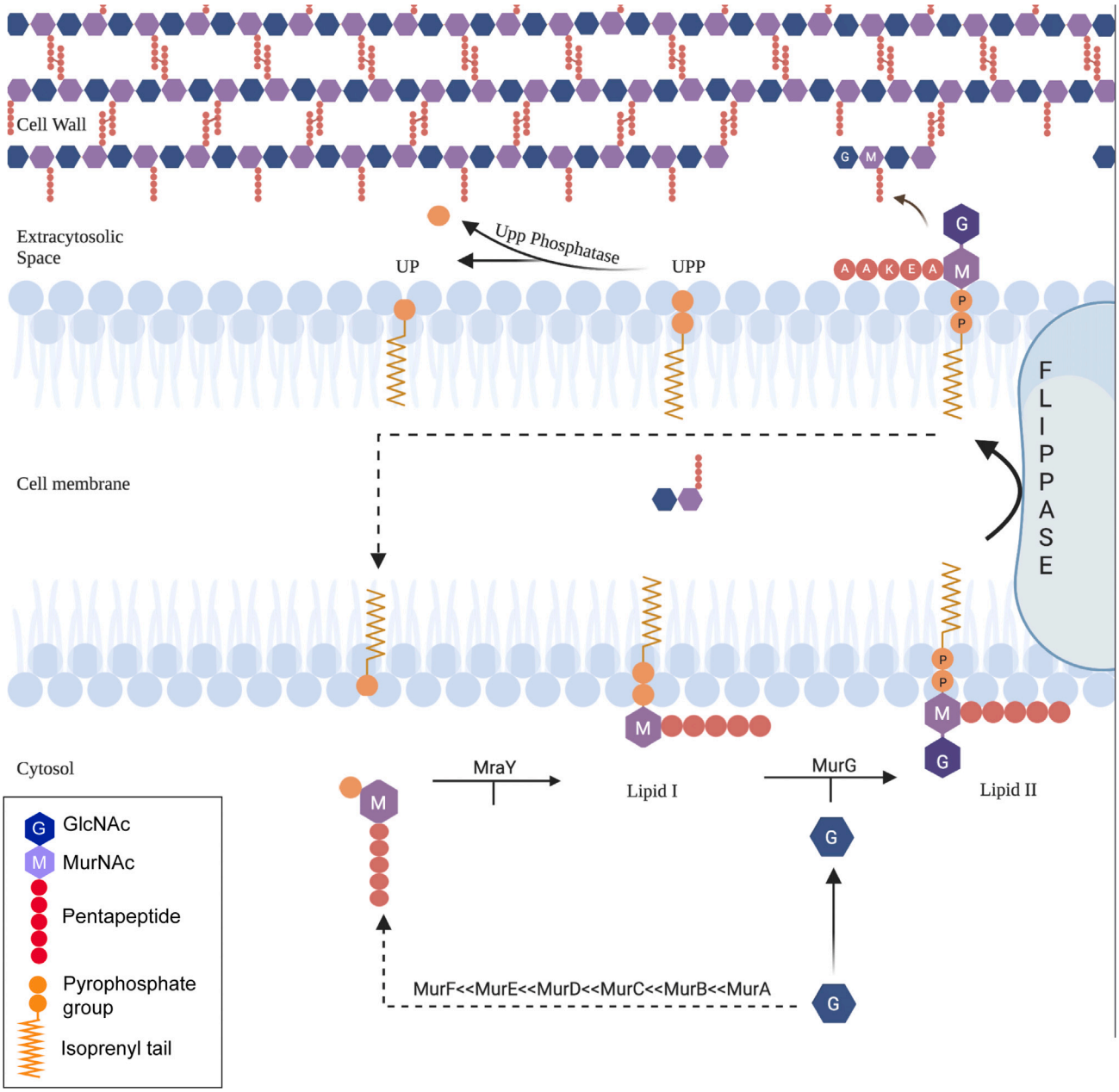

Figure S2. Schematic of peptidoglycan synthesis, related to Figure 3

Peptidoglycan synthesis is dependent on the lipid II cycle which is shown in the illustration. It shows the organization of the lipid II molecule on the inner leaflet, which is eventually flipped to the outer leaflet. When present in the outer leaflet lipid II deposits the disaccharide moiety (GlcNAc-MurNAc) and the attached pentapeptide to develop the peptidoglycan layer. The $C_{55}P$ moiety is then recycled to continue the cycle.

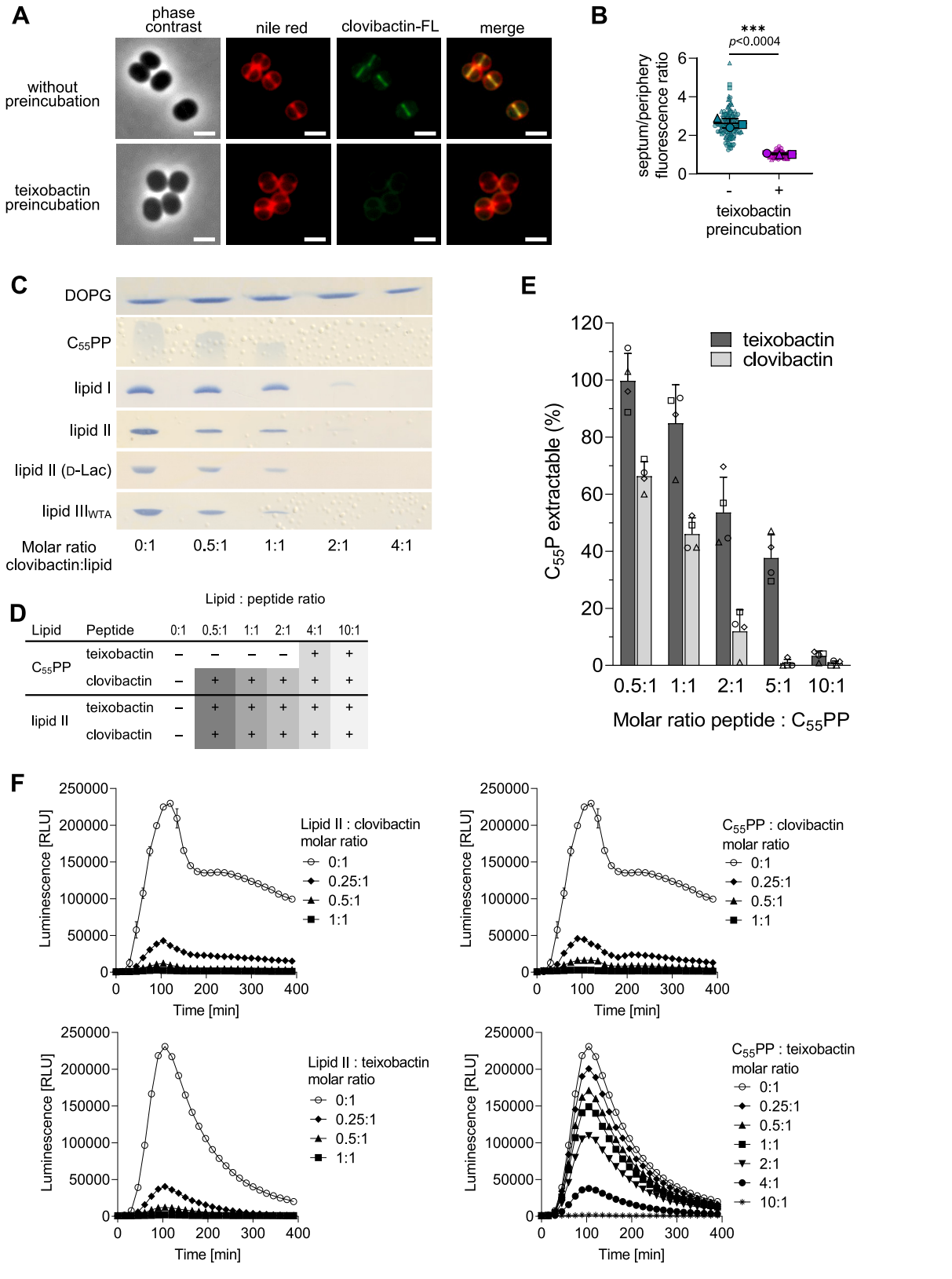

(legend on next page)

Figure S3. BODIPY FL-clovibactin localizes to the septum of *S. aureus* and forms extraction-stable complexes with undecaprenyl-pyrophosphate-containing cell wall precursors, related to Figure 3

(A) In cells preincubated with teixobactin (2 min), septal localization of FL-clovibactin is diminished. Nile red was used for membrane staining. Scale bars, 1 μm.

(B) Images of individual cells were used to calculate the fluorescence ratio (FR) of the septal versus peripheral fluorescence signal for cells pre-treated with teixobactin and lacking pre-treatment. FR > 2 indicates septal localization. At least n = 30 cells were evaluated for each condition from three biologically independent experiments. Significance was determined by unpaired Student's t test with a 95% confidence interval. ****$p < 0.0004$.

(C) Complex formation is indicated by a reduction of the amount of free lipid intermediates visible on the TLC. Cell wall intermediates are fully locked in a complex at a 2-fold molar excess of antibiotic. No complex formation was observed with the anionic phospholipid DOPG. Note that the molar clovibactin: lipid ratios are not representative for stoichiometries. The chromatograms are representative of three independent experiments.

(D) Antagonization of the antimicrobial activity of clovibactin and teixobactin by cell wall precursors. *S. aureus* was incubated with clovibactin (8 × MIC) in nutrient broth in microtiter plates, and growth was measured after a 24 h incubation at 37°C. HPLC-purified antagonists C_{55}PP and lipid II were added in molar ratios with respect to the antibiotic. Experiments were performed with biological replicates. + antagonization/growth; − no antagonization/no growth.

(E) Clovibactin inhibits dephosphorylation of undecaprenyl-pyrophosphate (C_{55}PP) by YbjG. Clovibactin and teixobactin were added in molar ratios from 0.5 to 10 with respect to the amount of the C_{55}PP substrate C_{55}PP. The reaction product (C_{55}P) synthesized in the absence of antibiotic was taken as 100%. Mean values from three independent experiments are shown. Error bars represent standard deviation.

(F) Clovibactin and teixobactin-induced *lial-lux* expression is antagonized when preincubated with lipid II (molar ratio of lipid II with respect to antibiotic). C_{55}PP antagonizes clovibactin activity at equimolar ratio, whereas at least a 10-fold higher concentration is required for teixobactin. Representative of three independent experiments.

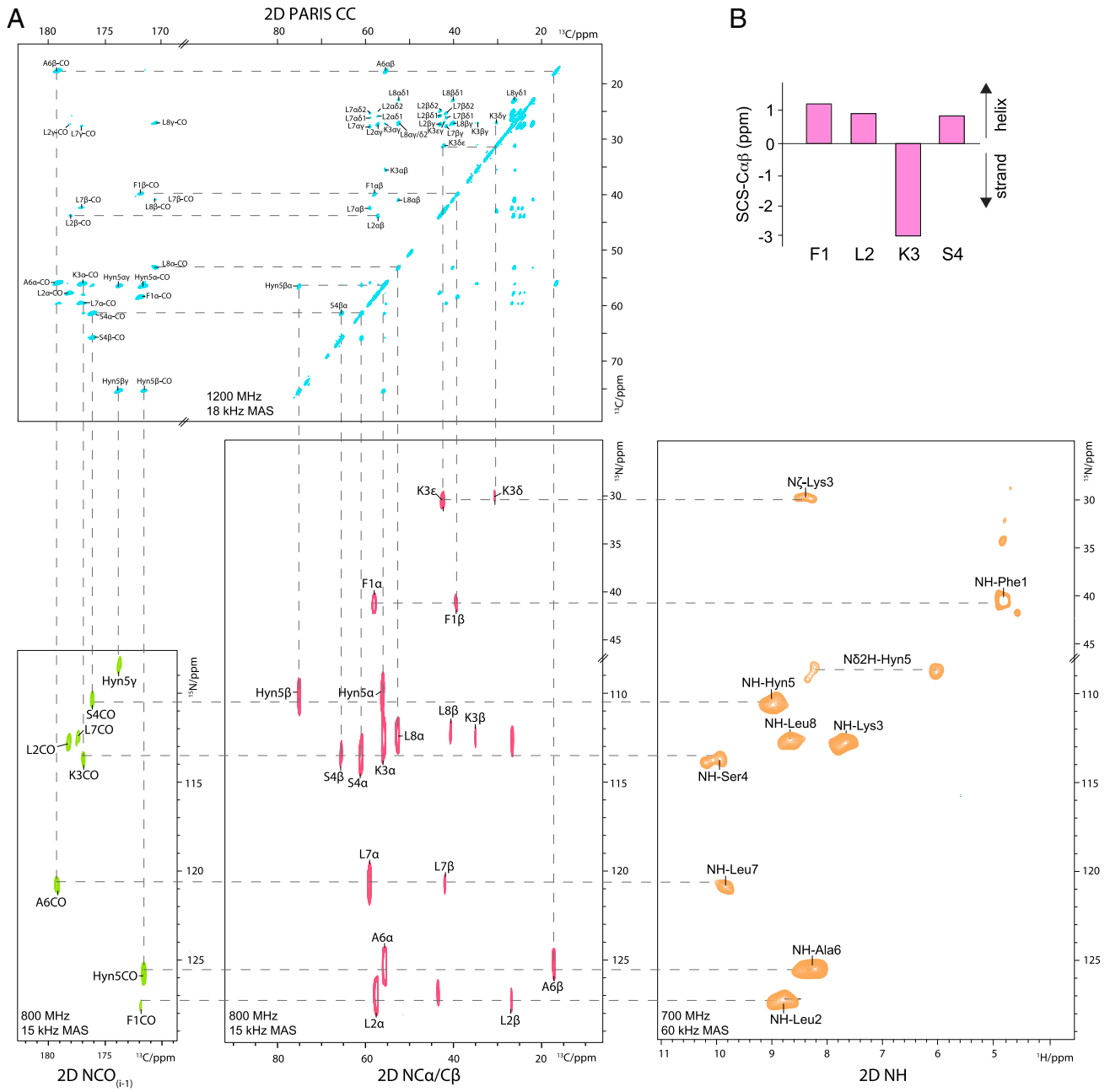

Figure S4. ssNMR assignments of clovibactin in the lipid II-bound state in DOPC liposomes, related to Figure 4

(A) Assignments were performed using a 2D PARIS CC experiments (in blue), 2D NCO(i-1) (in green), 2D NCA (in red), and 2D NH (in orange). 2D PARIS CC ssNMR experiment was recorded at 1,200 MHz magnetic field at 18 kHz magic angle spinning (MAS). 2D NCO(i-1) and 2D NCα experiments were recorded at 800 MHz magnetic field at 15 kHz MAS. The 2D NH experiment was recorded at 700 MHz magnetic field at 60 kHz MAS.

(B) Cαβ secondary chemical shifts (SCSs) do not show consistent β-structuring for the linear clovibactin N terminus. We note that it is unclear to which extent chemical shift information[27] applies to the very short N terminus with its unusual structure and non-canonical residues. We also note that for the chemical shifts of teixobactin,[10] residues D-N-Me-Phe1 and Ser7, i.e., the residue connected to the depsi-cycle, did not indicate β-structuring.

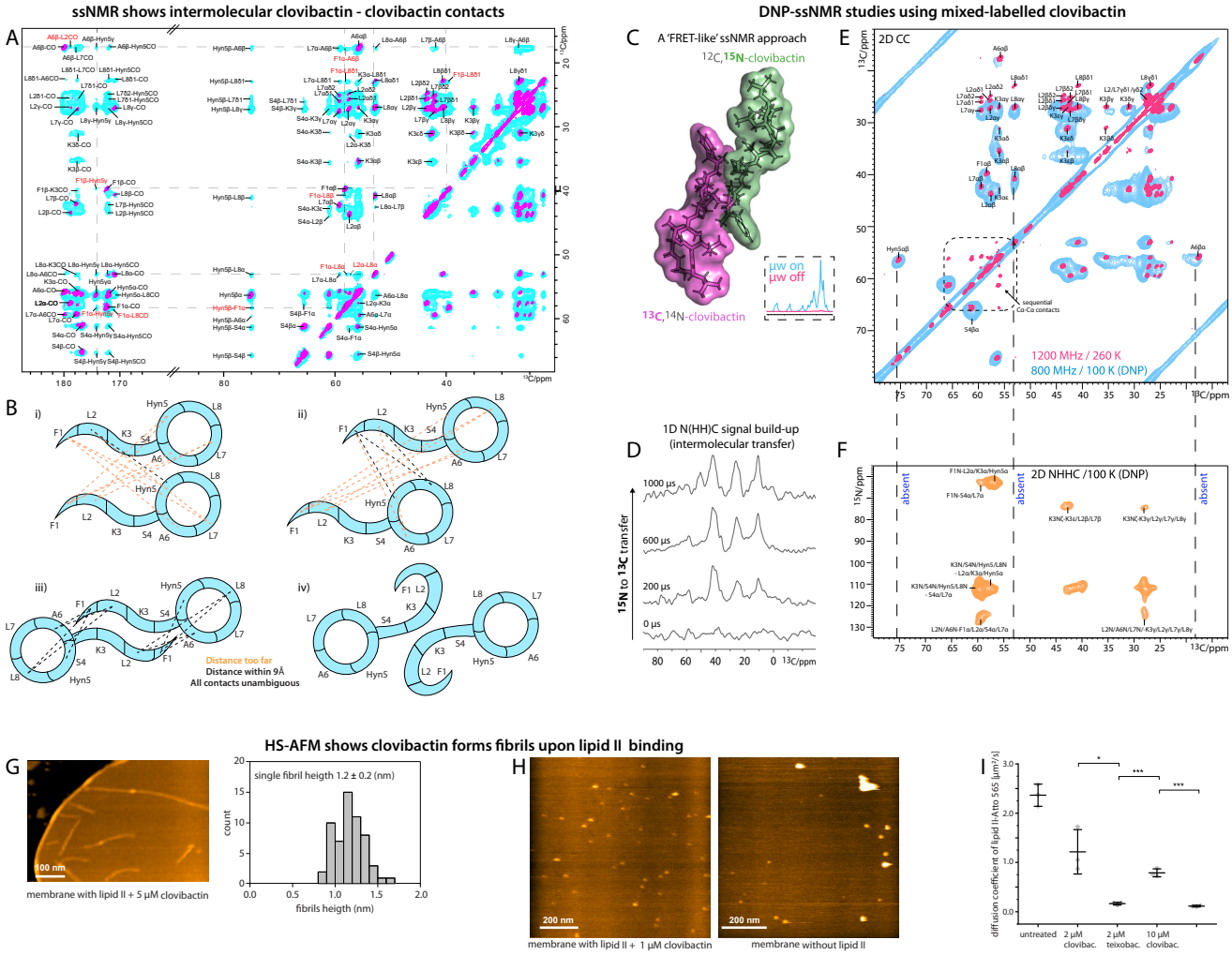

Figure S5. Supramolecular arrangement of the clovibactin dimer, related to Figure 4

ssNMR, confocal microscopy, and AFM data show that clovibactin assembles into fibrils upon lipid II binding. From ssNMR data, the nature of the fibrils can be gauged.

(A) Superposition of 2D PARIS CC spectra of clovibactin in the lipid II-bound state with 50 (magenta) and 300 ms (cyan) mixing time measured at 1,200 MHz magnetic field and 18 kHz MAS. The contacts (in red) very likely arise from intermolecular interactions between adjacent clovibactin molecules because they are beyond the 8 Å distance range of such an experiment.

(B) The illustrations show how these contacts are consistent with be an antiparallel arrangement (Biii) of the neighboring clovibactin molecules. The parallel (Bi) and out of register parallel (Bii) arrangements still contain many contacts that presumably would not be satisfied by the distance threshold of the experiment. In the antiparallel arrangement, the N- and C-terminal residues of adjacent clovibactin molecules come close enough to justify observing contacts such as F1α-L8α and F1α-A6β. (Biv) Due to the small size of clovibactin, we note that the ssNMR restraints could potentially also be fulfilled by alternative supramolecular arrangements in which the N terminus bends toward the C-terminal depsi-cycle. However, such an alternative arrangement appears difficult to align with the formation of fibrils observed by AFM.

(C–F) DNP-ssNMR studies in liposomes demonstrate that clovibactin assembles into oligomeric structures upon lipid II binding in liposomes. (C) The formation of a suprastructure can be probed with an equimolar mixture of ^{15}N- and ^{13}C-labeled clovibactin and dedicated ssNMR experiments such as NHHC.[73] The insert shows the DNP signal enhancement of a factor of 49 using the SNAPol-1[48] biradical at 800 MHz magnetic field. (D) A series of DNP-enhanced 1D ssNMR NHHC experiments, acquired at 800 MHz magnetic field, with increasing ^{1}H-^{1}H magnetization transfer times applied to mixed-labeled clovibactin (in membranes with 4% lipid II) show the presence of oligomeric clovibactin structures. (E) Superposition of 2D CC ssNMR spectra acquired at 260 K temperature (in red) and at 100 K under DNP conditions (in blue). (F) DNP-enhanced 2D NHHC ssNMR spectrum, acquired with mixed-labeled clovibactin. The black dashed-lines mark signals of the depsi-cycle residues Hyn5, Ala6, and Leu8 that are absent from the spectrum, consistent with their involvement in lipid II binding.

DNP-ssNMR studies: although signal broadening at 100 K and the moderate spectral sensitivity in this highly challenging experimental setup prohibited to clearly identify the type of supramolecular arrangement, the "FRET-like" ssNMR experiments provided valuable insights that support our structural model of the complex.

(1) Intermolecular (proton-mediated) ^{15}N to ^{13}C magnetization transfer clearly confirms that the supra-structures observed by fluorescence microscopy and AFM are mediated by direct clovibactin-clovibactin contacts.

(legend continued on next page)

(2) The high signal intensity of NH-Hα contacts demonstrate that clovibactin-clovibactin contacts are mainly mediated by backbone-backbone contacts, which aligns with our structural model of a fibrillar suprastructure.
(3) Interestingly, well-resolved signals of depsi-cycle residues Hyn5, Ala6, and Leu8 showed no signals and hence seem not involved in intermolecular clovibactin-clovibactin contacts (indicated by black-bashed lines in E and F). This is something that aligns well with our structural model, in the N terminus acts as oligomerization domain and the depsi-cycle as lipid II binding motif.
(4) Furthermore, the Lys3 side chain shows only side-chain-side-chain contacts, consistent with the membrane topology of our model, in which hydrophilic residues "stick out of the fibril" toward the water phase.
(G) HS-AFM experiments show the formation of the clovibactin fibrils only at high-concentrations of 5 μM and in the presence of lipid II. Also, the fibrils are loosely attached to the membrane and the average height of the fibrils is 1.2 ± 0.2 nm above the membrane. There was no visible membrane deformation, and this is in line with our permeabilization assays, which also show no effect on bacterial membrane depolarization.
(H) Control experiments with low clovibactin concentration (1 μM) at a membrane containing 4% lipid II (left image) and 5 μM clovibactin at a membrane containing no lipid II (right image) both show no fibrilization events.
(I) Lipid II mobility was also monitored using single-molecule tracking microscopy experiments in supported lipid bilayers. These experiments also align with the requirement of higher clovibactin concentrations to immobilize lipid II in lipid bilayers. This contrasts with the low concentrations of teixobactin required for maximum lipid II immobilizations. For every experimental condition three independently prepared samples were measured. Further statistical details are given in the STAR Methods.

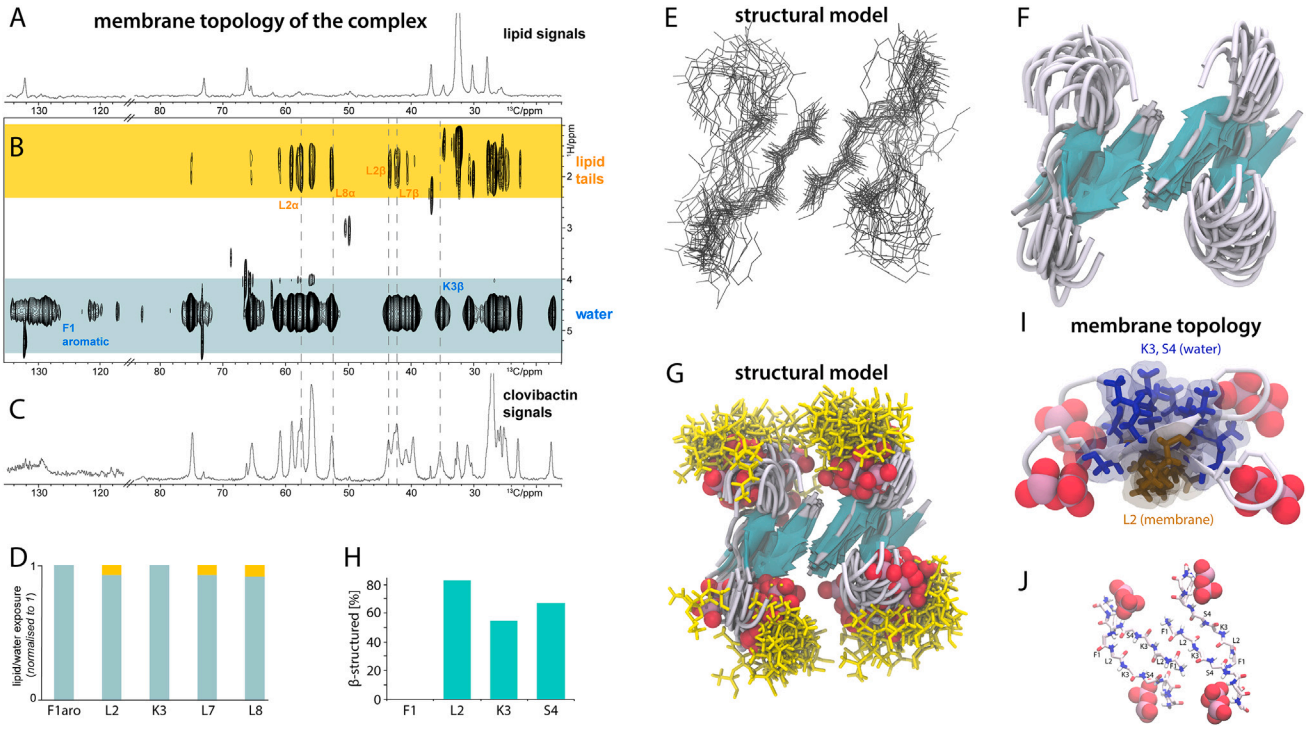

Figure S6. Membrane topology and structure of the complex, related to Figure 4

(A) and (B) show mobility-edited (T_2-filtered) $^{1}H(^{1}H)^{13}C$ ssNMR experiments[31] of ^{13}C,^{15}N-clovibactin bound to lipid II. Here, magnetization from mobile water and lipid molecules is transferred to the rigid clovibactin protons via ^{1}H-^{1}H mixing and eventually transferred to the ^{13}C nuclei of clovibactin via a short cross-polarization step (200 μs). A 2D implementation of this experiment demonstrates that the side chain of Leu2 is partially inserted in the membrane, whereas the side chain of Lys3 points to the water phase. In general, as shown in Figure 4I of the main text, clovibactin fibrils do reside on the membrane surface and do not insert deeply into the membrane. Spectra were measured at 1,200 MHz, 16.5 kHz MAS, and 300 K sample temperature.

(A) Control: 1D $^{1}H(^{1}H)^{13}C$ ssNMR spectrum (5,120 scans) using a T_2-filter of 2.5 ms without transfer to clovibactin (0 ms ^{1}H-^{1}H mixing). All signals relate to lipids, demonstrating the effectiveness of the T_2-filter.

(B) 2D $^{1}H(^{1}H)^{13}C$ ssNMR spectrum using 2.5 ms T_2 filter (1,792 scans) and 5 ms ^{1}H-^{1}H mixing.

(C) ^{13}C cross-polarization spectrum (200 μs contact time) of lipid II-bound clovibactin.

(D) Normalized relative signal intensities (peak heights) of the correlations with water (blue) and lipid (brown) protons for several residues. See Figure S6I for a structural representation of the topology.

(E and F) Superposition (2.50 ± 0.85 Å average backbone RMSD for clovibactin in the complex) of 22 calculated structural models of the clovibactin-lipid II complex. Lipid II is not shown for clarity.

(G) Same as (F) but including the PPi group (shown in spheres) and the MurNAc sugar of lipid II.

(H) Quantification[38] of secondary structure elements of the very short linear N terminus based on the calculated structural model. The N terminus adopts a secondary structure that contains elements of β-structuring and an elongated loop. This is also reflected in the calculated ensemble (E and F) that does not show consistent β-structuring for the N terminus.

(I) Membrane topology of clovibactin in the complex derived from ssNMR T_2-edited H(H)C experiments.[31] The long hydrophobic Leu2 side chain (in brown) is embedded in the membrane, whereas the cationic (Lys3) and polar (Ser4) side chains (in blue) of the N terminus are water-exposed and, at the same time, favorably interact with the anionic PPi group.

(J) Atomic force microscopy, confocal microscopy, and ssNMR data demonstrate that clovibactin and lipid II oligomerize into fibrils. ssNMR distance measurements are consistent with an antiparallel arrangement of clovibactin molecules, something that is also in line with the fibrils observed in AFM experiments. Based on these experimental data, we applied hydrogen bonding restraints to foster an antiparallel arrangement in the structural model.

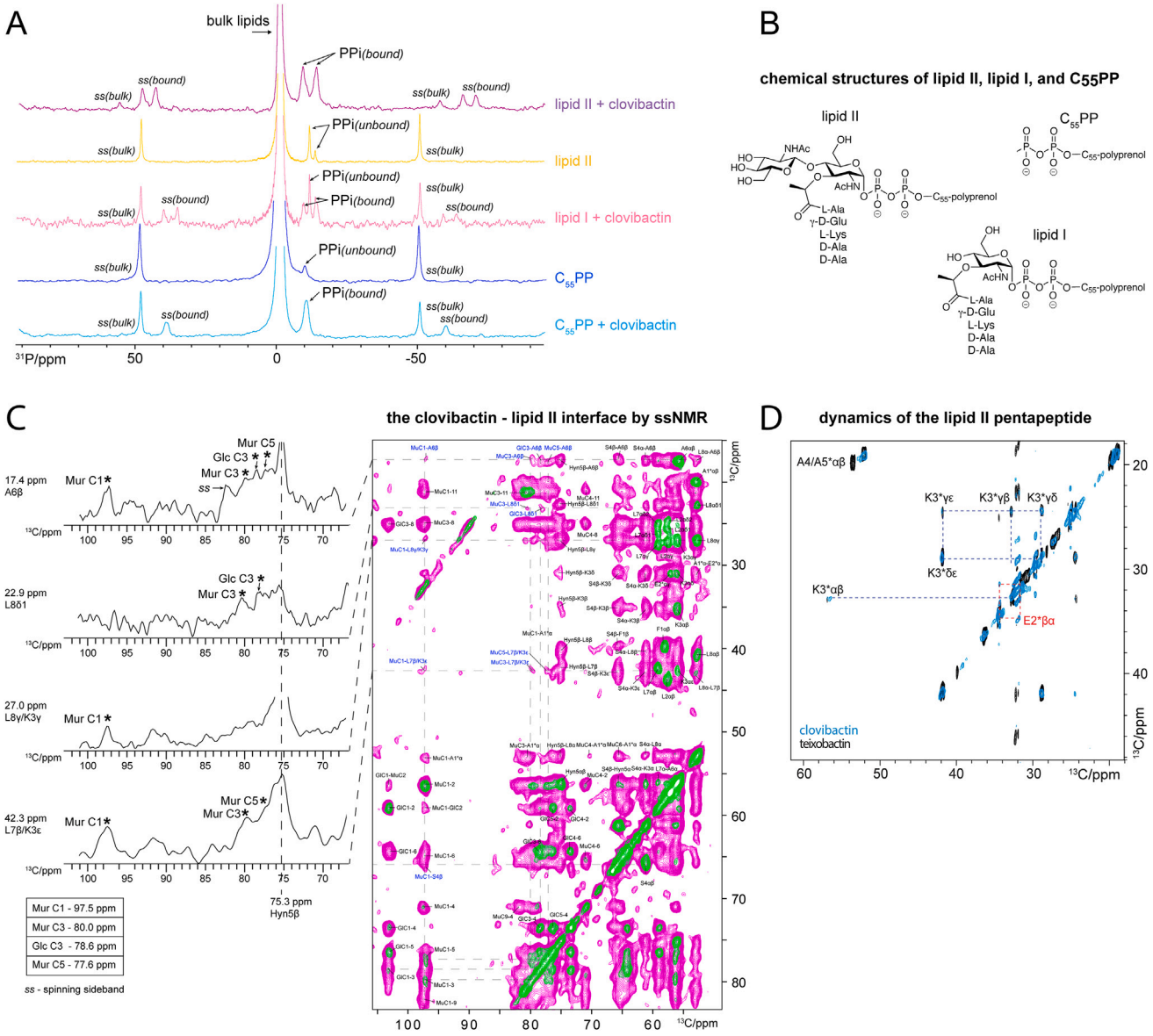

Figure S7. The clovibactin-lipid II binding interface seen by ssNMR, related to Figure 5

(A) Clovibactin binds to all cell wall precursors containing the C_{55}PP unit (C_{55}PP, lipid I, and lipid II). Changes in the chemical shifts of the pyrophosphate groups of lipid II and lipid I upon addition of clovibactin show the direct binding to the site. Furthermore, the emergence of strong spinning sidebands around +45/−55 ppm show that clovibactin binds and immobilizes C_{55}PP. Experiments were performed using MLV's containing 2 mol % of the cell wall precursor with and without the treatment with clovibactin at 500 MHz and 10 kHz MAS (lipid II + clovibactin was performed at 12 kHz MAS). Spinning sidebands (ss) of bound cell wall precursors and bulk lipids are annotated.

(B) Chemical structures of lipid II, lipid I, and C_{55}PP.

(C) (Right) 2D CC PARIS ssNMR spectra show multiple interfacial contacts illustrating the interaction between the depsi-cycle of clovibactin with the first sugar of lipid II. The experiments were performed at 950 MHz magnetic field with 15.5 kHz MAS using CC mixing times of 50 (green) and 300 ms (magenta). (Left) Horizontal cross-sections (rows) of long-range contacts extracted from 2D CC spectrum acquired with 300 ms CC mixing time.

(D) The scalar based TOBSY spectrum only shows highly mobile residues in the complex. Here, one can clearly see the presence of all the residues of the pentapeptide of lipid II, except for A1*. This indicates that the pentapeptide is highly mobile in the complex and not involved in the binding interface. The first A1* residue is linked to the first sugar (MurNAc) and therefore is more rigid and visible in the dipolar-based spectrum (Figure S7C). This contrasts with teixobactin's scalar spectrum (black) where residue E2 (in red) was not observed due to specific interactions of the MurNAc sugar with the enduracididine residue, leading to higher degree of rigidification of the pentapeptide.[10]

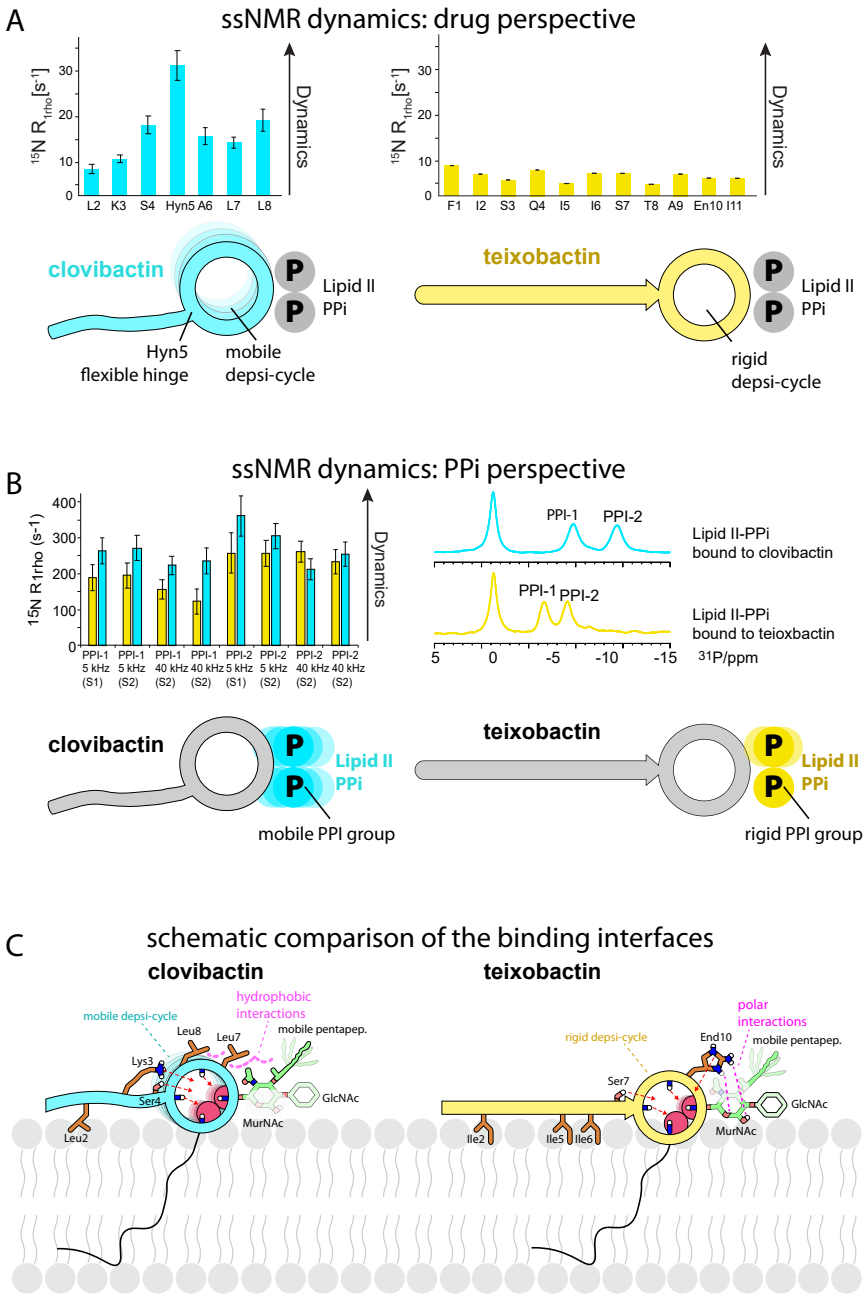

Figure S8. Comparison of the clovibactin-lipid II and teixobactin-lipid II interfaces, related to Figure 5

(A) Comparison of ^{15}N T_{1rho} ssNMR dynamics acquired for clovibactin (in cyan) and teixobactin (in yellow) in their lipid II-bound states in DOPC liposomes. Data were acquired using ^{1}H-detected ssNMR experiments[74] at 60 kHz MAS and 700 MHz static magnetic field at about 300 K sample temperature. The error bars show the standard error of the fit. The data show enhanced dynamics for the depsi-cycle of clovibactin, especially around the hinge-residue Hyn5. These enhanced slow dynamics compromise dipolar magnetization transfer, especially for clovibactin's depsi-cycle residues.

(B) Comparison of ^{31}P T_{1rho} ssNMR dynamics acquired for the lipid II PPi group bound to teixobactin (in yellow) and bound to clovibactin (in cyan) in DOPC liposomes. Data were acquired at 16 kHz MAS and 500 MHz static magnetic field (^{1}H-frequency) at about 300 K sample temperature. The data show clearly enhanced dynamics for the PPi group when bound to clovibactin compared to when bound to teixobactin. For each complex, measurements were conducted in duplicate (i.e., for two samples) using two different spin-lock fields of 5 and 40 kHz.

(C) Schematic comparison of the binding interfaces:

Clovibactin: clovibactin binds lipid II on the membrane surface. In the bound state, clovibactin's N-terminal domain (Phe1-Ser4) adopts a non-classical secondary structure that presumably contains β-structured elements. Clovibactin's N-terminal domain, which is presumably the self-assembly domain, is only loosely anchored into the membrane by a single long hydrophobic residue (Leu2). This (together with the lack of specific interactions with the lipid II sugars, see below) explains why clovibactin supra-structures are quite mobile, as seen by single-molecule tracking microscopy experiments (Figure S5I).

(legend continued on next page)

Target binding: clovibactin specifically targets the pyrophosphate group of lipid II using backbone amino protons (shown as blue-white sticks) of its depsi-cycle (Hyn5-Leu8). Binding of the anionic pyrophosphate group is presumably supported by the cationic Lys3 side chain and also by polar interactions with the hydroxyl group of Ser4. In the complex, the depsi-cycle and the lipid II pyrophosphate remain fairly mobile, as demonstrated by ssNMR relaxation data (Figures S8A and S8B). The side chains of the depsi-cycle that face the lipid II sugars are exclusively hydrophobic (Ala6, Leu7, and Leu8). ssNMR data show that these hydrophobic residues, especially Leu7 and Leu8, interact with the hydrophobic side of the MurNAc sugar (i.e., the methyl-groups of N-acetyl at the C2 position and of lactyl at the C3 position). The second lipid II sugar, GlcNAc, is distal from the complex interface. The pentapeptide is highly mobile and not involved in complex formation, which is a reason why clovibactin is not prone to the development of antimicrobial resistance. Clovibactin hence solely targets the conserved pyrophosphate group in a specific manner, which is the reason why clovibactin also targets other indispensable precursor molecules (lipid I and C55PP) with very good affinity. This multi-target mechanism is another major reason why clovibactin is so refractory to the development of antimicrobial resistance.

Teixobactin: teixobactin binds lipid II on the membrane surface. In the bound state, teixobactin's N-terminal domain (Phe1-Ser7) adopts a β strand conformation. The N-terminal domain is the self-assembly domain, forming antiparallel β sheets. Teixobactin is firmly anchored into the membrane by three long hydrophobic residues (Ile2, Ile5, and Ile6), which rigidifies the teixobactin supramolecular fibrils (together with the specific interactions with the lipid II MurNAc sugar, see below).

Target binding: teixobactin specifically binds the conserved pyrophosphate group of lipid II using backbone amino protons (shown as blue-white sticks) of its depsi-cycle (Thr8-Leu11).[10] Binding of the anionic pyrophosphate group is presumably supported by polar interactions with the hydroxyl-group of Ser7. In the complex, the depsi-cycle is highly rigid, as demonstrated by ssNMR relaxation data (Figures S8A and S8B). The pyrophosphate group is also rigid in the teixobactin-bound state, with slightly elevated dynamics on the second phosphate that is attached to MurNAc. The unusual cationic residue enduracididine10 (End10) of teixobactin dominates the interface and engages in tight, specific hydrogen bonding with the MurNAc sugar, presumably with the hydroxyl group of C6. The cationic End10 side chain also stabilizes the anionic pyrophosphate. Furthermore, pyrophosphate is coordinated by the cationic N terminus of N-Me-D-Phe1 of an adjacent teixobactin molecule in the suprastructure. The second sugar, GlcNAc, is distal from the complex interface. The pentapeptide is highly mobile and not involved in complex formation, which is a reason why clovibactin is not prone to the development of antimicrobial resistance.

clovibactin - lipid II

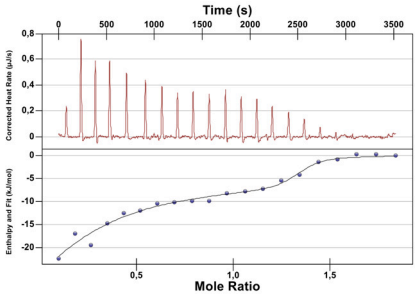

clovibactin - lipid I

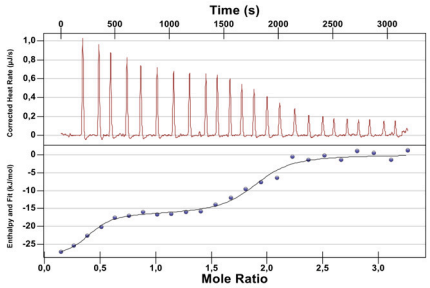

clovibactin - C_{55}PP

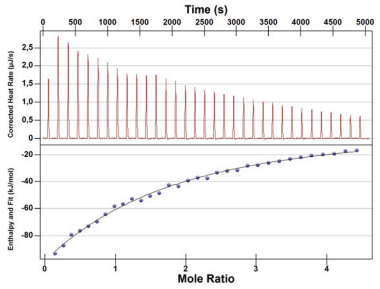

teixobactin - lipid II

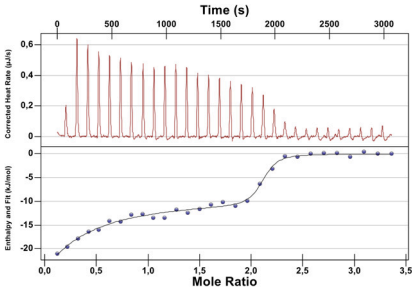

teixobactin - lipid I

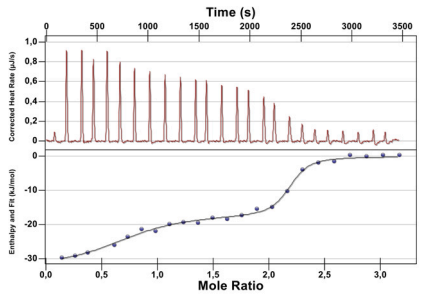

teixobactin - C_{55}PP

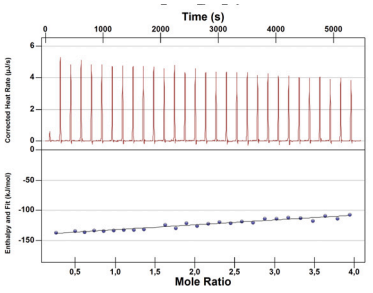

clovibactin - Na-pyrophosphate

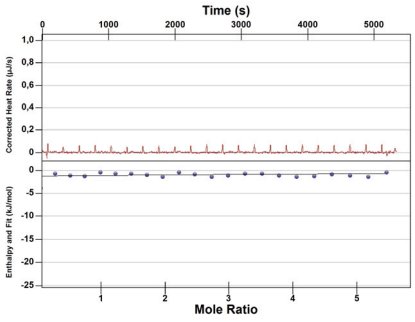

clovibactin - DOPC LUVs

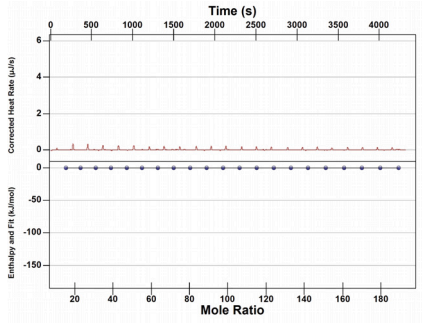

teixobactin - DOPC LUVs

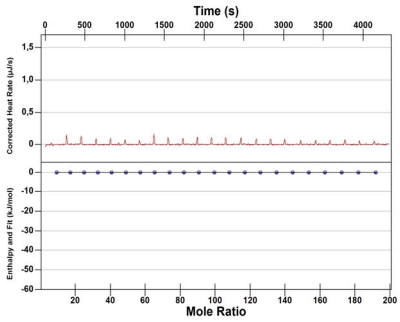

K_d (µM)	lipid II	lipid I	C_{55}PP
clovibactin	0.086 ± 0.007	0.081 ± 0.017	62.3 ± 2.6
teixobactin	0.015 ± 0.007	0.080 ± 0.007	137 ± 41.7

Figure S9. Comparative ITC data for clovibactin and teixobactin, related to Figure 5

The ITC data shows a binding isotherm for interaction between clovibactin and lipid II, lipid I, and C_{55}PP. All experiments were performed in duplicates. All the parameter values are shown as mean ± SD.

Teixobactin (1.46E−8 ± 2.00E−9) has a higher binding affinity for lipid II than clovibactin (8.62E−8 ± 7.30E−9). For lipid I, teixobactin's affinity diminishes (8.05E−8 ± 7.48E−9), whereas the affinity of clovibactin remains steady (8.07E−8 ± 8.07E−8). This decrease in affinity already indicates that teixobactin is more sensitive to the exact conformational arrangement of the lipid II sugars. This is strongly supported by the drastically reduced binding affinity of teixobactin for C_{55}PP (1.37E−4 ± 4.17E−5), whereas clovibactin still binds reasonably strong to C_{55}PP (6.23E−05 ± 2.60E−6).

There is no binding observed between clovibactin and soluble sodium-pyrophosphate.